

The Study of Some Physical Properties
of Selected Rare Earth Compounds

A Thesis submitted for the Degree of
Doctor of Philosophy by

William Alexander Westall B.S c.

Department of Chemical Physics
Faculty of Natural Sciences
University of Kent at Canterbury,

October. 1983.

Memorandum

The work described in this thesis was carried out in the University Chemical Laboratory, University of Kent at Canterbury, between October 1979 and October 1982 under the supervision of Dr. S.J. Lyle, Reader in Chemistry.

This thesis contains the results of some original research by the author; no part of the material offered has previously been submitted by the candidate for a degree in this or any other University. When use has been made of the results and conclusions of other authors in relevant studies, care has always been taken to ensure that the source of information is clearly indicated unless it is of such a general nature that indication is impracticable.

Acknowledgements

I am grateful to Dr. S.J. Lyle for his consistent help and encouragement throughout the course of this work. My thanks are also due to the Science and Engineering Research Council for their financial support; the entire technical staff of the Chemical Laboratory, University of Kent at Canterbury for their assistance in the construction and maintenance of equipment; my friends and colleagues for their helpful discussions and Mrs. L. Wellum for the preparation of the manuscript.

Finally these acknowledgements would not be complete without thanking my fiancée and family for their support and encouragement.

Abstract

The work set out in this thesis relates to studies of europium(II) and europium(III) containing solids. The primary mode of study was Mössbauer spectroscopy supported where useful, by information from chemical analysis, x-ray diffractometry, electrical conductivity, thermogravimetry, infra-red and mass spectrometry.

The thermal dehydration of $\text{EuCl}_3 \cdot 6\text{H}_2\text{O}$ and $\text{EuBr}_3 \cdot 6\text{H}_2\text{O}$ and subsequent conversion to oxyhalide and oxide was studied initially by thermogravimetry to define stable intermediates; these were afterwards prepared in amounts enabling their characterization. The chloride system gave a sequence of well-defined intermediate hydrates; but those for the bromide system were less well-defined. Neither anhydrous europium(III) halide was observed in contrast with previous reports. However in the absence of oxygen the thermal decomposition of the hydrated bromide resulted in the formation of some europium(II) at temperatures above 300°C .

The non-stoichiometric phase formed in the initial stages of the thermal reaction



has been studied. The temperature dependent Mössbauer spectra are consistent with an "electron hopping" mechanism similar to that involved previously to describe non-stoichiometric EuCl_3 . Electrical conductivity measurements on both chloride and bromide systems revealed two regions for each system; they were separated by a characteristic temperature of $198 \pm 2\text{K}$ and $222 \pm 2\text{K}$ respectively. Below these temperatures charge ordering in the lattice is considered to occur while above, electron hopping predominates. Activation energies calculated for electron hopping from spectral and conductivity data are in agreement.

Several europium-mercury compounds (EuHg_x where $x = 0.8, 1, 2, 3, 3.6$) have been prepared and studied. Correlation was found between the europium isomer shift and $\sqrt[3]{(n/v)}$ where n is the number of europium ions in a unit cell of volume v . The electron density at the europium nucleus together with an approximate electron configuration of the europium ion core have been determined for each of the samples. The compounds were found to be metallic in nature with some degree of normal valence character in bonding. The ionic core of europium was found to be divalent with the conduction electron density at the nucleus decreasing with decreasing europium concentration in the crystal lattice.

Contents

Chapter 1. Introduction	1
1.1 History of the Mössbauer Effect	1
1.2 Energetics of Recoilless Absorption and Emission of γ -rays	2
(a) Energetics of Free Atom Recoil and Thermal Broadening	2
(b) The Heisenberg Natural Line Width	5
(c) Energy and Momentum Transfer to the Lattice	8
(d) The Cross-Section for Resonant Absorption	9
1.3 The Mössbauer Spectrum	11
1.4 Hyperfine Interactions	12
(a) The Isomer Shift	12
(b) The Second Order Doppler Shift	18
(c) Quadrupole Interactions	19
(d) Magnetic Hyperfine Interactions	23
1.5 Aims and Objectives of the Work Presented in this thesis	25
Figures	28
References	31
Chapter 2. Experimental Apparatus and Techniques	33
2.1 Introduction	33
2.2 The Mössbauer Spectrometer	33
2.3 The Multichannel Analyzer	34
2.4 The Velocity Generator and Transducer	35
2.5 Detectors	36
2.6 Sources	37
2.7 Sample Preparation for Mössbauer Spectroscopy	39

2.8	The Variable Temperature Cryostat	40
2.9	The Glove Box	41
2.10	Electrical Conductance Cell and Bridge	43
2.11	Data Handling Techniques	44
(a)	Mossbauer Data	44
(b)	Conductivity Data	48
(c)	X-ray Data	48
	Figures	50
	References	57
Chapter 3. The Preparation and Characterization of the Samples for Study		59
3.1	Introduction	59
3.2	The Preparations of Anhydrous Europium Tribromide and Europium Trichloride	59
(a)	Preparation of Anhydrous Europium(III) Chloride	61
(b)	Preparation of Anhydrous Europium(III) Bromide	62
3.3	Preparation of Intermediate Hydrates of Europium Halides	67
3.4	Chemical Characterization of the Compounds	69
(a)	Titrimetric analysis for europium	69
(b)	Titrimetric analysis of the halide ion	70
3.5	Spectrophotometric Determination of Europium(II) in the Presence of Europium(III)	71
3.6	Other Analytical Techniques	76
	Figures	78
	References	82

Chapter 4. The Thermal Decomposition Reactions of Hydrated Europium(III) Chloride and Bromide	84
4.1 Introduction	84
4.2 Experimental Method	88
4.3 Results and Discussion	90
(a) Hydrated Europium(III) Chloride	90
(b) Hydrated Europium(III) Bromide	94
(c) Infra-red Spectra	99
(d) Mass Spectrometry	99
4.4 Conclusion	100
Tables	103
Figures	108
References	122
 Chapter 5. Electron Hopping in Anhydrous Europium Halides	 124
5.1 Introduction	124
5.2 Mechanisms by which Non-stoichiometric Phases Arise	127
5.3 The Observations of Electron hopping using the Mossbauer Effect and the Choice of System	130
5.4 Relaxation Effects and Mossbauer Spectra	133
5.5 Experimental	138
5.6 Results and Discussion	138
Tables	153
Figures	158
References	175

Chapter 6. A Preliminary Investigation into Europium	
Mercury Compounds	178
6.1 Introduction	178
6.2 Factors Influencing the Character of Intermetallic Compounds	180
6.3 Electrons in Metals	184
6.4 Experimental	189
6.4.1 Preparations	189
6.4.2 Chemical Analysis	192
(a) Total Metal Analysis	193
(b) Europium Analysis	193
6.5 Results	194
6.6 Discussion	196
Tables	205
Figures	209
References	221
 Chapter 7. Summary of Results, Conclusions and Suggestions for Further Work.	 223
7.1 Introduction	223
7.2 The Thermal Decomposition of Hydrated Europium(III) Chloride and Bromide	223
7.3 Electron Hopping in Anhydrous Europium(III) Chloride and Europium(III) Bromide	224
7.4 The Europium-Mercury System	226
7.5 Experimental Apparatus	227
References	229

Chapter 1

Introduction

1.1 History of the Mössbauer Effect

The Mössbauer effect is the phenomenon of emission or absorption of a γ -ray photon without loss of energy due to recoil of the nucleus or thermal broadening. The effect is named after its discoverer, R.L. Mössbauer^{1,2,3} who in 1957 observed, contrary to expectation, that a decrease in temperature resulted in an increase in resonant absorption of the 129 KeV γ -radiation in ^{191}Ir metal.

The resonant absorption of light, i.e. optical fluorescence was predicted by Rayleigh⁴ in 1894 and first observed by Wood⁵ in 1904 in his famous "sodium D line" experiment. Just as resonant absorption is observed in atoms and molecules, so there is every reason for observing γ -ray resonance in the nucleus. The search started⁶ in 1926 and continued for twenty years without success. Up until Mössbauer's discovery, nuclear resonance had been observed but under very special conditions so the investigation did not receive wide attention. The reasons for difficulty in observing recoilless nuclear resonance of γ -rays lie in the energies involved in the process; these will be discussed in the next section.

In the early stages, the Mössbauer effect was restricted to low energy nuclear physics i.e. the determination of excited state lifetimes and nuclear magnetic moments. The chemical shift was reported in 1960 by Kistner and Sunyar⁷ in a quadrupolar perturbed magnetic spectrum of $\alpha\text{-Fe}_2\text{O}_3$. The

Mössbauer effect had now become a useful spectroscopic technique for observing properties related to the electronic shell of the atom due to the great resolving ability allowing such hyperfine effects to be observed.

1.2 Energetics of Recoilless Absorption and Emission of γ -rays

(a) Energetics of Free Atom Recoil and Thermal Broadening

Resonant emission and absorption of a γ -ray photon will only occur if the energy of the γ -ray is not degraded in any way. One of the primary reasons for the failure in observing resonance is the high recoil energy associated with the emission of a γ -ray photon from the nucleus.

If an isolated atom in the gas phase is considered the energies involved in the emission and absorption process can be evaluated remembering that the atom has translational kinetic energy, hence a relative velocity. Let the energy of transition be E

$$E = E_e - E_g \quad (1.1)$$

where E_e and E_g are the energies of the excited and ground states respectively. In one dimension for simplicity the atom has a velocity V_x hence an energy of $E + \frac{1}{2}MV_x^2$ and a momentum MV_x . After the emission of a γ -ray of energy E_γ , the atom suffers recoil which imparts a velocity v to the atom. The velocity is now $V_x + v$ and the energy is

$$E_\gamma + \frac{1}{2}M(V_x + v)^2 \quad (1.2)$$

and the momentum is

$$M(V_x + v) + \frac{E_\gamma}{c} \quad (1.3)$$

As energy is conserved

$$E + \frac{1}{2}Mv_x^2 = E_\gamma + \frac{1}{2}M(Vx + v)^2 \quad (1.4)$$

So

$$\delta E = E - E_\gamma = \frac{1}{2}Mv^2 + MvVx^2 \quad (1.5)$$

or

$$\delta E = E_R + E_D \quad (1.6)$$

It can be seen that the degradation of the γ -ray is due to energy lost in recoil, E_R and the energy due to the velocity of the atom, E_D . Non-relativistic mechanics can be used since V_x and $v \ll c$. The mean kinetic energy per translational degree of freedom for a free gas atom is

$$\bar{E}_k = \frac{1}{2} M \bar{V}_x^2 \approx \frac{1}{2} KT \quad (1.7)$$

where K is Boltzmann's constant and T is the absolute temperature. From this

$$\bar{E}_D = 2 \sqrt{E_k E_R} \quad (1.8)$$

$$\text{Writing } E_R = \frac{1}{2} Mv^2 = \frac{P^2}{2M} \quad (1.9)$$

where P is the momentum of the atom due to recoil the momentum of the γ -ray in the opposite direction is $-P_\gamma$

$$P_\gamma = \frac{E_\gamma}{c} \Rightarrow P = -\frac{E_\gamma}{c}$$

$$\therefore E_R = \frac{E_\gamma^2}{2Mc^2} \quad (1.10)$$

and
$$E_D = E_\gamma \sqrt{\frac{2\bar{E}_k}{(Mc^2)}}$$

It is now apparent that the γ -ray distribution is displaced by E_R and broadened by $2\sqrt{\bar{E} K E_R}$ with a Gaussian distribution.

The extent of the absorption of electromagnetic radiation depends on the overlap of the energy profiles of the excited and exciting states, figure 1 shows the overlap as the shaded area. The emitted γ -ray loses an energy E_R due to recoil therefore for it to excite a second nucleus another amount of energy, E_R is required; hence the energy must be $E + E_R$. A comparison of the energies involved between a nuclear system and those for resonance in the ultra-violet region reveals that there is strong absorption in the ultra-violet region.

for $M = 100$ a.m.u. and $E = 6.2$ eV

$$E_R = 2.1 \times 10^{-10} \text{ eV}$$

$$E_D = 3 \times 10^{-6} \text{ eV}$$

but only weak absorption of a γ -ray.

for $M = 100$ a.m.u. and $E_\gamma = 10^4$ eV

$$E_R = 5.4 \times 10^{-4} \text{ eV}$$

$$E_D = 5 \times 10^{-3} \text{ eV at } 300^\circ\text{C}$$

First attempts to compensate for the recoil energy, $2E_R$, involved a large closing velocity,

$v = \frac{E_\gamma}{Mc}$, ⁸ Moan in 1950 used an ultra centrifuge and obtained a velocity of about 7×10^5 mms⁻¹ to observe nuclear resonance in ¹⁹⁸Hg.

Other attempts involved the use of high temperatures to increase the overlap of absorption and emission profiles. These attempts only resulted in a marginal improvement in absorption. It is worth remembering that energy loss due to recoil is not compensated for in the Mössbauer effect.

(b) The Heisenberg Natural Line Width

In the previous section we have seen that the width of the energy distribution is given by $2\sqrt{E_K E_R}$. However, since the Mössbauer effect does not require thermal broadening to exhibit nuclear resonance it will be more suitable to consider the width of the energy distribution due to the uncertainty in the lifetime of the excited state; the Heisenberg natural line width.

From Heisenberg's uncertainty principle

$$\Delta E \Delta t \geq \hbar$$

where $\hbar = h/2\pi$ and h is Planck's constant. The full width at half height of the energy Γ , represents the uncertainty in the energy of the excited state having a mean lifetime, τ . The ground state has an infinitely long lifetime therefore has no uncertainty in its energy.

The mean lifetime is related to the half-life, $t_{1/2}$ of the state by

$$\tau = t_{1/2} / \ln 2$$

The inequality may now be written

$$\Gamma \tau \geq \hbar \quad (1.11)$$

It can be seen that the natural line width is very much less than \bar{E}_R and \bar{E}_D , for a free atom it can be neglected. If E_R and \bar{E}_D can be eliminated then the energy distribution with a width Γ would represent a highly monochromatic radiation, in the next section it will be seen that the degradation of the γ -ray energy can be overcome.

For a many emission process, Lipkin⁹ has shown that the average energy transferred to the lattice per event must be equal to E_R . If a fraction of events, f , occur without transfer of energy to the lattice, then to a first approximation $(1-f)$ events transfer one phonon of energy $\hbar W$

so

$$E_R = (1-f) \hbar W \quad (1.12)$$

The recoil free fraction, f is dependent upon the host lattice of the emitting nucleus, it will be helpful to outline a more quantitative account of the probability of a zero phonon γ -ray emission from a nucleus in a solid. Consider a nucleus embedded in a solid which emits a γ -ray photon and simultaneously changes its vibrational state from $|i\rangle$ to $|f\rangle$. From dispersion theory⁹⁻¹¹ the probability of a zero phonon emission W , is given

$$W \propto | \langle f | \mathcal{H} | i \rangle |^2 \quad (1.13)$$

where the operator depends on the position co-ordinates of the nucleus and the momentum and spins of the particles within the nucleus. Lamb¹² has shown that inter nuclear forces are short range whereas the forces holding the lattice together are long range. This allows the matrix element to be split into two parts since the nuclear decay and vibrational state are treated as being independent. The matrix element is reduced to one term for the transition of the vibrational state from the initial state L_i to the final state L_f . The probability W is now

$$W = \text{const} \times | \langle L_f | e^{i\mathbf{k}\cdot\mathbf{x}} | L_i \rangle |^2 \quad (1.14)$$

\mathbf{x} is the position of the centre of mass of the decaying nucleus, \mathbf{k} is the wave vector for the emitted γ -ray photon. For a zero phonon emission, the lattice modes are unchanged so

$$f = \text{const} | \langle L_i | e^{i\mathbf{k}\cdot\mathbf{x}} | L_i \rangle |^2 \quad (1.15)$$

since \underline{Li} is normalized

$$f = e^{-\underline{k}^2 \cdot \underline{x}^2} \quad (1.16)$$

Replacing \underline{x}^2 with $\langle x^2 \rangle$, the mean square vibrational amplitude of the emitting nucleus in the γ -ray direction and $\underline{k}^2 = \frac{4\pi}{\lambda^2} = \frac{E^2}{(\hbar c)^2}$

$$f = \exp \frac{-E^2 \langle x^2 \rangle}{(\hbar c)^2} \quad (1.17)$$

It is apparent that the recoil free fraction decreases with increasing γ -ray energy and increasing $\langle x \rangle$. To gain a more physical understanding of how the recoil free fraction is affected by the surroundings of the emitting nucleus, the results of the Debye model are considered. The Debye model while not a complete description of a solid in that it does not take into account anharmonicity it is still useful to predict the physical properties of a solid. Only the relevant results are mentioned here but a more complete account of the model can be obtained from most solid state physics texts of which Kittel¹³ is typical.

The Debye model gives

$$\underline{k}^2 \cdot \underline{x}^2 = \frac{\hbar}{2M} \int_0^{w_D} \frac{N(w)}{w} \coth\left(\frac{\hbar w}{2K_B T}\right) dw \quad (1.18)$$

w is the frequency of vibration, w_D is the Debye frequency and $N(w)$ is the distribution of frequencies. From the above an expression for the recoil-free fraction is obtained.

$$f = \exp \left\{ \frac{-6E_R}{K \theta_D} \left[\frac{1}{4} + \left(\frac{T}{\theta_D}\right)^2 \int_0^{\theta_D/T} \frac{x}{e^x - 1} dx \right] \right\} \quad (1.19)$$

or

$$f = e^{-2w} \quad (1.20)$$

$\theta_D = \frac{\hbar w_D}{K_B}$ where θ_D is the Debye temperature of the lattice

(c) Energy and Momentum Transfer to the Lattice

We have seen how a free atom recoils when emitting a γ -ray in the gas phase, now consider what happens to an atom bound tightly in a crystal lattice. Lattice energies and chemical binding energies are in the order of between 1 and 10eV; this is very much larger than the recoil energy so if the emitting nucleus can not recoil, i.e. be ejected from the lattice, the recoil is suffered by the entire lattice. Considering the smallest crystalite contains around $10^{15} - 10^{17}$ particles, then from the equation

$$E_R = \frac{E\gamma^2}{2Mc}$$

we see that the increase of a factor $10^{15} - 10^{17}$ in M makes E_R negligible. This picture is oversimplified. A real lattice does not contain atoms or ions rigidly held in place but atoms or ions which vibrate about a mean position. The Einstein model for lattice vibrations in a solid has the lattice as a large number of independent simple harmonic oscillators vibrating at a frequency which is an integral multiple of $\hbar W_E$ (i.e. $0, \hbar W_E, 2\hbar W_E \dots$) where W_E is the Einstein frequency. Here we can see that the recoil energy can only be transferred to the lattice if it is equal or greater than the energy to excite the lattice to the first excited phonon state. The recoil energy is made up of two parts, that which goes in translational energy which has been shown to be negligible and that which goes to exciting lattice vibrations. It is the lattice which requires further examination.

W is known as the Debye-Waller factor and was originally derived for Bragg x -ray scattering theory. In its application to the Mössbauer effect it is more widely known as the Lamb-Mössbauer factor. It should be noted that even at absolute zero the recoil-free fraction is less than unity.

$$f_{T=0} = \exp \left\{ \frac{-3E_R}{2K_B \Theta_D} \right\} \quad (1.21)$$

From the expression for the recoil-free fraction it can be seen that,

- (i) f decreases with increasing temperature
 - (ii) f decreases with increasing γ -ray energy; for example the upper limit of observable γ -ray energy in Mössbauer spectroscopy is currently the 187KeV transition in ^{190}Os
 - (iii) f increases with increasing Debye temperature this being a measure of the strength of the bonds between the Mössbauer atom and the lattice.
- Clearly studies of the recoil-free fraction will reveal much of the nature of the host lattice of the Mössbauer atom. However, the recoil-free fraction is not the only factor affecting the resonant absorption of γ -rays.

(d) The Cross-Section for Resonant Absorption

The distribution of energy about the γ -ray energy, E_γ is given by the Breit-Wagner¹⁴ formula as a Lorentzian distribution

$$N(E)dE = \frac{fs\Gamma_s}{2\pi} \frac{dE}{(E-E_\gamma)^2 + (\Gamma_s/2)^2} \quad (1.22)$$

fs is the recoilless probability

Γ_s is the natural line width of the γ -ray of the source.

The resonant absorption cross-section $\sigma(E)$ can be expressed in a similar way

$$\sigma(E) = \sigma_0 \frac{(\Gamma_a/2)^2}{(E-E_0)^2 + (\Gamma_a/2)^2} \quad (1.23)$$

where

$$\sigma_0 = 2\pi\lambda^2 \frac{2I_e + 1}{2I_g + 1} \frac{1}{1 + \alpha}$$

Γ_a is the natural line width of the absorber I_e and I_g are the nuclear spin quantum numbers of the excited and ground states respectively.

α is the internal conversion coefficient. A proportion of γ -rays eject electrons from the atomic orbitals leading to x-rays and conversion electrons. The internal conversion coefficient is therefore the ratio of conversion electrons produced to the number of γ -rays emitted σ is usually expressed in barns

$$(1 \text{ barn} = 10^{-24} \text{ cm}^2)$$

The resonant absorption of γ -rays is not the only process of attenuation it is in competition with other processes such as photo-electric absorption and Compton scattering. It is important for the cross-section of resonant absorption to be higher than that for the other processes. The exact evaluation of the transmission of γ -rays through a solid in general is impossible but Margulies and Ehrman¹⁵ showed the basic behaviour, to a first approximation is quite simple. Taking the natural line width of the source and absorber to be equal, i.e. $\Gamma = \Gamma_a + \Gamma_s$, for an ideally thin

absorber at thickness, $t \rightarrow 0$, the intensity, $I(\epsilon)$ of the radiation is given by

$$I(\epsilon) = \frac{\Gamma_r}{2\pi} \frac{1}{(\epsilon - E_\gamma)^2 + \Gamma_r/2} \quad (1.24)$$

$$\text{where } \Gamma_r = \Gamma_a + \Gamma_s = 2\Gamma$$

The distribution is still Lorentzian but has been broadened. For absorbers of a finite thickness containing t_a resonant atoms per unit area of cross-section with a recoil-free fraction of f_a the effective thickness, a dimensionless parameter is defined

$$T_a = f_a \sigma_0 t_a \quad (1.25)$$

To accumulate a good Mössbauer spectrum, the resonant absorption must be high, hence a large number of resonant absorbers is needed. However, as the number of absorbing atoms increase, so the width of the absorption increases with a loss of resolution. The ideal amount of sample is a compromise found by experience.

1.3 The Mössbauer Spectrum

If an energy range is being scanned using the conventional Doppler drive then a plot of transmission against energy is obtained. Of all the γ -rays emitted from the source only a fraction are resonantly absorbed. Figure 1.2 shows self evidently the various factors affecting a transmission spectrum. It should be noticed that if an absorbing nucleus is excited, then it too can emit a γ -ray when it relaxes. However, the newly emitted γ -ray may suffer internal conversion, or if not it can be emitted at any angle over a range 0 to 4π radians, hence reducing the probability of detection on the spectrum.

1.4. Hyperfine Interactions

A hyperfine interaction is one between an electron and the nucleus other than the Coulombic interaction. Electric and magnetic hyperfine interactions may be distinguished as the nucleus may have an electric quadrupole moment or a magnetic dipole moment.

Such hyperfine interactions make the Mössbauer effect a valuable spectroscopic tool. The interaction between the nucleus and the electrons may be observed and since the electronic environment of the nucleus is affected by the chemical and physical environment of the nucleus, much information can be gained from the system on a microscopic level.

The main interactions are:

- (a) the electric monopole interaction or isomer shift E_0 .
- (b) the second order doppler shift.
- (c) the electric quadrupole moment, E_1 .
- (d) the magnetic dipole moment, H_1 .

(a) The Isomer Shift

The Coulombic interaction between the nucleus and the extra-nuclear electrons is considered. Of the latter only those electrons whose wave functions overlap with the nuclear wave function are of consequence; they are the s -electrons and the $p_{\frac{1}{2}}$ electrons. The latter are not usually considered as this state is not usually encountered in Mössbauer spectroscopy. Although the p , d and f electrons are not directly involved in this interaction they do affect the s -electron density by the shielding effect.

The energy of interaction between a nucleus of charge $+Ze$ and electrons of charge $-e$ can be found by first considering a point nuclear charge, the intergrated electrostatic energy will be

$$E_0 = \frac{-Ze^2}{k} \int \rho_e \frac{d\tau}{r} \quad (1.26)$$

k is the dielectric constant of a vacuum

r is the radical distance from the nucleus

$-\rho_e$ is the charge density of orbital electrons in the volume element $d\tau$

This equation is only valid for $r < R$ where R is the nuclear radius. so for a nucleus of finite size (ie radius R) the electrostatic energy for $r < R$ is

$$E = e \int \rho_n \phi_e d\tau \quad (1.27)$$

where ϕ_e is the electrostatic potential of the electrons.

ρ_n is the charge density of the nucleus.

Assuming a simple model for the proton charge density inside the nucleus, taking this to be uniform¹⁷.

The charge W , in electrostatic energy caused by the finite radius of the nucleus can therefore be expressed as

$$W = e \int_0^R \rho_n \phi_e d\tau - \frac{Ze^2}{K} \int_0^R \rho_e \frac{d\tau}{r} \quad (1.28)$$

The probability density of an s-electron in the neighbourhood of a point charge is given by Dirac theory as

$$\rho_e = \frac{2(\rho+1) |\psi_S(0)|^2}{\Gamma^2(2\rho+1)} \left(\frac{2Z}{a_H}\right)^{2\rho-2} r^{2\rho-2} \quad (1.29)$$

$$\text{where } \rho = \sqrt{1-\alpha^2 Z^2} \quad \alpha = \frac{e^2}{hc}$$

a_H is the first Bohr radius

$\psi_S(0)$ is the non-relativistic Schrodinger wave function at $r = 0$

$\Gamma(n)$ is the gamma function

$$\Gamma(n) = \int_0^{\infty} e^{-x} x^{n-1} dx \quad n > 0$$

It should be noted that the equation ignores the distortion in $\psi_S(0)$ due to the finite nuclear size which will cause an over estimation of the isomer shift. Taking the nuclear charge density as a uniform sphere as stated above the change in electrostatic energy between the point charge and finite radius models is given by

$$W = \frac{24\pi (\rho+1) |\psi_S(0)|^2 Z e^2}{K 2\rho (2\rho+1) (2\rho+3) \Gamma^2(2\rho+1)} \left(\frac{2Z}{a_H}\right)^{2\rho-2} R^{2\rho} \quad (1.30)$$

the difference in energy caused by the nuclear radius change δR will then be

$$\Delta W = \frac{24\pi(\rho+1) |\Psi_s(0)|^2 Z e^2}{K(2\rho+1)(2\rho+3) \Gamma^2(2\rho+1)} \left(\frac{2Z}{a_H} \right)^{2\rho-2} R^{2\rho} \frac{\delta R}{R} \quad (1.31)$$

The chemical isomer shift, δ , as measured in a Mossbauer experiment is an energy difference between two chemical environments, A and B. From the above, an equation can be derived taking into account the differences in $|\Psi_s(0)|^2$ between A and B. The equation is simplified by assuming

$$K = \rho = 1$$

leading to the familiar expression for the isomer shift:

$$\delta = \frac{4}{5} \pi Z e^2 \left\{ |\Psi_s(0)_A|^2 - |\Psi_s(0)_B|^2 \right\} R^2 \frac{\delta R}{R} \quad (1.32)$$

The isomer shift, δ is normally measured as a Doppler velocity v where

$$v = \left(\frac{c}{E_\gamma} \right) \delta$$

So far only non-relativistic wave functions have been considered but this is acceptable for the lighter elements up to about iron. For the heavier elements the wave functions will be modified by relativistic effects, especially near the nucleus. To allow for such effects, Dirac wave functions and first order perturbation theory have been used¹⁸. The correction is made as a dimensionless factor $S'_{(Z)}$ which is introduced into the expression for the isomer

shift as

$$\delta = \frac{4\pi}{5} S'(z) Ze^2 \left\{ |\psi_s(0)_A|^2 - |\psi_s(0)_B|^2 \right\} R^2 \frac{\delta R}{R} \quad (1.33)$$

Values of the 'relativity factor', $S'(z)$ have been compiled by Shirley¹⁹. As the isomer shift is measured for a fixed transition $S'(z)$ remains the same for both environments hence it is not always of practical importance.

It can be seen that the isomer shift depends on two variables, the change in nuclear volume and the difference in s -electron densities in the environments A and B. The nucleus is not necessarily spherical so the mean square value of the radius may be used from the relationships

$$\delta \frac{\langle R^2 \rangle}{\langle R^2 \rangle} = \frac{2\delta R}{R}$$

and

$$\langle R_e^2 \rangle - \langle R_g^2 \rangle = \frac{6}{5} R^2 \left(\frac{\delta R}{R} \right)$$

The excited nucleus is usually larger than the ground state nucleus, ie δR is positive, this implies an increase in electron density at the nucleus from B to A will yield a positive isomer shift. The change in nuclear radius is not always positive, for example in the 57.6 KeV transition in ^{127}I , $\frac{\delta R}{R}$ is negative, the radius decreases when the nucleus when the nucleus is excited²⁰.

For a given transition δ_R/R remains constant so it is possible to study the changes in electron density at the nucleus directly and the expression for the isomer shift can be written

$$\delta = \text{const} \times \left(|\Psi_S(o)_A|^2 - |\Psi(o)_B|^2 \right) \quad (1.34)$$

In this application where s-electron densities at the nuclei are compared, isomer shifts must be measured relative to a known standard. For the 21.6 KeV transition in ^{151}Eu the conventional standards are, monoclinic Eu_2O_3 and EuF_3 (anhydrous) neither of which are ideal standards. Cohen and Kalvius²¹ have examined the problem of a suitable standard for ^{151}Eu Mössbauer measurement, they have defined the following criteria in order of significance:

- (i) The spectrum should show no unresolved electric or magnetic hyperfine interactions.
- (ii) The compound should be of definite stoichiometry and chemical composition.
- (iii) The compound should be easy to prepare and be stable under laboratory conditions.
- (iv) It should be convenient for Mössbauer spectroscopy.

The aforementioned standards do not comply with these criteria exactly. Eu_2O_3 has more than one crystal structure in addition to non-stoichiometric phases. The fluoride is air sensitive leading to doubts about its chemical composition²². Cohen and Kalvius suggest EuS as a standard as it

has the NaCl structure hence no quadrupole interaction unlike many other standards chosen in the past. In this thesis all isomer shifts are quoted relative to anhydrous EuF_3 unless otherwise stated. The range of isomer shifts for ^{151}Eu is quite large, taking EuF_3 as $\delta = 0 \text{ mms}^{-1}$ figure 1.3 shows the extent of ^{151}Eu Mössbauer isomer shifts. It is interesting to note that europium (II) isomer shifts are negative relative to europium (III) this is a consequence of the different shielding of the closed shell s-electrons by the $4f^7$ and $4f^6$ configurations respectively. There are many sources of isomer shift data for europium compounds some of which are given at the end of this chapter.²³⁻²⁸

(b) The Second Order Doppler Shift.

Although no use of this is made in the work described in this thesis, the second order Doppler shift will be mentioned. The emitting or absorbing atom is vibrating on its lattice site with a frequency of oscillation of about 10^{12} Hz , so the average displacement during the Mössbauer event is zero. The average velocity is also zero but $\langle v^2 \rangle$ is non-zero. Pound and Rebka²⁹ and also Josephson³⁰ independently pointed out the existence of a relativistic temperature dependent contribution to the chemical isomer shift. The relativistic equation for the Doppler effect³¹ on an emitted photon gives an observed frequency, ν' for a closing velocity v as

$$\nu' = \left(1 - \frac{v}{c}\right) \left(1 + \frac{v^2}{2c^2}\right) \quad (1.34)$$

The modification to the isomer shift is

$$\frac{\delta E_{\gamma}}{E_{\gamma}} = \frac{\delta \nu}{\nu} = \frac{-\langle v^2 \rangle}{2c^2} \quad (1.35)$$

This small change in the isomer shift can be seen to be related to the lattice

dynamics of a system and is relevant in interpreting very small differences in isomer shift.

(c) Quadrupole Interactions

Previously the nucleus has been assumed to be spherical and the charge distribution to be uniform, but this need not be the case. The non-uniform charge distribution may be represented by a sum of potentials of the multipoles into which the distribution may be divided. The electric dipole moment or higher odd dipoles do not exist on the grounds of symmetry. The electric quadrupole moment exists and is the most important term as it shows the strongest hyperfine interaction. The electric quadrupole moment, eQ interacts with an electric field gradient (E.F.G.) outside the nucleus having the effect of splitting the nuclear energy levels but not altering the centre of gravity of the spectrum. If Q is positive the nucleus is cigar shaped or oblate, if Q is negative the nucleus is pancake shaped or prolate.

The electric quadrupole interaction may be expressed in terms of the quadrupole Hamiltonian which takes the general form

$$H(E2) = \hat{Q} \cdot (\nabla E) \quad (1.36)$$

where \hat{Q} is the operator of the electric quadrupole moment and $(\nabla\hat{E})$ is the tensor operator. The E.F.G. is represented by a second rank tensor and is the second derivative of the potential, V . The E.F.G. can be written as:

$$\text{E.F.G.} = - \begin{pmatrix} V_{xx} & V_{xy} & V_{xz} \\ V_{yx} & V_{yy} & V_{yz} \\ V_{zx} & V_{zy} & V_{zz} \end{pmatrix} \quad (1.37)$$

$$\text{where } V_{ij} = \frac{\delta^2 V}{\delta i \delta j} \quad i, j = x, y, z.$$

this can be simplified by assuming "principal axes" such that

$|V_{zz}| \gg |V_{yy}| \gg |V_{xx}|$ leaving only the diagonal elements which are themselves related as Laplace's equation requires this tensor to be traceless so that

$$V_{xx} + V_{yy} + V_{zz} = 0 \quad (1.38)$$

leaving only two independent parameters V_{zz} and η where

$$\eta = \frac{V_{xx} - V_{yy}}{V_{zz}} \quad (1.39)$$

the choice of the principal axes means that

$$0 \leq \eta < 1$$

The quantity η is known as the asymmetry parameter. The E.F.G. has two main contributors, the lattice and the valence contributions. The electrons

around the Mossbauer nucleus need not lie symmetrically distributed in their orbitals, if the symmetry is lower than cubic then this gives rise to the valence contribution of the E.F.G. The p and d electrons contribute to this but the s-electrons, since their distribution is spherical, do not. A negligible contribution comes from the f-electrons since they are rarely involved in bonding remaining as a 'quasi-degenerate' core hence remain unsplit. The lattice contribution arises from charges on the surrounding ions in a lattice interacting with the nucleus. Putting $\eta = 0$, which is the simplest case, a general form of the quadrupole q is

$$q = (1 - \sigma_{\infty})q_{\text{lattice}} + (1 - R)q_{\text{valence}} \quad (1.40)$$

where R and σ_{∞} are the Sternheimer anti-shielding factors³² which take into account the polarization of the inner electrons which may magnify the effect of q_{lattice} or q_{valence} . The interaction between the nucleus of nuclear spin, I and quadrupole moment, Q and an E.F.G. may be expressed by the Hamiltonian³³.

$$H(E2) = \frac{e Q V_{zz}}{4 I(2I-1)} \left[3\hat{I}_z^2 - \hat{I}^2 + \eta (\hat{I}_x^2 + \hat{I}_y^2) / 2 \right] \quad (1.41)$$

\hat{I} is the nuclear spin operator

$$\hat{I}^2 = \hat{I}_x^2 + \hat{I}_y^2 + \hat{I}_z^2$$

\hat{I}_x , \hat{I}_y , \hat{I}_z are the nuclear component spin component operators. The eigen

values are

$$E_Q = \frac{e Q V_{zz}}{4 I(2I-1)} \left[3m_I^2 - I(I+1) \right] \left(I + \eta/3 \right)^{\frac{1}{2}} \quad (1.42)$$

m_I is the nuclear magnetic spin quantum number. The equation reveals that a nucleus with $I > \frac{1}{2}$ will split into $2I + 1$ degenerate states, $|I, \pm m_I\rangle$ without shifting the centre of gravity of the spectrum. The quadrupole splitting gives useful information on the environment of the Mössbauer nucleus such as bond properties (ie hybridization), symmetry and electronic structure.

The 21.6 KeV transition in ^{151}Eu goes from the $I = 7/2$ excited state to the $I = 5/2$ ground state leading to the spectrum being split into eight lines, the intensities of which are given by the Clebsh Gordon³⁴ or Wigner coefficients. There is no valence electron contribution to the E.F.G. in europium for either Eu(II) or Eu(III) as the electronic ground states of the $4f^7$ and $4f^6$ configurations are 7F_0 and $^8S_{7/2}$ which do not produce a contribution. The only contribution to a quadrupole moment is from the lattice which is small resulting in a broadening of the peak rather than the resolution of eight lines. A small quadrupole interaction together with a large number of lines means that quantitative information is difficult to obtain; this has, nevertheless, been done by Gibb³⁵ on orthorhombic perovskites. Dulaney and Clifford³⁶ have studied the line widths of ^{151}Eu Mossbauer spectra in order to obtain a more monochromatic source; this was an attempt to reduce the quadrupole splitting. The quadrupole interaction remains of mainly qualitative use in ^{151}Eu Mossbauer spectroscopy.

(d) Magnetic Hyperfine Interactions

A nucleus with a non-zero spin possesses a magnetic dipole moment, this dipole gives rise to a magnetic field in its vicinity and with this field the magnetic moments of the electrons interact. The effect may be described by the Hamiltonian

$$\mathcal{H} = -\hat{\mu} \cdot \hat{H} = -g_N \mu_N \hat{I} \cdot \hat{H} \quad (1.43)$$

and has the well-known eigen values

$$E = -\mu H m_I / I = -g_N \mu_N H m_I \quad (1.44)$$

where μ is the magnetic dipole moment

$$\mu_N \text{ is the nuclear magneton} = \frac{e\hbar}{2Mc}$$

(M is the mass of the nucleus)

g_N is the nuclear g factor

H is the magnetic field at the nucleus.

The magnetic field at the nucleus can originate from several sources, a general expression may be written:

$$H = H_0 - DM + \frac{4\pi}{3} M + H_S + H_L + H_D$$

H_0 is the field generated by an external magnet.

$-DM$ is the diamagnetic field

$\frac{4}{3}\pi M$ is the Lorentz field (the coefficient is for cubic symmetry)

H_S is the Fermi contact term arising from the interaction of the nucleus with an imbalance in s-electron spin density at the nucleus.

$$H_S = - \left(\frac{16\pi}{3} \right) \mu_B \sum_i S_i^z \delta(r_i)$$

μ_B is the Bohr magneton

r_i is the radial coordinate of the i^{th} electron.

H_L is the orbital angular momentum term. (If the orbital magnetic moment of the parent atom is non-zero then this will give a contribution.)

H_D arises from the dipolar interaction of the nucleus with the spin moment of the atom.

The sign of the internal magnetic field can be determined by the application of an external magnetic field altering the effective field at the nucleus to $H + H_0$. The external field may be applied parallel or antiparallel to H . This method was described by Hanna et al³⁷.

The effect of the magnetic hyperfine interaction is to split the nuclear state into $2I + 1$ non-degenerate, equally spaced substates $|I, m_I\rangle$ which are characterized by the size and magnitude of the nuclear magnetic spin quantum number m_I . The transitions between states as in Mössbauer spectroscopy can be found from the selection rules, $\Delta I = 1$ and $\Delta m = 0, \pm 1$ the intensities are again found from the Clebsch-Gordon coefficients.

Magnetic hyperfine splitting in ^{151}Eu metal was first observed at 4.2K in 1963³⁸ confirming $I = 7/2$ for the excited state and $I = 5/2$ for the nuclear ground state. In all, eighteen transitions are observed but they are not usually resolved as the spectral lines will overlap with each other.

1.5 Aims and Objectives of the work presented in this thesis.

The Mössbauer effect is a very versatile technique enabling small changes in the electronic environment of the Mössbauer nucleus to be observed on a microscopic scale. The information obtained from Mössbauer spectra concerns individual species rather than averaged or bulk properties; it is this feature which has proved useful in the work to be presented in this thesis.

Chapter four describes the work performed to determine the various stages in the thermal decomposition of fully hydrated europium (III) chloride and europium (III) bromide. The decomposition of the europium halide hydrates are of interest in the preparation of the anhydrous europium (III) halides reported in chapter three. There are some claims in the literature that both anhydrous europium (III) chloride and anhydrous europium (III) bromide are intermediate species formed in the thermal decomposition of the relevant europium halide hydrate. The lack of success in preparing the anhydrous europium (III) halides by this method in our laboratory coupled with disagreement found in the literature concerning the intermediate species formed led to the undertaking of the present study. The aims of this study are to follow the thermal decomposition reactions of hydrated europium (III) chloride and europium (III) bromide, to characterize the intermediate species formed thus determining whether the anhydrous europium (III) halides do occur as intermediate species.

Chapter five provides an account of an extension of the investigations carried out by Ball³⁹ and Jenden⁴⁰ on electron hopping in europium (III) chloride. Europium (III) chloride undergoes a thermal decomposition reaction:



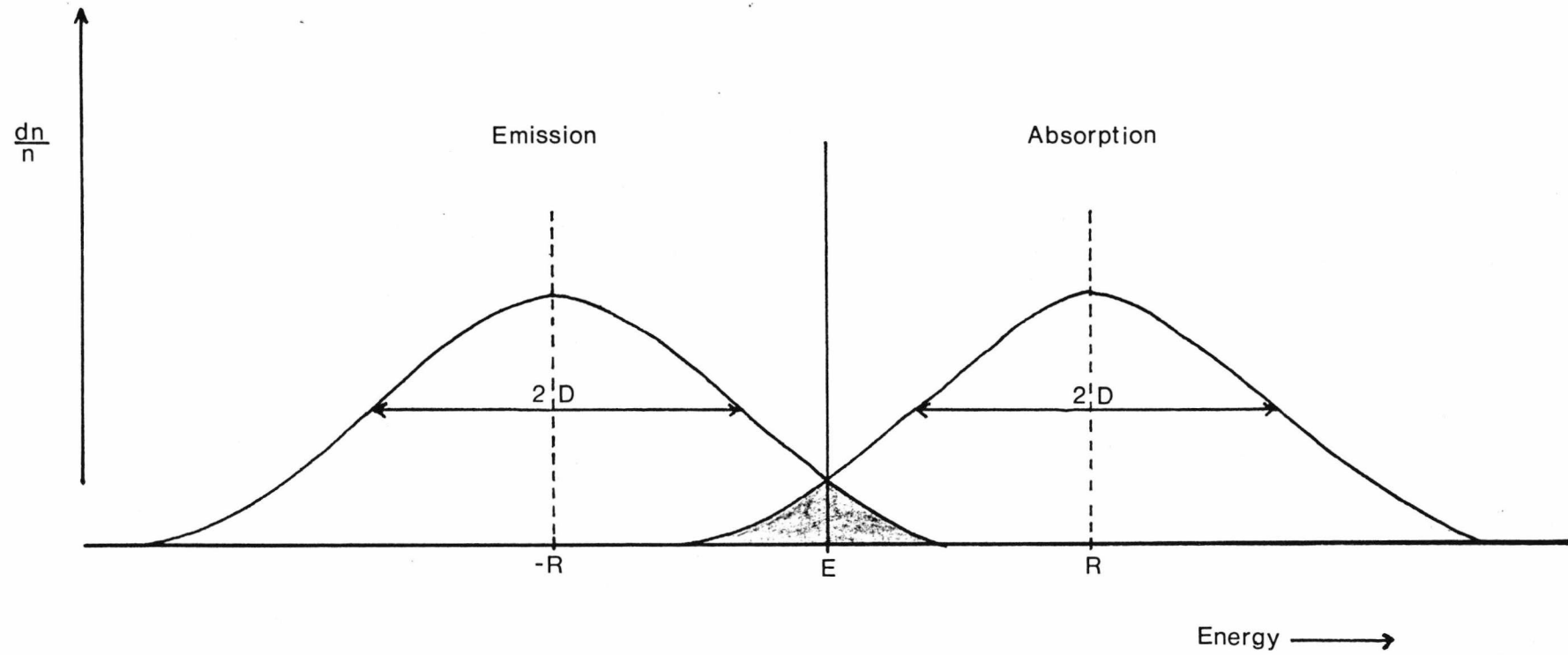
In the initial stages of the reaction a non-stoichiometric phase, slightly deficient in chlorine is formed. Both Eu(III) and Eu(II) exist together within this phase. Temperature dependent Mössbauer spectra were observed for non-stoichiometric europium chloride phases similar to those observed for Eu_3S_4 . The oxidation states Eu(III) and Eu(II) both exist in Eu_3S_4 in the ratios 2:1 respectively. The extra electron from the Eu (II) is considered to be itinerant and to "hop" to adjacent Eu(III) sites. The temperature dependence of the Mössbauer spectra can be ascribed to the temperature dependence of the relaxation time of the hopping electron. Thus an activation energy can be obtained. Such an activation energy has been found for non-stoichiometric europium (III) chloride⁴⁰. The activation energy can also be found from electrical conductivity measurements and the present study sought to corroborate the previously found activation energy with electrical conductivity measurements. An extension of the study to a second europium halide non-stoichiometric phase will allow further investigation of the mechanism of electron hopping. From the conditions for observing electron hopping in non-stoichiometric phases³⁹ anhydrous europium(III) fluoride was not considered a good example due to the high decomposition temperature and anhydrous europium(III) iodide is not known to exist⁴⁰. However, anhydrous europium(III) bromide is known to exist and is expected to decompose at a lower temperature than the corresponding chloride so

making it a suitable example for further study. The temperature dependence of the electrical conductivity and the Mössbauer spectra will be studied so that an activation energy for electron hopping may be found and comparisons between the two systems be made.

Chapter six describes an initial study of europium-mercury intermetallic compounds. Little information exists on this system although europium has been separated from lanthanide mixtures by electrolysis using mercury as a cathode. The europium forms an amalgam with the mercury. Some studies of rare earth intermetallic compounds published in the literature have included europium-mercury systems and the structures of various compounds have been determined. From the crystal structure data, the unit cell dimensions of intermetallic compounds containing europium and ytterbium suggest these elements exist with a divalent ionic core. Very little is known of the chemical and physical nature of the europium-mercury system. The aim of the present study is to determine the nature of europium-mercury systems using the general observations of Hume-Rothery and others as a guideline. In addition Mössbauer spectroscopy will allow the electronic environment of the europium nuclei to be studied and the effect of the mercury on it may be observed.

Figure 1.1

The Overlap between Energy Distributions



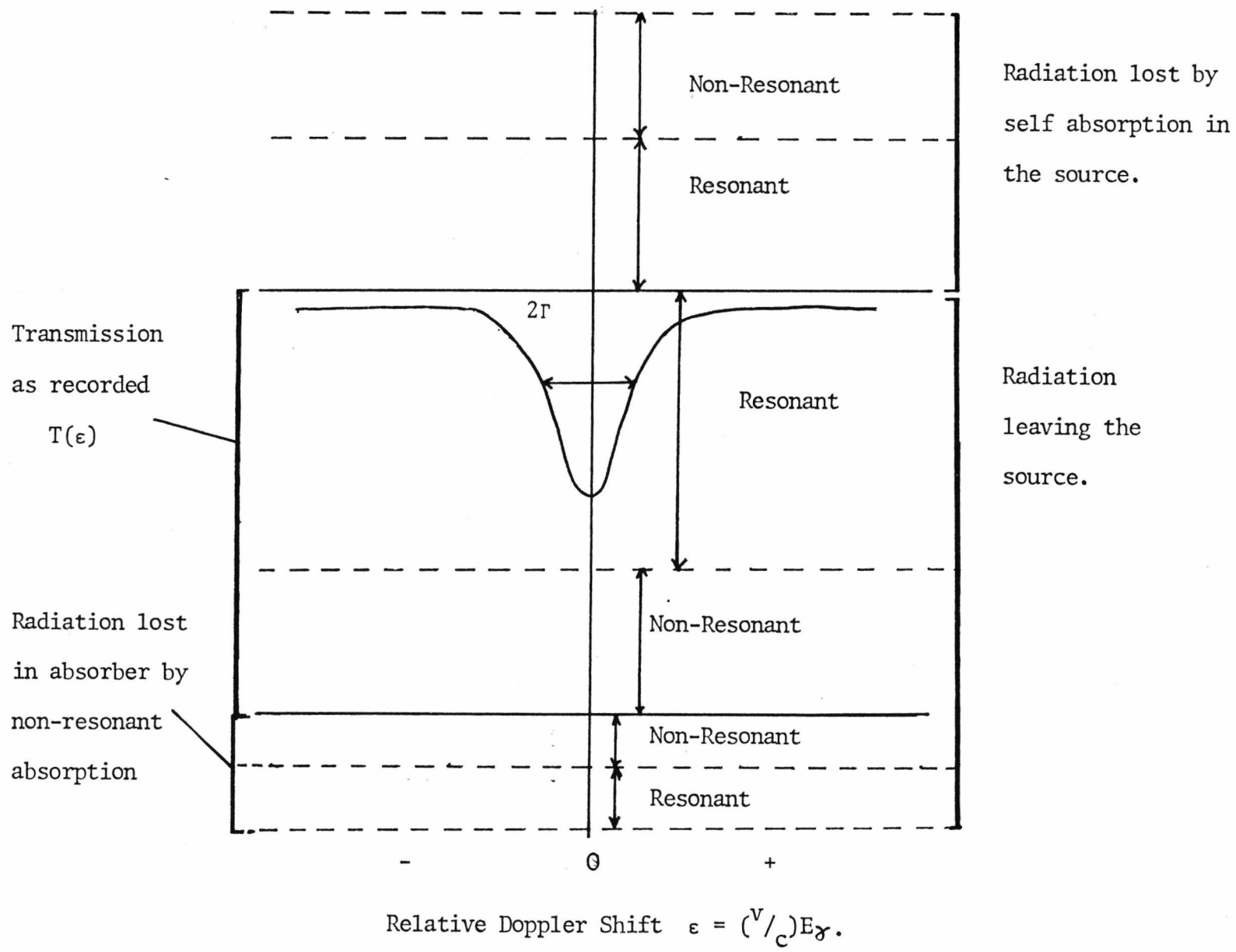
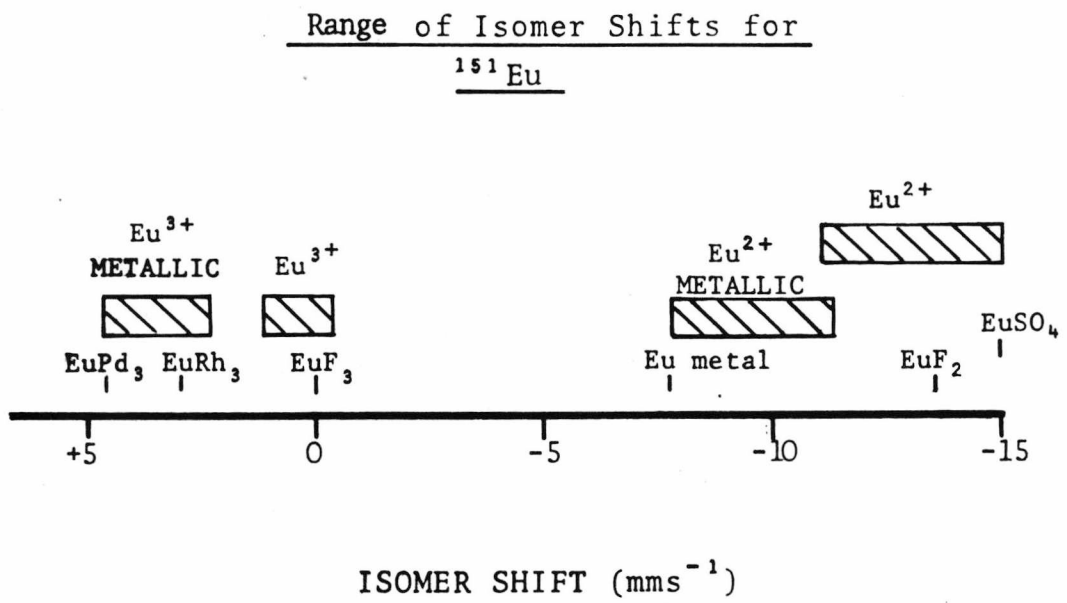


Figure 1.2 A Mossbauer transmission spectrum

Figure 1.3



Chapter OneReferences

1. R.L. Mössbauer, Z. Physik, 1958, 151 124.
2. R.L. Mössbauer, Naturwissenschaften, 1958, 45, 538.
3. R.L. Mössbauer, Z. Naturforsch, 1954, 14A, 211.
4. Lord Rayleigh, 'The Theory of Sound', Reprinted by Dover Press, New York, 1894.
5. R.W. Wood, Physical Optics, McMillan Press, New York, 1939.
6. W. Kuhn, Phil. Mag, 1929, 8, 625
7. O. Kistner and A.W. Sunyar , Phys. Rev. Lett, 1960, 4, 229.
8. P.B. Moon, Proc, Phys, Soc., 1950, 63, 1189.
9. H.J. Lipkin, Ann. Phys., 1960, 9, 194.
10. W.E. Lamb Jr, Phys. Rev., 1939, 55, 190.
11. W.M. Visscher, Ann. Phys., 1960, 9, 194.
12. W.E. Lamb Jr. Phys. Rev. 1936, 49, 514.
13. W.E. Kittel, 'Introduction to Solid State Physics', 5th edition, John Wiley & Sons Inc, New York, 1976.
14. G. Breit & E. Wigner, Phys Rev, 1936, 44, 519
15. S. Margulies & J.R. Ehrman, Nucl. Instr. Methods, 1961, 12, 131.
16. N.N. Greenwood & T.C. Gibb, 'Mössbauer Spectroscopy', Chapman & Hall Ltd., London, 1971.
17. L.R. Walker & G.K. Wertherim & V. Jaccarino, Phys. Rev Lett, 1961, 6, 98.
18. G.K. Wertherim, 'Mössbauer Effect Principles & Applications', 1st edition, Academic Press, New York, 1968.
19. D.A. Shirley, Rev. Mod. Phys., 1964, 36, 339.
20. T.C. Gibb, 'Principles of Mössbauer Spectroscopy', Chapman & Hall, London, 1976.
21. R.L. Cohen & G.M. Kalvins , Nucl Inst Meth, 1970, 86 209.

22. J. Burges & J. Kijowski, 'Advances in Inorg. Chem & Radio Chem', 1981, 29, 57.
23. S. Hufner, P. Kienle, D. Quitmann & P. Brix, Z. Physik, 1965, 187, 67.
24. E. Steikhele, Z. Physik, 1967, 201 331.
25. G. Gerth, P. Kienle & K. Luchner, Phys Letters, 1968, 27A, 557.
26. O. Berkooz, J. Phys and Chem Solids, 1969, 30, 76.
27. P. Brix, S. Hufner, P. Kienle & D. Quitmann. Phys Letters, 1964, 13, 140.
28. F.A. Deeney, J.A. Delaney & V.P. Ruddy, Phys.Letters, 1967, 25A, 370.
29. R.V. Pound & G.A. Rebka Jr, Phys.Rev.Lett, 1960, 4, 274.
30. B.D. Josephson, Phys.Rev.Lett, 1960, 4, 341.
31. W.G.V. Rosser, 'An Introduction to the Theory of Relativity', Butterworth, 1964, 114.
32. R.M. Sternheimer, Phys.Rev, 1950, 80, 102, Phys.Rev, 1951, 84, 244. 1963, 130, 1423.
H.M. Foley, R.M. Sternheimer & D. Tucko, Phys. Rev, 93, 734.
R.M. Sternheimer & H.M. Foley, Phys.Rev, 1956, 102, 731.
33. A.A. Abragam 'The Principles of Nuclear Magnetism', Oxford Uni Press, Clarendon Lon, 1961.
34. P.W. Atkins, 'Quanta Handbook of Concepts', Clarendon Press, Oxford, 1974.
35. T.C. Gibb, JCS Dalton, 1981, 11, 2245.
36. G.W. Dulaney & A.F. Clifford, 'Mössbauer Effect Methodology', Vol 5, Plenum Press, N.Y., 1970, P65.
37. J.J. Hanna, J. Heberle, G.J. Rerlow, R.S. Bresbon and D. Vincent, Phys.Rev.Lett, 1960, 4, 513.
38. P.H. Barrett & D.A. Shirley, Phys Rev, 1963, 131, 123.
39. J. Ball, PhD Thesis, University of Kent at Canterbury, 1978.
40. C.M. Jenden, PhD Thesis, University of Kent at Canterbury, 1980.

Chapter 2

Experimental Apparatus and Techniques.

2.1 Introduction

An outline of the apparatus used for the work described in this thesis is provided together with a description of the techniques used in the production of the results reported here. Much of the equipment used for obtaining Mössbauer spectra is explained in general terms elsewhere¹⁻³ so only a brief description is given here. The emphasis of this chapter will be placed on a description of the equipment built or adapted for use in this laboratory.

2.2 The Mössbauer Spectrometer

The Mössbauer spectrometer records the transmitted intensity of γ -rays as a function of energy. The change in energy is achieved by the use of a Doppler velocity, so the spectrometer will record the number of counts for a given Doppler velocity, this requires synchronization of the counting and the Doppler velocity drive. Figure 2.1 shows schematically how this is achieved. The Doppler velocity is provided by means of an electromechanical transducer similar to a loud speaker coil. The γ -rays transmitted through the absorber impinge upon the detector and the resulting electrical pulses are amplified. The amplified pulses are shaped and after discrimination by the single channel analyzer are sent to the multichannel analyzer (MCA). The counts are stored in the MCA in memories determined by the Doppler velocity or in effect the timing control; in this way the spectrum may be accumulated over a period of time. Each of the units will be examined in more detail.

2.3 The Multichannel Analyzer

The MCA used in this laboratory was custom built to a design prepared by Brandenburg Ltd⁴. The machine served both as a single channel analyzer and a multi channel analyzer with a total of 512 channels usually split into two subgroups of 256 in normal operation. The MCA was of modular design and consisting mainly of Harwell²⁰ 6000 units on a frame constructed by Brandenburg. The MCA was capable of operating in the dual mode ie accumulating two spectra simultaneously, by the use of buffer registers.

Before a spectrum was accumulated the S.C.A. 'windows' had to be set up. This set the energy range of interest so that unwanted γ -ray transitions could be eliminated. The window range was set up by first obtaining a pulse-height analysis from which the appropriate transitions could be indentified. The window was set to cover this region with the channel and threshold potentiometers respectively. To accumulate a spectrum the MCA was put into the multiscalar mode to scan the transmission through the absorber over the velocity range set by the waveform generator. Accumulation was monitored on a cathode ray oscilloscope.

Once the spectrum had accumulated the information was read out in the form of punch tape using an ASR33 teletype. The paper tape was the input for the computer necessary for the analysis of the data.

2.4 The Velocity generator and Transducer.

The energy modulation required for the Mössbauer spectrum has been provided in a number of ways⁵, the most convenient being the electro-mechanical transducer. The transducer operates in the same way as a loud speaker with the source attached to a drive rod which is connected to the transducer. A suitable oscillating voltage is supplied to the drive coil causing oscillatory motion of the drive rod. This motion is monitored by a second coil, the "velocity coil", the resulting induced current is monitored and forms part of a feedback loop allowing a high degree of linearity during the velocity sweep.

The wave form supplied to the transducer is generated in the form of an assymmetric double ramp or sawtooth; other types of wave form can be used such as a symmetrical double ramp, or sine wave. The sawtooth wave form gives a constant acceleration over about 80% of the sweep. The wave form is the motion of the source hence the velocity is synchronized with the counting so that each velocity corresponds to one of the 256 channels in the MCA. The design of the waveform generator and synchronization was based on that of Cranshaw⁶ and was supplied by 20th Century electronics⁷. It comprised of a servo amplifier, velocity attenuator (so that the total energy sweep could be varied), and a dual channel wave form generator. Duplication of the waveform generator was necessary so that the dual mode of the MCA could be utilised. Recent improvements in the design of the transducer equipment have been reported by Kanteleit at the Cracow Mössbauer conference⁸.

2.5 Detectors.

Two types of detector were used in the course of the work described here, a NaI/Tl scintillation counter for the detection of the 21.6KeV γ -ray of ^{151}Eu and a proportional counter for the detection of the 14.4 KeV γ -ray of ^{57}Fe used for calibration purposes.

The resolution for a scintillation counter decreases with decreasing gamma ray energy, however, the efficiency is high. Such counters can only be used if the back ground radiation is low and there are no other x-ray or γ -ray lines close in energy to the Mössbauer transition under study. Fortunately for ^{151}Eu this is the case. The scintillation counter consisted of a 1mm thick sodium iodide disc doped with thalium which becomes luminescent in a γ -ray flux. The luminescent light is amplified by a photo amplifier tube; the resultant electrical pulses are proportional to the γ -ray flux.

The proportional counter used for the detection of the 14.4 KeV γ -rays of ^{57}Fe was purpose built by Harwell²⁰. A proportional counter will give a higher resolution at the expense of a lower efficiency than the scintillation counter but this is necessary in the case of ^{57}Fe . The counter functions by the ionizing effect of γ -rays on the gas filling, in this case xenon. The gas filling includes a quenching gas such as methane in this case about 10% of the mixture is methane.

In addition to the counters mentioned there are semiconductor detectors in which γ -rays cause electrons to be excited into the conduction band and the resulting current can be measured. Usually lithium doped germanium is used. However, the sensitivity is poor and the device requires to be kept at liquid nitrogen temperatures, otherwise permanent damage will result.

The electronic modules in the counting circuit consist of the relevant detector, a preamplifier with power supply (Harwell 2000 series) a main pulse amplifier and single channel analyzer (Harwell 6000 series incorporated in the MCA).

2.6 Sources.

Two sources were used in the course of this work, they contained either ^{57}Fe or ^{151}Eu . The former was employed in the calibration of the spectrometer using the magnetic hyperfine splitting to calibrate the velocity scale. The latter was used in the remainder of the work. The source employed for Mössbauer spectroscopy ideally will give rise to only one transition (ie. without hyperfine splitting), will have a high recoil free fraction and have a well-known composition. Population of the excited spin state required should be efficient allowing a relatively long lived precursor. Precursors emitting α -radiation should be avoided where possible as radiation damage is caused to the source during this process. Energetically related x-ray and γ -ray

transitions to the transition of interest should be avoided as the discrimination against unwanted events becomes difficult. The sources used in this work were manufactured at the Radiochemical Centre, Amersham⁹.

(a) ^{57}Fe .

The source used consisted of 10mCi of ^{57}Co dispersed in a rhodium matrix. The source line width was 0.098mms^{-1} and the recoil-free fraction was 0.76. The two γ -rays which can be used are the 136.6 KeV and 14.4 KeV transitions. The former is not commonly used due to its high energy and associated problems discussed in chapter 1. The 14.4 KeV transition is the most widely used, but the internal conversion coefficient is high (approximately 9). The calibration of the spectrometer was achieved by running a spectrum of iron foil enriched in ^{57}Fe . The positions of the resultant six peaks of the spectrum are well known¹⁰ from external calibration methods¹¹. The spectrum consists of six peaks symmetrically arranged about a centre line, both in position and intensity. The intensities are in the order 3:2:1 the lowest intensities being associated with the centre peaks. The out side peaks should not be used for calibration as saturation effects will impare the accuracy of their measured position. The centre of the spectrum ($V = 0$) is the centre of gravity of the spectrum but this has an isomer shift relative to the source. The isomer shift has to be taken into account but fortunately it is known to be -0.114 mms^{-1} relative to the source.

(b) ^{151}Eu

There are two naturally occurring isotopes of europium, ^{151}Eu and ^{153}Eu , and their abundancies are approximately equal. Both have been used for Mössbauer spectroscopy. However, ^{151}Eu is more suitable in Mössbauer work as it has only one excited level giving a Mössbauer transition whereas ^{153}Eu has three. Either ^{151}Sm or ^{151}Gd can be used as precursors. The former is more convenient and economical as the latter has a much shorter half life. The source used in this laboratory consisted of 50mCi ^{151}Sm in a europium(III) fluoride lattice. The full width at half height is given as 2.2mms^{-1} and the isomer shift relative to anhydrous EuF_3 is 0.122mms^{-1} . The decay schemes for the two sources are given in figure 2.2.

2.7 Sample Preparation for Mössbauer Spectroscopy

All the Mössbauer spectroscopic measurements described in this thesis were made using a transmission geometrical arrangement with the source, absorber and detector all lying on the same vertical axis. Since many of the samples were either known or thought to be air sensitive, nearly all of the preparations were carried out in a dry, argon-filled glove box. The sample holders were designed to prevent contact of the sample with the atmosphere in the transfer from the glove box to the spectrometer. The sample holder (figure 2.3) for Mössbauer spectroscopy consists of two hollowed out copper discs which surround an inner perspex holder containing the sample. The sample material is finely ground, using an agate mortar and pestle and an amount containing

approximately 10mg of europium is placed in a cylindrical depression (10mm diameter by 2.5mm deep) in the perspex holder. The sample is spread evenly and held in place by a Perspex lid (10mm dia by 0.5mm thick) and the Perspex holder is placed in a cylindrical hole in the lower copper disc. The arrangement is made gas-tight by placing an 'O' ring over the lid and this is pressed down by the top copper disc which is held in place by three brass nuts and bolts. Concentric holes in the copper discs allow the transmission of γ -rays; aluminized 'Mylar' windows are required to cover the holes to seal the assembly. Transfer of the sample is usually carried out in the glove box and the filled sample holder may then be removed and secured in the variable temperature cryostat.

2.8 The Variable Temperature Cryostat.

Most of the europium compounds encountered in the work described in this thesis were found to have low recoil free fractions at room temperature, hence Mössbauer measurements were carried out at lower temperatures. The investigation of electron hopping in non-stoichiometric anhydrous europium tribromide required spectra to be recorded at varying temperatures so a variable temperature cryostat was used for most Mössbauer measurements.

The cryostat (Figure 2.4) was supplied by 20th Century Electronics Ltd⁷ from a design by Wiedmann et al¹² and was modified by a previous worker¹³ to overcome deficiencies in its performance. The cryostat was designed to operate in the 300K to 77K range and maintained both the source and the absorber at the same temperature to reduce the second order Doppler shift. The cooling is effected by liquid nitrogen or cold nitrogen gas being pumped from the

resevoir through a series of pipes in the copper block surrounding the sample holder and source. The pipes act as a simple heat exchanger and the source and sample chamber is filled with nitrogen gas to assist heat exchange within the cryostat. The nitrogen gas escapes from the system through the pump and temperature control is achieved by controlling the flow of nitrogen by the use of an electromagnetic valve situated between the cryostat and the pump. Temperature sensors are fitted inside the copper block, they consist of one platinum resistance thermometer for temperature control, a second for external temperature measurement if required and a copper constantin thermocouple for temperature monitoring. The opening and closing of the electromagnetic valve is controlled by a temperature controller operating on the principle of an A.C. wheatstone bridge, with the platinum resistance thermometer as one of its arms. A temperature can be selected using a potentiometer and if the sample is warmer than the selected temperature then the electromagnetic valve opens and the nitrogen cools the sample. Originally heaters were fitted in the copper block to aid temperature control, these became unserviceable but were found to be unnecessary and so were not replaced. The original temperature controller supplied by 20th Century electronics was later replaced by a Eurotherm¹⁴ 070,071 which operates in the same way. Thermal insulation is provided by means of a vacuum jacket which is evacuated continuously throughout the operation of the cryostat.

2.9 The Glove Box.

As previously mentioned, most of the samples were sensitive to the atmosphere, necessitating the use of a reliable glove box.

The box itself was supplied by Lintott Engineering Ltd¹⁵, and the system was built by previous workers in these laboratories. (Figure 2.5). The box is of stainless steel and is approximately 100cm long by 80cm by 80cm with large windows at the front at top. Glove parts holding the neoprene gloves are situated on the front window; these can be sealed by removable doors when not in use to prevent water diffusing through the gloves. A large mild steel exchange chamber (15cm dia by 38cm long) is attached to one end with a door between the glove box and chamber and a second at the end of the chamber. The doors are made gas tight with 'O' ring seals. The glove box contains argon dried using molecular sieve (4Å) and phosphorus pentoxide; oxygen is removed from the argon by running the gas over hot copper turnings in an oven between the argon cylinder and the glove box. Objects to be transferred to the glove box are placed in one of the two exchange chambers (an additional small chamber (5cm dia x 15cm) for small objects is included) and the outer door sealed. Argon is admitted to the glove box from the cylinder through the heated tube containing copper turnings and a tube containing molecular sieve. The exchange chamber is evacuated and then flushed with argon from the glove box by means of a two way tap. The exchange chamber is flushed three times before the inner door is opened and the objects transferred. Using the glove box as a reservoir in this way ensures that the argon is regularly circulated and replaced. The atmosphere inside the glove box is monitored by a Shaw hygrometer and the water content is typically in the region of 3ppm to 10ppm during operation.

2.10. Electrical Conductance Cell and Bridge

Electrical conductivity measurements were performed to complement the Mössbauer measurements between room temperature and 77K. The measurements were performed on pressed powder pellets typically using about 200 mg of sample. The pellet press (Figure 2.6) is made from stainless steel and can be operated by hand or tightened with the aid of a spanner inside the glove box. The press is assembled excluding the top barrel and disc, the finely ground sample is poured onto the bottom disc with the aid of an aluminium funnel. The top disc is placed polished face downwards on top of the sample and the top barrel is screwed tightly in place. The bottom barrel is then removed and the top barrel screwed down, thus pushing the pellet out of the press. The pellet is then placed between the platinum electrodes of the conductance cell.

The conductance cell is based on a design by Bransky et al¹⁶ and consists of two mutually insulated copper rods supporting the sample surrounded by a stainless steel outer jacket. (Figure 2.7). The outer jacket is continuously evacuated, connection between the vacuum system and the cell being made by a ground glass joint. The cell may be isolated from the atmosphere by means of a ground glass tap between the glass to metal seal and the ground glass socket. The sample is held between two 15mm platinum foil discs held on copper supports. The top support is sprung to ensure a constant pressure of the electrodes on the sample. Copper-constantin thermocouples are situated in the copper supports immediately above and below the sample and the conductivity leads are attached to each of the copper rods. All electrical leads exit from the cell

through the vacuum outlet and through the glass tube by tungsten rods sealed into the glass. The cell is supported by two wooden rods to provide electrical insulation (ie a floating earth) in a Dewar filled with the cooling agent. Various cooling agents consisting of an organic liquid, ie carbon tetrachloride or chloroform, mixed with liquid nitrogen to form a slush bath are employed. For the lowest part of the temperature range, liquid nitrogen alone is used as the cooling agent. The electrical conductance is measured using an A.C. bridge, either a WayneKerr B 221 or B 641 at a frequency of 1592 Hz. The pellets used were 9mm diameter and had (typically) a thickness of between 1 and 2 mm.

2.11 Data Handling Techniques

(a) Mössbauer Data

The contents of each of the 256 channels of the MCA were read out in the form of paper tape. The information contained therein was transferred to disc file on the I.C.L. 2960 computer at the University of Kent. The data files were edited at Canterbury and run on a least squares spectral curve fitting program¹⁷. The programs were run at the University of London Computing Centre on a CDC 7600 machine through a G.P.O. link.

The fitting program could fit up to sixteen strongly overlapping lines to either Lorentzian or Gaussian line-shapes. The program relied on a least squares fitting routine, the function to be fitted $f(x,p)$ has the form:

$$f(x,p) = P_{L+1} + \sum_{j=3m-2}^L F(p_j, p_{j+1}, p_{j+2}, x)$$

P_{L+1} represents the background

p_j represents the centroid

p_{j+1} represents the full height

p_{j+2} represents the full width at half height of

the m^{th} line.

The function F has the form

1) for a Gaussian

$$F(p_j, p_{j+1}, p_{j+2}, x) = p_{j+1} \exp \left\{ -4(\ln 2) \left(\frac{x - p_j}{p_{j+2}} \right)^2 \right\}$$

2) for a Lorentzian.

$$F(p_j, p_{j+1}, p_{j+2}, x) = p_{j+1} \left\{ 4 \left(\frac{x - p_j}{p_{j+2}} \right) + 1 \right\}^{-1}$$

The quantity to be minimised is the weighted sum of the squares:

$$\chi^2 = \sum_{i=1}^N W_i [y_i - f(x_i, P)]^2$$

using the condition for a minimum:

$$\frac{\delta \chi^2}{\delta P_j} = 0 = -2 \sum_i^N W_i [y_i - f(x_i, P)] \left(\frac{\delta f}{\delta P_j} \right)_{x=x_i}$$

Initial estimates are made for the parameters, P_j^0 , so that $p_j = P_j^0 + \delta_j$, so that δ_j is the correction. The function $f(x_i, p)$ is expanded by a Taylor series to obtain a set of equations for the correction δ_j

$$0 = \sum_i W_i (y_i - f_i - \sum_r \delta_r f_i^r) f_i^j$$

where $f_i = f(x_i, p^0)$

$$f_i^j = \left(\frac{\delta f}{\delta P_j} \right)_{\substack{x=x_i \\ p=p^0}}$$

writing the equation as

$$0 = \underline{d} - \underline{A}\delta \text{ or } \delta = \underline{C}d$$

Where A is defined as the matrix

$$A_{jr} = \sum_i W_i f_i^j f_i^r$$

and the vector \underline{d} as:

$$d_j = \sum_i W_i (y_i - f_i^j) f_i^j$$

The matrix C is known as the variance-covariance matrix and is the inverse matrix \underline{A} .

This equation provides an iterative formula for determining the correction δ_j to the initial estimates P_j^0 of the parameters. Linear constraints are incorporated into the theory by introducing a constrained covariance matrix. It is these constraints which enable the spectra to be fitted to real physical situations such as magnetic hyperfine spectra; by choosing the constraints to hold a number of parameters in a fixed relationship to one another as determined by a theoretical model.

The fitted data is then plotted together with the experimental data using the G-PLOT package on the ICL 2960. G-PLOT is a general graph plotting package enabling many types of graphical representation to be obtained.

The Mössbauer spectra obtained for the anhydrous non-stoichiometric europium (III) chloride and bromide samples were fitted additionally to a relaxation curve. A theoretical relaxation spectrum was generated from an equation derived by Wickmann¹⁸ using a simple BASIC program. The parameters for this curve were provided from the

data obtained from the fitted spectrum, plus a relaxation time τ . Spectra were generated for various values of τ , normalized to the experimental intensities and plotted with the experimental data for a comparison of the fit. The goodness of fit was judged by eye and the fit could be improved by adjusting the value of τ for each case. All the programs for generating, normalizing and the preparation of data for the theoretical fitting were written in BASIC.

(b) Conductivity Data

Plots of the logarithm to base 10 of the conductivity (σ) versus the inverse of the absolute temperature were required. The data ($\log_{10}\sigma$ and $1000/T$) were typed into the file above and plotted by the G-PLOT package using a linear least squares fitting routine. From the gradients of the graphs the activation energies were obtained.

(c) X-ray Data

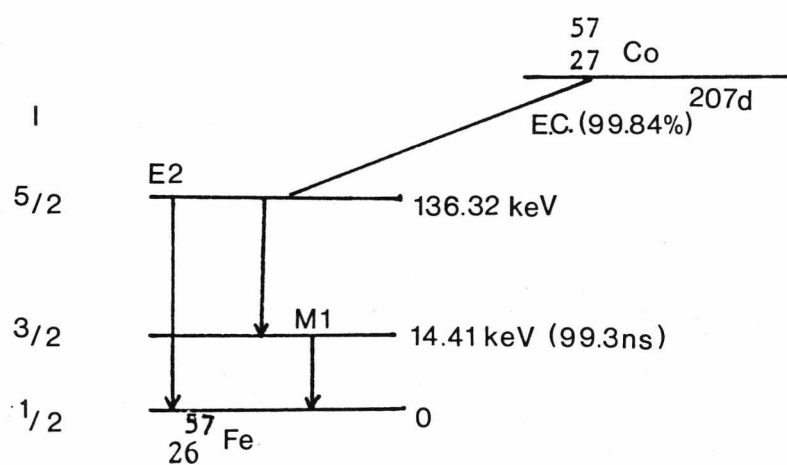
To obtain the lattice parameters from powder X-ray diffraction patterns of samples, requires each line representing an angle of reflection to be assigned to the appropriate set of Miller indices; this is not always easy. Various methods for the assignment of Miller indices exist such as Bunn Charts or computing the diffraction angles for given sets of Miller indices and comparing these to the experimental data. The latter was found to be the most suitable for the purpose of this work. A program¹⁹ is available on the CDC 7600 at the University of London Computing Centre. It consists of two parts, namely "Lazy" to decode and prepare the data for "Pulverix" which calculates the powder pattern. The program requires the user to provide the approximate cell parameters, space

group and special positions for the atoms in the cell; using a data base it will give the diffraction angle and associated data, the intensity, structure factor, real and imaginary parts of the structure factor, phase angle, multiplicity of the line and the Lorentz-polarization factor for a given Miller index set.

Figure 2.2

Decay Schemes for the Precursor Isotopes

(a) iron-57



(b) europium -151

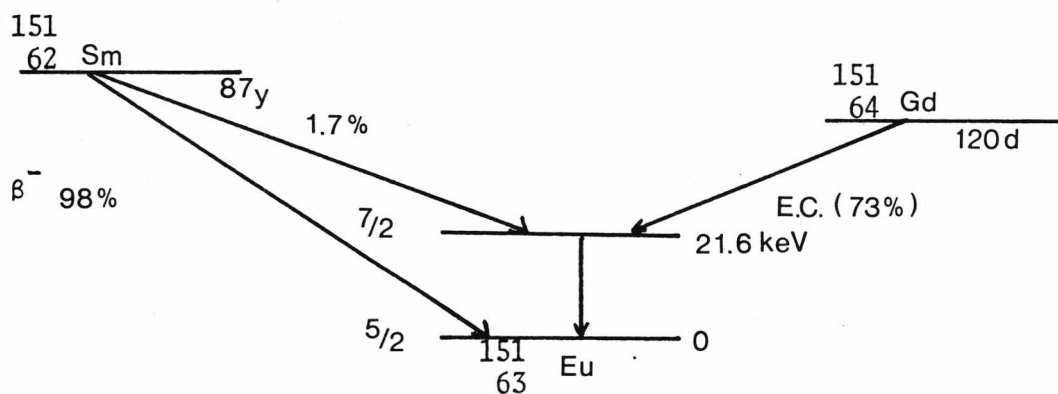


Figure 2.3

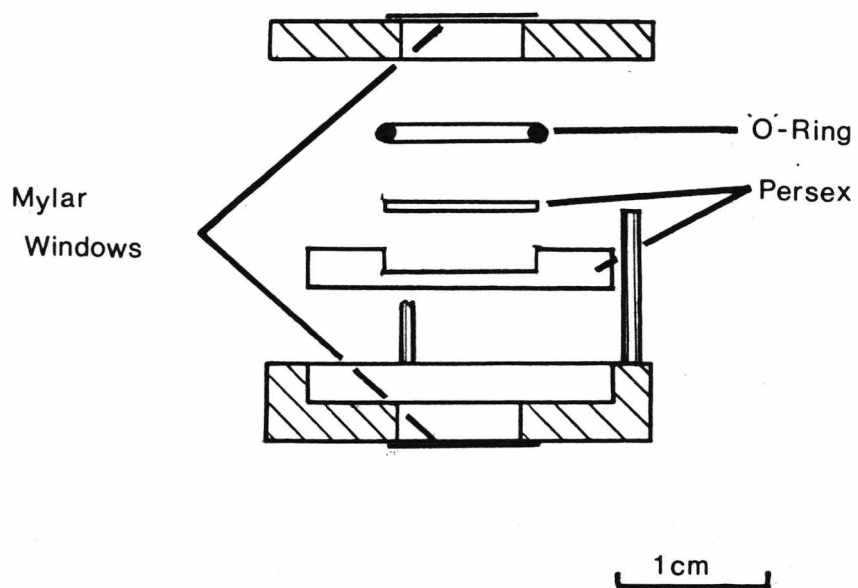
Sample Holder for Mössbauer Spectroscopy

Figure 2.4 The Variable Temperature Cryostat

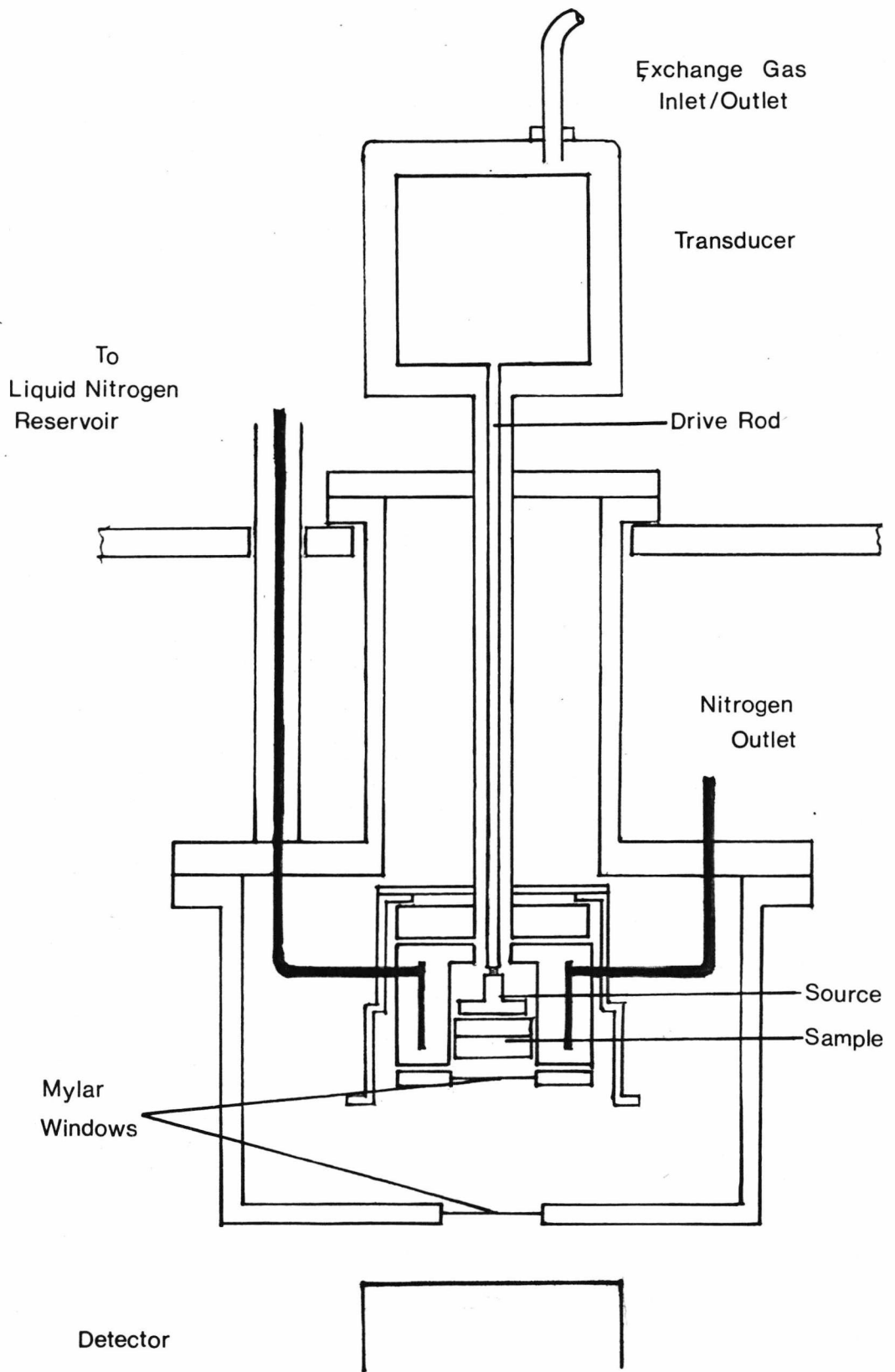


Figure 2.5

The Glove Box System

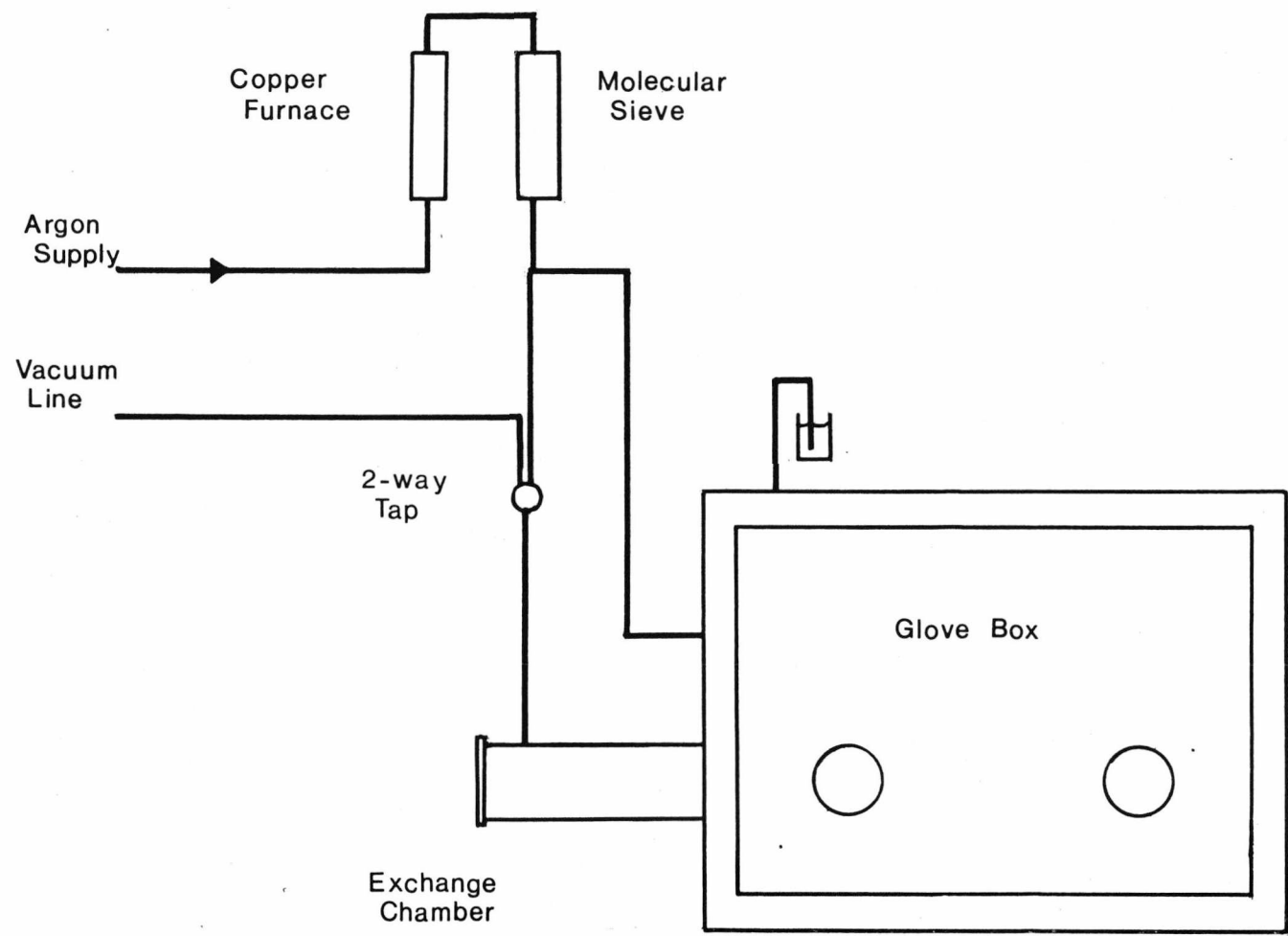


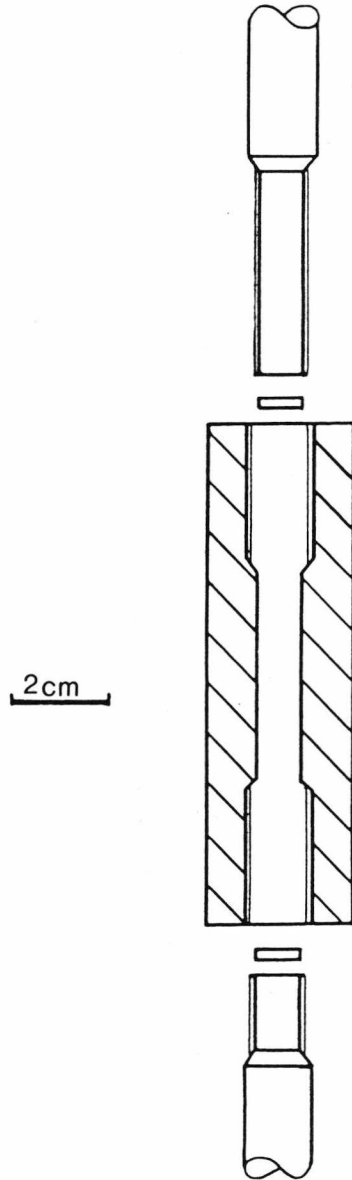
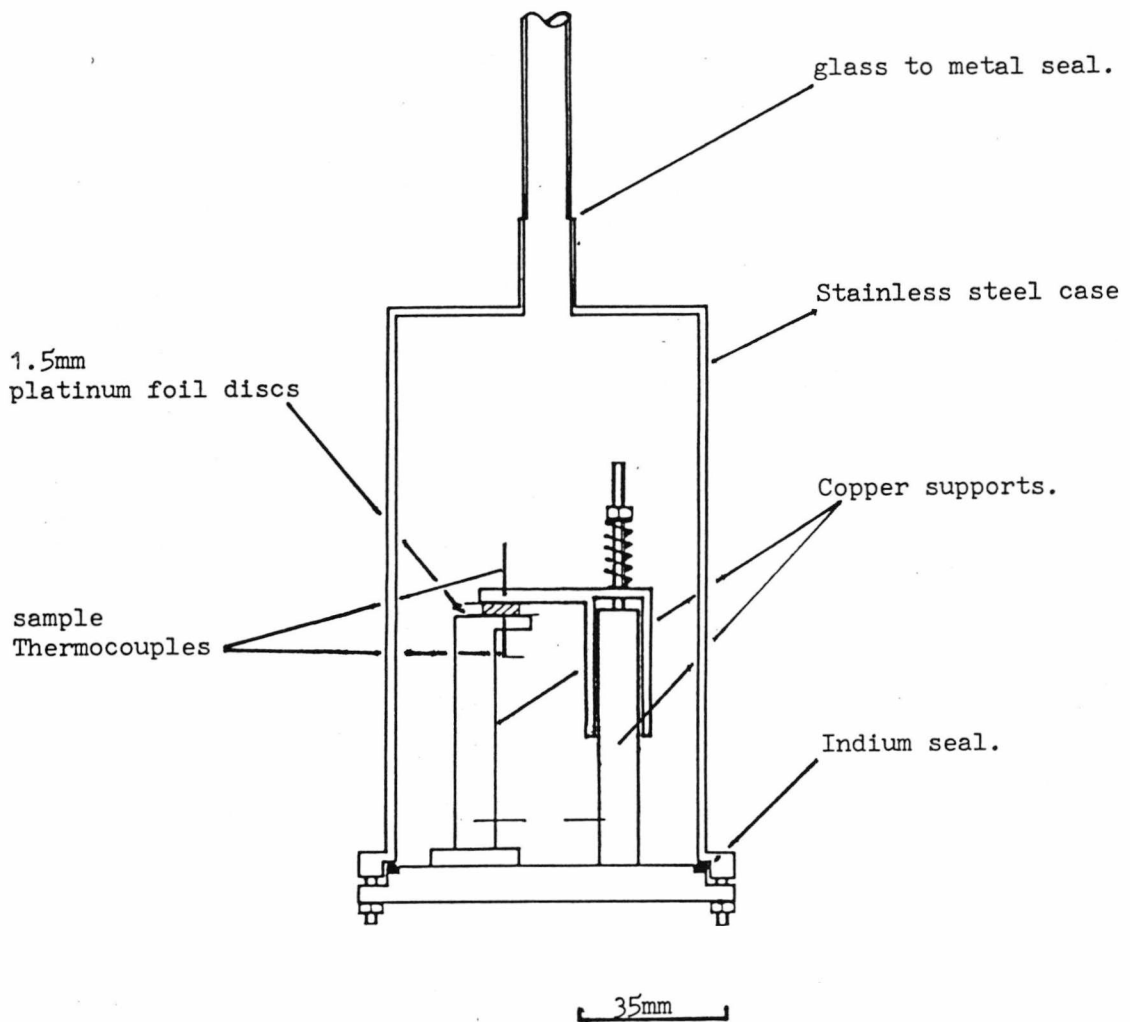
Figure 2.6The Pellet Press

Figure 2.7Variable Temperature Conductivity Cell

Chapter 2References

1. N.N. Greenwood and T.C. Gibb, 'Mössbauer Spectroscopy', Chapman and Hall Ltd, London 1971.
2. G.K. Shenoy and F.E. Wagner (Ed.), 'Mössbauer Isomer Shifts', North Holland Publishing Co., Amsterdam, New York, Oxford, 1978.
3. V.I. Goldonski and R.H. Herber (Ed.), 'Chemical Applications of Mössbauer Spectroscopy', Academic Press, New York and London, 1968.
4. Brandenburg Ltd., 939 London Road, Thornton Heath, Surrey, CR4 6JE, England.
5. G.K. Wertheim, 'Mössbauer Effect Principles and Applications' Academic Press, New York, 1964.
6. T.E. Cranshaw, Nucl Inst. Methods, 1964, 20, 101.
7. 20th Century Electronics Ltd., King Henry's Drive, New Addington, Croydon, Surrey.
8. E. Kankeleit, Proc. Int. Conf. on Mössbauer Spectroscopy, Cracow, Poland, Vol 2, (1975).
9. The Radiochemical Centre, Lion Road, Amersham, Buckinghamshire.
10. J.G. Stevens and V.E. Stevens, 'Mössbauer Effect Data Index', Plenum, New York, 1970.
11. R. Fritz and D. Schultze, Nucl. Instr. Meth., 1963, 62, 317.

12. W. Wiedemann, W.A. Munot and D. Kullmann, *Cryogenics*, 1964, 5, 94.
13. C.M. Jenden, PhD. Thesis, University of Kent at Canterbury, 1980.
14. Eurotherm.Ltd., Faraday Close, Durrington, Worthing, Sussex, England.
15. Lintott Engineering Ltd., Horsham, Sussex, England.
16. I. Bransky, N.M. Tallan and A.Z. Hed., *J. App. Phys.* 1970, 41, 1787.
17. E. Von Meerwall, *Computer Physics Comm.* 1975, 9, 117.
18. H.H. Wickmann, 'Mössbauer Effect Methodology', Vol. 2, Plenum Press, 1966, P39.
19. K. Yvon, W. Jeitschko and E. Parthé, Laboratoire de Crystallographie aux Rayons Université de Geneve, 24, Quai Erre CH1211 Geneva 4, Switzerland.
20. Harwell Mössbauer Group, AERE, Hangar 8, Didcot, Oxon

Chapter 3

The Preparation and Characterization of the Samples for Study

3.1 Introduction

This chapter describes the preparation and characterization of the europium halide samples which are to be studied. They are:

- (i) Anhydrous europium tribromide and europium trichloride.
- (ii) Hydrated europium (III) chloride and hydrated europium(III) bromide together with their related intermediate compounds formed in the thermal decomposition reactions.
- (iii) Europium oxybromide and europium oxychloride in the same thermodecomposition studies.

3.2 The Preparations of Anhydrous Europium Tribromide and Europium Trichloride

This study mainly concerns non-stoichiometric europium tribromide. However, to complement a previous study by Jenden¹ in these laboratories, samples of anhydrous europium trichloride have been produced. It is convenient to start with the description of the preparations of anhydrous europium trichloride.

Many references to the preparation of anhydrous europium trichloride may be found; the methods they represent fall into four main types.

- (i) Direct combination of the metal with either chlorine or hydrogen chloride.
- (ii) High temperature chlorination of the oxide or other compounds of europium.

- (iii) Dehydration of the hydrated europium trichloride
- (iv) Thermal decomposition of organic compounds of europium.

The first of these methods was discarded as it was thought that surface oxidation on europium metal, which occurs readily, would lead to the unacceptable contamination of the product. In addition the purification of the chlorine gas to the standard required would prove difficult.

Z Jenden attempted to produce anhydrous europium trichloride by the chlorination of europium oxalate as described by Johnson and Mackenzie². This method was found to be unsuccessful; it is thought that the high affinity oxygen has for europium and the requirement for this strong bond to be broken is responsible. It is for this reason that preparations involving the chlorination of the oxide were discarded.

X The thermal decompositions of hydrated rare earth trichloroacetate has been reported by Mathur & Bhat³. They claimed their thermogravimetric study in air and nitrogen showed the anhydrous europium chloride to be stable up to about 1000°C. However, this is not the case and the method was discarded due to variable product composition.

A Studies on the thermal decomposition^{4,5,6} of the hydrated europium trichloride mainly show that phases approximating to anhydrous europium trichloride decompose to europium oxychloride.

An exception to this general conclusion was published by Ashcroft & Mortimer⁷ who claimed that by careful heating anhydrous europium trichloride could be produced. The small size of the sample 1-5 mg leaves doubts concerning its purity.

Taylor & Carter⁸ have described a general method of producing anhydrous rare earth halides. This method utilizes the appropriate ammonium halide which is molecularly dispersed with the hydrated rare earth halide. When the mixture is heated in vacuo the water and ammonium halide are expelled leaving the anhydrous rare earth halide. This method was adopted in the present work with a little modification, especially to the recommended heating time (8 hours) at the final temperature.

(a) Preparation of Anhydrous Europium (III) Chloride

Unless otherwise stated all reagents used were of A.R. grade from Fisons Ltd⁹.

Between 300 and 500 mg of Eu_2O_3 ¹⁰ (99.9% purity) were dissolved in 6 M HCl along with the NH_4Cl in molar ratio 1:20:10 respectively. The solution was heated to near dryness under conditions such that the temperature did not exceed 150°C to avoid forming any oxyproducts. The slurry was transferred to a silica boat and placed at the closed end of the pyrex reaction tube. The dehydration apparatus was assembled as shown in figure 3.1 and the system was evacuated to better than 1×10^{-3} torr. The temperature was raised to 80°C to remove the excess water and after one hour it was increased to 130°C and maintained at this temperature for half an hour. Then, it was increased to 320°C at the rate of 4°C

per minute; this final temperature was maintained for two hours. Samples of different stoichiometry were produced by varying the final heating temperature. Figure 3.2¹¹ shows the relationship between the stoichiometry and the sample and the final heating temperature. The product, allowed to cool slowly under vacuum, was recovered under argon in the glove box previously described. Chemical analysis showed the sample to be anhydrous trichloride slightly deficient in chlorine content (between 5 and 10%) Anhydrous europium trichloride had the appearance of a fine yellow powder which was very soluble in water, the dissolution process being noticeably exothermic.

(b) Preparation of Anhydrous Europium(III) Bromide

Published methods for the production of anhydrous rare earth trichlorides have recently been reviewed¹².

The methods for producing anhydrous europium tribromide broadly fall into the same categories as those for anhydrous europium trichloride. However, the literature on the subject is less extensive.

(i) Direct Bromination of Europium with Bromine

It might be expected that this method would not offer a simple and reliable means of making anhydrous europium tribromide allowing for the limitations previously discussed with respect to the trichloride preparation. Of all the rare earth tribromides only that of Scandium¹³ has been prepared by this method.

(ii) Conversion of the Oxide to Anhydrous europium tribromide A

The high stability of europium (III) oxide hinders the conversion of it to anhydrous europium tribromide with either bromine or hydrogen bromide gas. This preparation has been claimed by Moeller & Griffin¹⁴ to be successful when the oxide is heated in a stream of dry hydrogen bromide and bromine gas. Cullen¹⁵ has reported conversion of the carbonate by this method. A reducing agent, ie carbon may be added to the oxide and the oxide converted to the anhydrous tribromide as in the method of Moeller & Griffin. Petra et al¹⁶ have claimed success with this method. In all these methods there is a marked tendency to form oxybromide. These methods were not adopted due to problems associated with formation of this impurity.

(iii) Dehydration of hydrated europium tribromide

Few thermal decomposition studies have been performed on hydrated Lanthanide tribromides. However, in common with the hydrated trichloride, the end product is the oxyhalide rather than the anhydrous lanthanide trihalide.

Mayer & Zolatov¹⁷ suggest from their thermogravimetric study on hydrated europium tribromide that anhydrous tribromide is formed as an intermediate.

Brown et al¹⁸ have reported making anhydrous europium tribromide by careful thermal dehydration of the hydrate in a vacuum. Due to the strong possibility of contamination by europium oxybromide these methods were not adopted.

The method of Taylor & Carter⁸ was found to produce only anhydrous europium dibromide. This is not surprising since the temperature required to sublime the ammonium bromide (338°C) is higher than the decomposition temperature of europium tribromide (185°C) under vacuum. The europium dibromide formed by this method could be used as the starting material for the preparation of anhydrous europium tribromide according to the reaction $2\text{EuBr}_2 + \text{Br}_2 \rightarrow 2\text{EuBr}_3$.

The first attempt to brominate the anhydrous europium dibromide involved mixing the reactants at room temperature. The bromide was dried prior to use by means of phosphorous pentoxide from which the dried bromine could be distilled when required and condensed directly onto the sample. A

No significant bromination occurred by this method.

A variation on this method of brominisation has been described by Haschle & Eick¹⁹. In it an excess (1-2ml) of bromine are introduced to 0.3 - 0.7g of europium dibromide contained in a heavy walled quartz ampoule and the ampoule is sealed and heated for between 12-18 hours. It was found that at temperatures above 110°C this method yielded anhydrous europium tribromide to good purity. An adaptation of this method was therefore used.

The anhydrous europium dibromide was produced by a method similar to that of Taylor & Carter⁸.

Europium III oxide¹⁰ (0.7-1g) is dissolved in 48% hydrobromic acid along with ammonium bromide in the molar ratios of 1:20:10 respectively. The solution evaporated to near dryness and the slurry transferred to a silica boat which is in turn placed in the dehydration apparatus previously mentioned. (figure 1). The system is evacuated to a pressure less than 1×10^{-3} torr and the heating sequence commenced. The temperature is slowly increased to 100°C allowing excess water to be expelled. Then it is increased at a rate of 3°C per minute to a final temperature of 350°C, which is maintained for 90 minutes. The sample is allowed to cool slowly and is recovered under argon in the glove box. The authentic anhydrous europium dibromide has the appearance of a fine white powder, off white or grey samples were found, by chemical analysis to be contaminated with europium oxybromide. The anhydrous europium dibromide is found to dissolve in water with the aid of dilute nitric acid to prevent hydrolysis.

The anhydrous europium tribromide is prepared from the previously mentioned europium dibromide. Europium dibromide (0.5 - 0.7g) is placed in a medium walled pyrex ampoule under argon in the glove box. The tap attachment is fixed onto the ampoule, thus sealing the sample from the outside atmosphere. The apparatus is transferred from the glove box to the vacuum line and the bromine reservoir is attached (figure 3.3). The bromine reservoir contains a relatively large volume of previously dried bromine and phosphorous pentoxide. The bromine in the reservoir is frozen with a mixture of acetone and Cardice and

the system is evacuated to a pressure less than 1×10^{-3} torr. When a good vacuum had been achieved the tap to the reservoir is closed and the Cardice-acetone mixture removed allowing the bromine to warm up. Once the bromine has reached room temperature the reservoir and the ampoule are isolated from the vacuum line by closing tap A. The tip of the ampoule is cooled with liquid nitrogen and the tap to the reservoir slightly opened allowing the bromine to slowly distill over onto the europium dibromide.

Only enough bromine is introduced to cover the europium dibromide, the tap to the reservoir is closed and that to the vacuum line is reopened. Thus the ampoule is sealed at the constriction and placed in a mild steel container fitted with a screw top as a guard against the effects of an implosion of the contents. It is heated in an oven at 190°C for between 12 and 18 hours and then allowed to cool slowly. When required the ampoule may be broken in the glove box and transferred to the pyrex reaction tube into which it is sealed by means of the head assembly. Excess bromine is pumped off on the vacuum line. For depleted sample preparations this product is carefully heated under vacuum to a temperature of about 185°C and maintained at this temperature for one hour. The degree of depletion can be varied by changing the temperature to which the sample is heated, the relationship between the temperature and the stoichiometry is given in figure 3.4.

The sample is cooled under vacuum and recovered under argon in the glove box.

Both the stoichiometric and partially depleted anhydrous europium tribromide have the appearance of a fine rust brown coloured powder which is very soluble in water, the dissolution process being very exothermic.

No large concentration gradients were found in the samples from empirical measurements, even though they could not be annealed satisfactorily.

It is considered that, since migration of defects should be fast in these compounds, in order for electron hopping to occur, then large concentration gradients should not exist.

3.3 Preparation of Intermediate Hydrates of Europium Halides

There have been several studies of the thermal decomposition of hydrated lanthanide(III) chlorides^{4,7,20,21}. However, there is disagreement regarding the intermediate products of the decomposition. In contrast to the lanthanide chloride hydrates, only one study of the lanthanide bromide hydrates¹⁷ has been reported. In most of the previous studies the major experimental technique employed was thermogravimetric analysis and this formed the main evidence for the composition of the intermediate products with supportive data derived from the x-ray powder diffraction methods.

In the present study an attempt was made to prepare the intermediate products in large enough quantity to enable

accurate chemical analysis to be performed. Additional information on the nature of intermediate compounds was obtained from Mössbauer spectroscopy.

In both studies, the starting material was the hydrated europium trihalide.

About 1g of Europium (III)oxide was treated with a minimum volume of either 5 M hydrochloric acid or 48% hydrobromic acid and the solution carefully evaporated to near dryness. The sample was finally dried at room temperature over phosphorous pentoxide.

The hydrated europium(III) chloride or corresponding bromide were then used to make the intermediate reaction products by the same general method. About 200mg of the hydrated europium(III) halide was spread over a silica boat which was inserted into the reaction tube previously described (Section 3.2(a)). With the tube head in place the tube was flushed with nitrogen. The sample was then heated in the tubular furnace to a temperature selected from the thermogram. The temperature was maintained for 30 minutes when the sample was quenched and the tube evacuated to a pressure less than 10^{-3} τ . The sample was recovered under argon in the glove box, a chemical analysis performed and, where relevant, Mössbauer spectra run and x-ray powder diffraction patterns produced.

In addition to the intermediate reaction products previously described, the europium oxyhalides were separately prepared to aid the characterization of the intermediate decomposition products.

Both the europium oxychloride and europium oxybromide were produced by similar methods. About 500mg of the hydrated europium(III) halide hydrate was placed in the silica boat which in turn is inserted into the reaction tube as before. The tube head is placed in position and an air supply passing through a Dreschel bottle containing water is connected. The sample is heated to 500°C with a stream of water saturated air passing over it for one hour, the air supply is removed and the tube evacuated. The temperature is maintained for a further hour when the sample is allowed to cool slowly under vacuum. Once cool the sample is recovered under argon in the glove box. Both the europium oxychloride and the europium oxybromide were obtained as fine white powder, insoluble in water. Chemical analyses show the products produced by the method to be europium oxychloride and europium oxybromide of good purity.

3.4 Chemical Characterization of the Compounds

All of the compounds, with the exceptions of europium (III) chloride hexahydrate and europium(III) bromide hexahydrate, were handled under argon in the glove box. Portions (50mg) of the samples were chemically analysed for europium and halide by titration against E.D.T.A and Mercury(II) nitrate respectively.

(a) Titrimetric analysis for europium.

Here the europium is determined by a direct complexometric titration with an aqueous solution of ethylenediaminetetraacetic acid (E.D.T.A.). Lyle & Rahman²³ have reported a method using

xylene orange indicator in the pH range 5.8 to 6.4, this method was adapted for use on these compounds.

An aqueous solution of 5×10^{-3} M E.D.T.A. is prepared from the disodium salt and standardized using a standard europium solution. A 10ml aliquot of the unknown europium solution is pipetted into a 250ml conical flask and neutralized with 0.01N HNO_3 or 0.01N NaOH using bromophenol blue as the indicator. To the contents of the flask, 0.5ml of 0.01 N HNO_3 one drop of pyridine and 0.2 of sodium acetate-acetic acid buffer (200g sodium acetate in 900ml water with the pH adjusted to 4.5) are added in succession. The solution is warmed to about 60°C and between 4 and 6 drops of 0.1% xylene orange indicator in a 1:1 water ethanol mixture are added. The solution is titrated against E.D.T.A. to give a sharp red to golden colour change at the end point.

(b) Titrimetric determination of the halide ion

Bromide or chloride ions were determined using a mercurometric titration in which the sample in aqueous ethanol is titrated against mercuric nitrate at an apparent pH of 3.6 as described by White²⁴.

A solution of 5×10^{-3} M mercuric nitrate is prepared at a pH of 2.6 and is standardized against a 0.01 M solution of $\text{K}_2\text{Cr}_2\text{O}_7$.

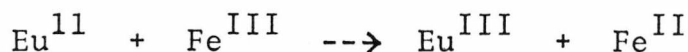
A 10 ml aliquot of the unknown halide solution is pipetted into a 250 ml conical flask and neutralized using 0.01 N HNO_3 or 0.01 N NaOH using bromophenol blue as indicator. An excess of 0.5 ml of 0.01 N HNO_3 is added together with 100 ml of absolute

ethanol and 12 drops of 0.1% diphenylcarbazone in ethanol. The solution is titrated slowly with the mercuric nitrate, swirling the flask after each addition of mercuric nitrate, to a sharp colourless to purple end point.

3.5 Spectrophotometric Determination of Europium(II) in the Presence of Europium (III)

In order to determine accurately the amount of depletion in a non-stoichiometric sample of the anhydrous europium halide system it is necessary to determine the amount of europium(II) directly.

The europium(II) determination was carried out spectrophotometrically by two methods. The first of these used the redox reaction,



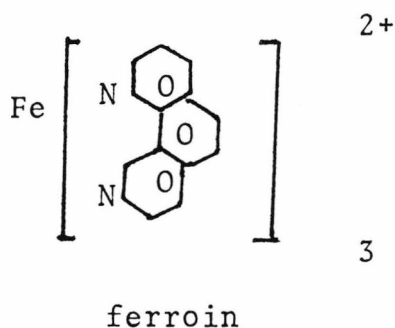
between europium (II) and excess iron(III).

The iron (II) formed gives an orange coloured complex with 1,10-phenanthroline, the absorbance of which is measured and so from it the amount of europium (II) can be found.

The second method is a selective spectrophotometric determination of europium (II) using the reduction of molybdophosphoric acid.

The method using the redox reaction between europium(II) and iron(III) is described first.

Ferric ions in a solution of ammonium ferric sulphate are reduced by the europium(II) ions present when the europium salt is dissolved in the iron solution. The iron(II) produced in this reaction forms a complex ('ferroin') with 1,10-phenanthroline.



This complex is coloured, hence a quantitative determination can be made from absorbance measurements.

Iron is chosen for the redox reaction due to its favourable half cell electrode potential relative to europium.

$$E_{\text{O}} [\text{Fe(III)}/\text{FeII}] = 0.76$$

$$E_{\text{O}} [\text{Eu(III)}/\text{EuII}] = -0.43\text{v}$$

The Nerntz equation requires that the direction of the reaction is dependent upon the activities of the species present, therefore by having a large excess of ferric ions the reaction is seen to proceed as required.

The method of analysis is an adaptation of that reported by
25
the Analytical Methods Committee of the Royal Society of Chemistry.

A calibration curve of absorbance against the amount of Fe(II) present is constructed. For this aliquots of 2,3,5,7,10 and 13 ml of standard (0.02 g/l) ammonium iron(III) sulphate were pipetted into separate 100 ml volumetric flasks.

The ammonium iron(III) sulphate solution had previously been adjusted to pH 2 using sulphuric acid. The iron(III) solution in each flask is reduced to iron(II) by the addition of 1 ml of 100 g/l ascorbic acid solution which had been freshly prepared. Each solution buffered to pH 4.5 using 20 ml of sodium acetate-acetic acid buffer. The buffer solution consisted of 200g of sodium acetate dissolved in about 900 ml of distilled water. The pH was adjusted to 4.5 using glacial acetic acid and the solution made up to one litre. After the addition of the buffer, 10 ml of 1,10-phenanthroline solution, 1 g/l, is added and each solution is made up to 100 ml with freshly boiled out doubly distilled water.

The absorbances of each solution are measured after fifteen to thirty minutes at 512 nm using a Hitachi-Perkin Elemer 139 UV-visible spectrophotometer in quartz cells of 1 cm path length. From these measurements a graph of absorbance against iron content is plotted and used for subsequent determinations of unknown amounts of iron(II). The molar absorption coefficient found from the calibration curve is $11521 \pm 230 \text{ l mole}^{-1} \text{ cm}^{-1}$ which is in agreement with Verbeck²⁶.

The determination of the amount of Eu(II) in non-stoichiometric europium halide samples could then be carried out. A weighed amount of the sample is dissolved in 10 ml of 3.30×10^{-2} M iron(III) ammonium sulphate which had previously been purged with nitrogen. The solution is transferred to a 100 ml volumetric flask where 20 ml of buffer solution and 10 ml of 1,10-phenanthroline solution are added. The solution is made up to 100 ml with freshly boiled out double distilled water and the absorbance measured after 15 minutes. Since the sample solution is not particularly stable to atmospheric oxidation, all the solutions were degased by bubbling nitrogen through them before use.

Ball¹¹, in a preliminary study, established the stability of the iron(II)-phenanthroline complex formed by the addition of europium(II) chloride to a solution of 1,10-phenanthroline and iron(III). Jenden performed two experiments to check the usefulness of this method in the presence of excess iron(III) and europium(III) ions. The experiments showed that these ions did not significantly impair quantitative performance.

Since the present work involved the determination of europium(II) in samples of europium(III) bromide, the effect of the presence of bromide ions was investigated. A standard (0.02g/l) ammonium iron(II) sulphate solution and a solution of approximately 0.015 M europium(III) bromide are prepared. Aliquots of 2,3,4,5 and 10 ml of standard iron(II) solution are pipetted into separate 50 ml volumetric flasks, 1 ml of the europium(III) bromide solution, 10 ml of buffer solution and 10 ml of 1,10-phenanthroline solution are added and the

solutions made up to 50 ml with freshly boiled out doubly distilled water. The absorbances of each of the solutions are measured and a plot of absorbance versus iron content revealed that the presence of the bromide ions does not significantly effect the determination of the iron(II).

The second method is that reported by Lyle and Zatar²⁷ in which the europium(II) reduces molybdophosphoric acid to a molybdenum blue, the absorbance of which can then be measured at 810 nm and thus the amount of Eu(II) determined. The sample containing europium(II) (0.04 - 5 mg of Eu(II)) is dissolved in 10 ml of 1 M HCl. The solution is transferred to a 100 ml volumetric flask containing 10 ml of freshly prepared molybdophosphate solution. The molybdophosphate solution is prepared by dissolving 15 g of molybdenum oxide in 100 ml of 1 M NaOH and the pH adjusted to 7 by the addition of 1 M HCl. Sodium dihydrogen phosphate dihydrate (7.5g) is added and the volume made up to 1 litre. The sample solution is left for about 40 minutes then 15 ml of 11.5 M HCl is added and the contents of the flask made up to 100 ml with distilled water. The absorbance is measured after 10 minutes using a Hitachi-Perkin Elmer 139 spectrophotometer in a glass cell of 1 cm path length at 810 nm. against a reagent blank taken through the reduction and colour development stages.

A calibration curve is constructed by measuring the absorbance of known europium(II) concentrations. Standard

europium(II) solutions are prepared by reducing known volumes of a standard europium(III) solution (0.5g Eu_2O_3 dissolved in a minimum of concentrated HCl and made up to 1 litre) in a Jones reductor²⁸. For samples containing small amounts of europium(II) (0.04 - 0.4 mg) a modified procedure can be employed. After the solution has been made up to 100 ml in the previously mentioned procedure, 10 ml of n-amyl alcohol is added. The mixture is shaken for 1 minute to partition the phosphomolybdenum blue into the alcohol phase. The alcohol phase is centrifuged to remove the entrained water and the absorbance is measured at 790 nm in a 1 cm glass cell with an amyl alcohol extract of the reagent taken through the measuring procedure as a reference. Bromide and Chloride ions do not interfere in this method up to high concentrations.

Both the methods for the determination of europium(II) have been employed. Initially the ferroin method was used until the molybdenum blue method became available. The latter is favoured since the coloured product is not susceptible to atmospheric oxidation to the same degree and the analysis is more easily performed than the previous method.

3.6 Other Analytical Techniques

A large number of the samples were subjected to analysis by the x-ray powder method. The samples for x-ray analysis were ground to a fine powder, packed into Lindemann tubes²⁹ and sealed with a hot wire inside the glove box. The

Lindemann tube was mounted in a Debye-Scherrer powder camera and irradiated for about 6 hours using CuK_α radiation from a Phillips PW 1008/80 generator. The diffraction patterns produced were of poor quality due to europium having an L absorption edge at the CuK_α line. This limited the usefulness of the method in a number of ways such as observing minority impurity phases. The lattice parameters obtained from the powder diffraction patterns could not be obtained to good precision as the lines in the region of $\theta = 90^\circ$ were not observed clearly. Hence, the associated errors³⁰ from the lines corresponding to lower angles of diffraction were higher than desired.

Infra-red spectroscopy was used to obtain information on the presence of small molecules such as water in the samples or about the halogen-europium bending and stretching frequencies in the far infra-red region. Samples for infra-red study were finely ground into a mull with dried nujol; a small amount of the mull was smeared between two cesium iodide discs under argon in the glove box. Infra-red spectra were recorded between 4000 and 200 cm^{-1} using a Perkin Elmer 683 infra-red spectrophotometer.

Figure 3.1

Apparatus used for Dehydration type Preparations

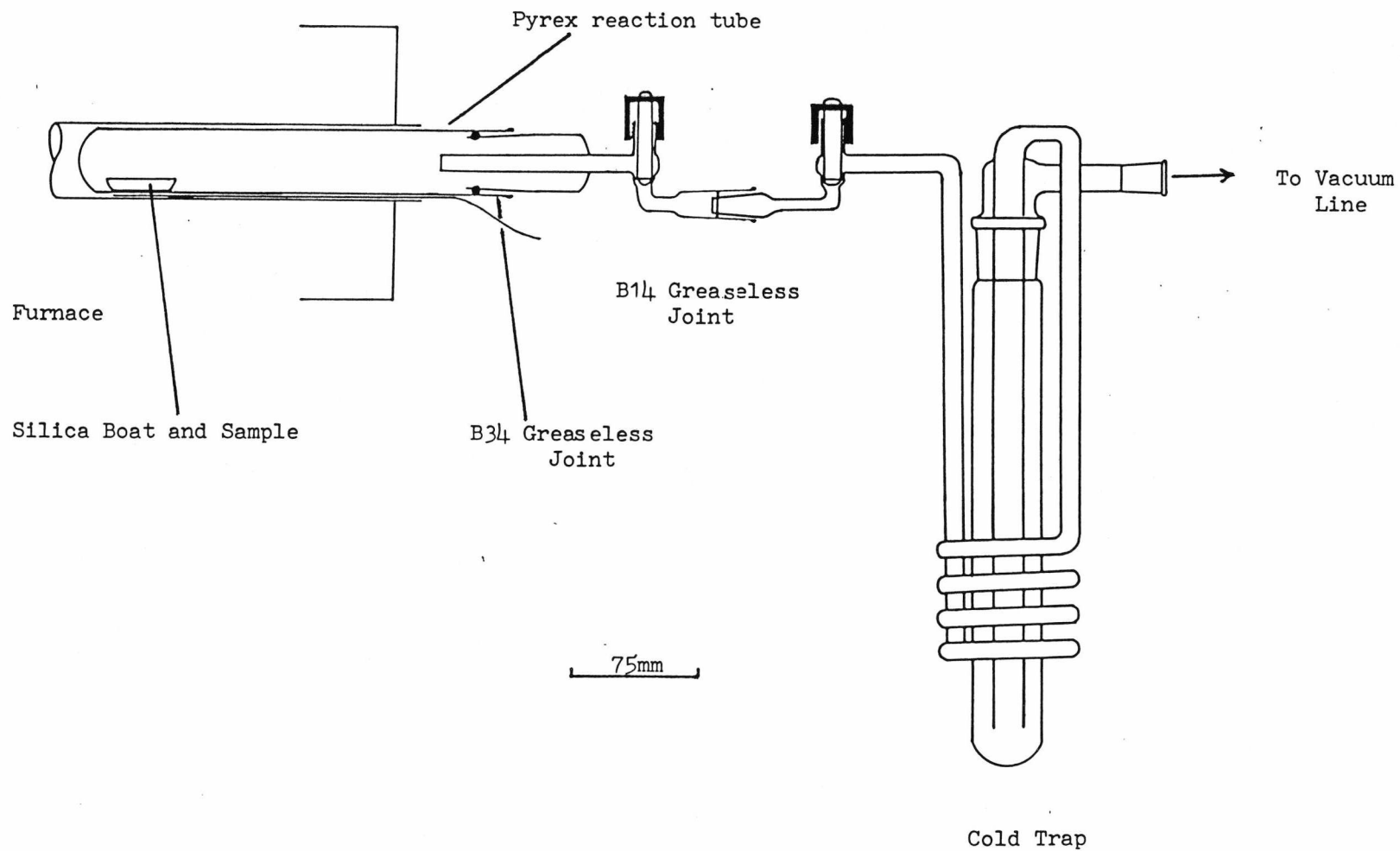


Figure 3.2

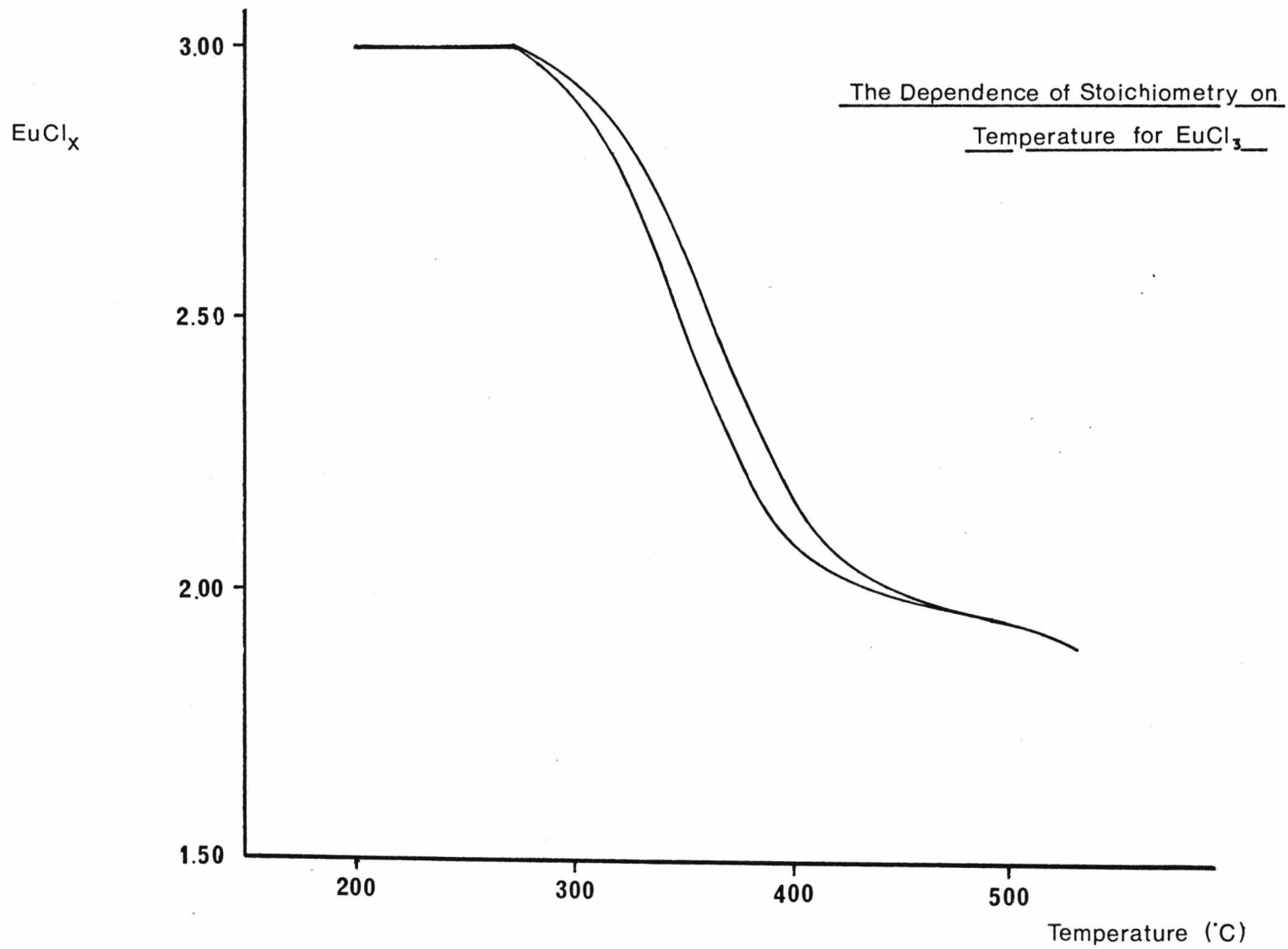


Figure 3.3

Apparatus for the Production of Anhydrous Europium Tribromide

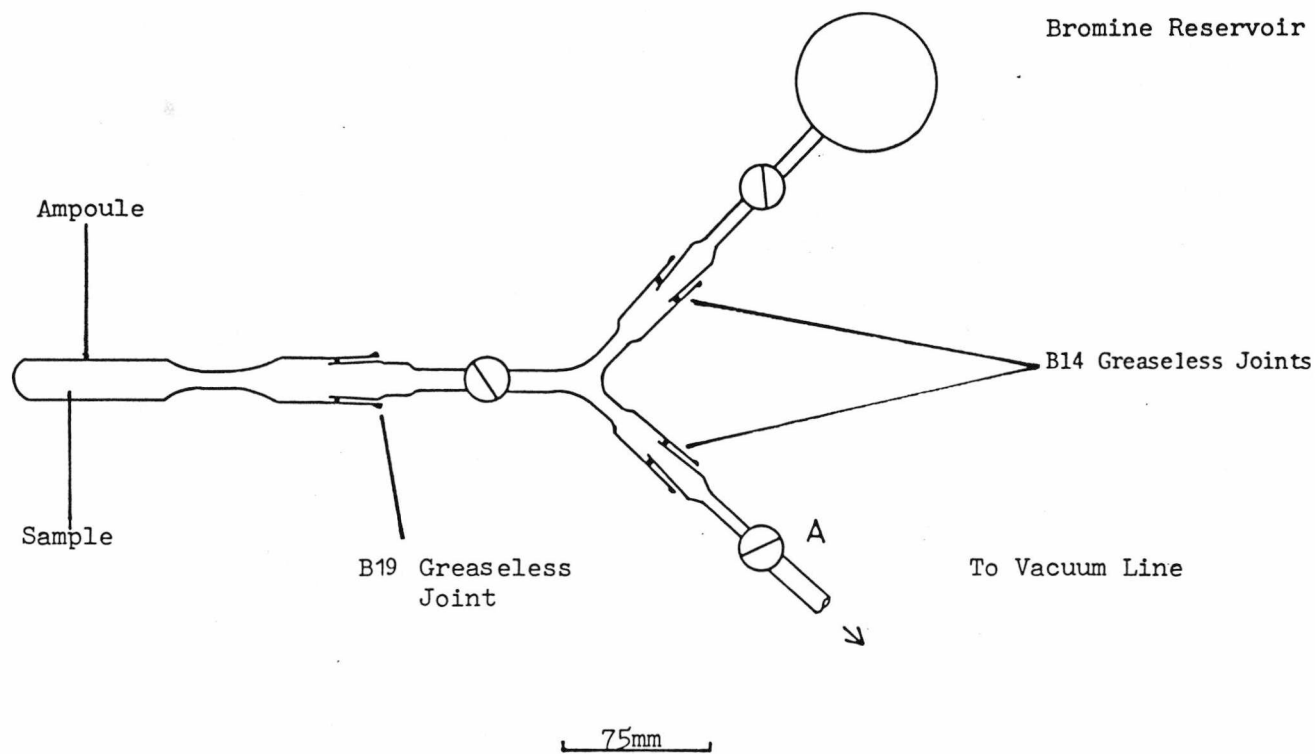
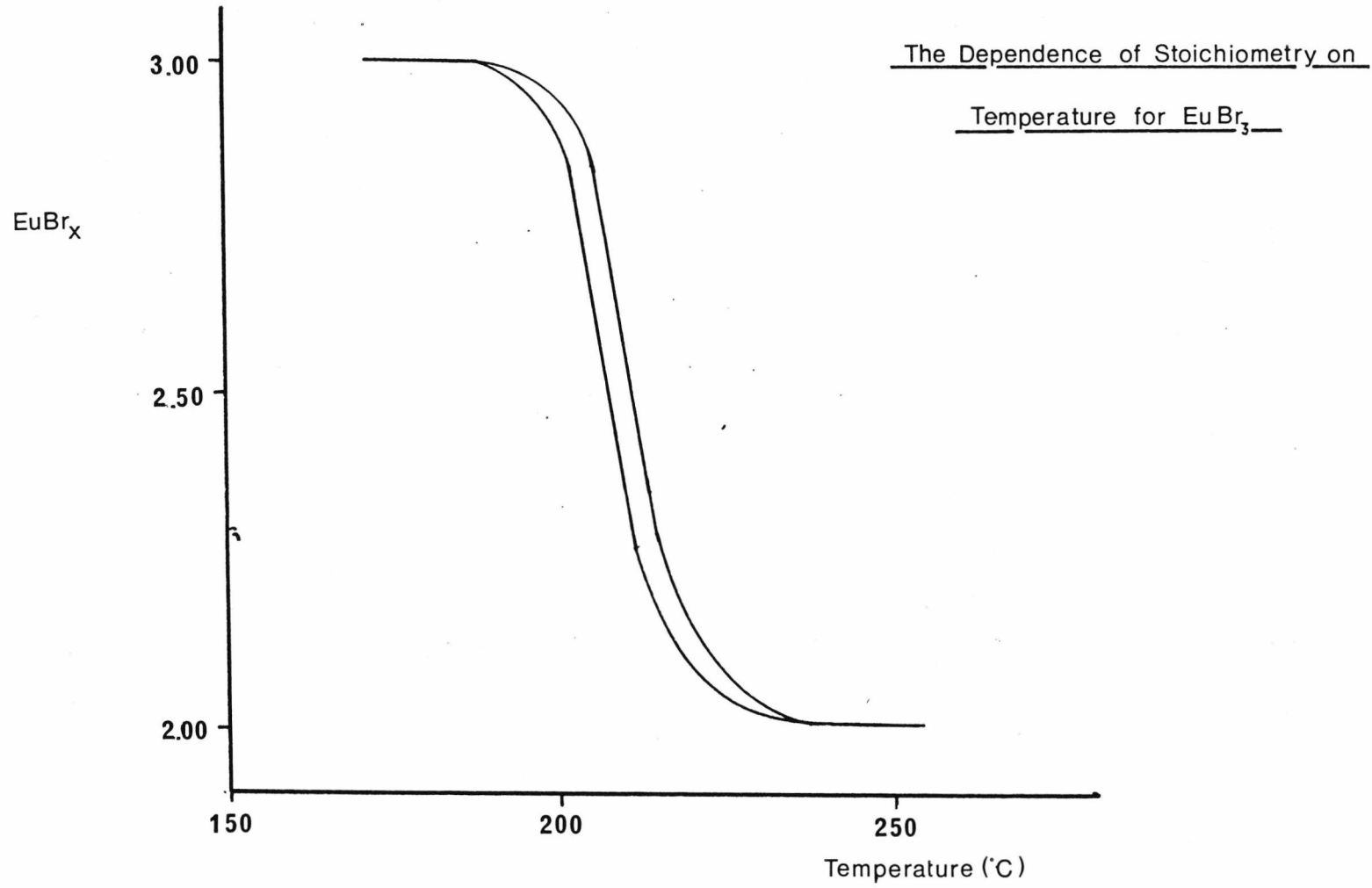


Figure 3.4



References Chapter Three

1. C.M. Jenden PhD Thesis University of Kent at Canterbury, Canterbury, England 1980.
2. K.E. Johnson & J.R. Mackenzie, Journal Inorg. Nucl. Chem., 1970, 32, 43.
3. B.S. Mathur & T.R. Bhat, Z Anorg. Allgem. Chemie, 1966, 343, 220.
4. W.W. Wendlant, J. Inorg. Nucl. Chem. 1957, 5, 118.
5. W.W. Wendlant, J. Inorg. Nucl. Chem., 1959, 9, 136.
6. W.W. Wendlant, & J.L. Bear, Anal. Chem. Acta, 1959, 21, 439.
7. S.J. Ashcroft & G.T. Mortimer, J. Less Common Metals, 1968, 14, 403.
8. M.D. Taylor & C.P. Carter, J. Inorg. Nucl. Chem., 1962, 24, 387.
9. Fisons Ltd. Loughborough, Leicestershire, England.
10. Rare Earth Products Ltd., Waterloo Rd., Widnes, Cheshire, WA8 OQH, England.
11. J. Ball, PhD Thesis, University of Kent at Canterbury, Canterbury, England, 1978.
12. J. Burgess & J. Kijowski, Advances in Inorganic Chemistry and Radio Chemistry, vol. 24, 1981.
13. A.A. Merlkov & L.N. Kommissarova, Russ. Journal Inorg. Nucl. Chem. 1964, 3, 1137.
14. T. Moeller & G. Griffin, B.P. Rep., 1959, 136162, 104.
15. G.W. Cullen, PhD Thesis, Univ. Illinois Urbana U.S.A. 1959.

16. F. Petru, P. Polivka, D. Lezal & B. Hajek, 56 Uys, Sk. Chem-Technal Praze, Anorg. Chem Technol., 1972, B 15, 15.
17. I. Mayer & S. Zolator, J. Inorg. Nucl. Chem., 1965, 27, 1905.
18. D. Brown, S. Fletcher and D.G. Holah, J. Chem. Soc.(A) 1968 in Press.
19. J.M. Haschke & H.A. Eick, J. Inorg. Nucl. Chem., 1970, 32, p2158.
20. J.E. Powell & H.R. Burkholder, J. Inorg. Nucl. Chem., 1963, 74, 65.
21. F. Matthes & G. Ha seler, Z. Chem., 3Jg, 1963, 2, 72.
22. F. Matthes & G. Ha seler, J. Less Common Metals, 1965, 9, 133.
23. S.J. Lyle & M. Rahmann, Talanta, 1963, 10, 1177.
24. D.C. White, Mikrochim, Acta, 1961, 3, 449.
25. Analytical Methods Committee, Analyst, 1978, 103, 391.
26. F. Verbeck, Bull. Soc. Chim. Belg., 1961, 70, 423.
27. S.J. Lyle & N.A. Za'tar, Analytica Chima. Acta, 1982, 135, 137.
28. R. Belcher & A.J. Nutten, Quantitive Inorganic Analysis, 3rd edition, Butterworths, London, 1970, p225.
29. Distributors, Pentak E.M.I. Ltd., Vale Road, Windsor, Berks.
30. Azâroff, L.V. Elements of X-ray Crystallography, McGraw Hill New York, 1968.

Chapter 4The Thermal Decomposition Reactions of Hydrated Europium(III)
Chloride and Bromide4.1 Introduction

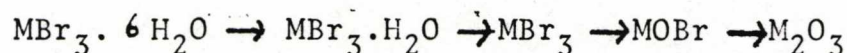
The literature concerning the preparations of anhydrous europium(III) chloride and bromide shows that some workers have claimed that the anhydrous halides are intermediates in the thermal decomposition reactions of the respective halide hydrates¹⁻³. Attempts have been made in this laboratory to prepare the anhydrous halides of europium from the thermal decomposition of the halide hydrates without success. Further investigation of the literature has revealed few but conflicting reports of the thermal decomposition reactions, the disagreement being in the proposed composition of the reaction intermediates.

The thermal decomposition of rare earth trichlorides has been studied⁴⁻⁹, and while all workers agree that the final stages of this reaction pass through the rare earth oxychloride (MOCl) and finally to the oxide, there are differences of opinion concerning intermediate steps. There are two proposed paths for the reaction. Wendlandt⁷ suggests that in the initial stages of the decomposition, water is lost until about one half of a molecule of water is present relative to each europium(III) chloride molecule. After this europium oxychloride forms through an intermediate stage corresponding approximately to $2\text{EuCl}_3 \cdot \text{EuOCl}$.

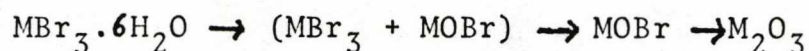
Matthes and Haesler⁸ have reported that $\text{Eu}(\text{OH})\text{Cl}_2$ is an intermediate species in place of the europium(III) chloride - europium oxychloride mixture. The studies were performed by thermogravimetric analysis; the thermograms are represented in figures 4.1 (a) and (b) respectively. The only evidence for the reported species is apparently from the observed weight loss from the thermograms, which are in good agreement with the calculated weight losses for both the proposed species.

Only one paper concerning the thermal decomposition reaction of hydrated rare earth tribromide has been published¹⁰. In it the decomposition reactions were considered to fall into two groups:

M = Pr to Eu



M = Gd to La



Their results show a similarity with the thermal decomposition of the hydrated rare earth trichlorides. The authors suggest the ease of forming the oxybromide increases with the decreasing ionic radii in agreement with Wendlandt's^{4,5} findings for hydrates of the rare earth trichlorides. The decomposition reactions¹⁰ were studied by thermogravimetric analysis supported by X-ray diffraction data of intermediate products in a few cases. The thermogram for the decomposition of hydrated europium(III) bromide is represented in figure 4.2 The intermediate species

anhydrous europium(III) bromide has been claimed to exist but on examination of the data the agreement between the observed and calculated weight loss for the species is poor. The explanation offered for the difference is that formation of europium oxybromide occurs even in the early stages of the decomposition.

The study described in this chapter sets out to provide more data on the thermal decomposition reactions of hydrated europium(III) chloride and bromide so that the intermediate species can be more definitely characterised.

Methods of thermal analysis include differential thermal analysis (D.T.A.), differential scanning calorimetry (D.S.C.), and thermogravimetric analysis (T.G.A.). The first two types of analysis involve the detection of energy changes within the sample with changing temperature. The energy changes may occur due to chemical reaction or a change in the physical properties of the sample, such as a phase change. In D.T.A. and D.S.C. heat is supplied to a sample pan and a reference pan at a constant rate, the temperature of each is monitored. When the sample undergoes a chemical or physical change it will be associated with an energy change leading to a temperature difference, ΔT between the sample and reference. The temperature difference can be recorded as a function of temperature, hence showing the temperatures at which changes occur. The experimental methods of D.T.A. and D.S.C. differ in that D.T.A. measurements are made using a single heater for sample and reference with the temperature of each being measured independently. In D.S.C. separate heaters are employed for sample and reference and the system works on the "null balance" principle where any

temperature difference is compensated for by the sample heating circuit, the energy required for this is recorded as a function of temperature. The inherent accuracy of D.S.C. is greater than that for D.T.A. as the assumption that the temperatures of both the sample and reference are the same is valid.

Reviews¹¹⁻¹⁷ on D.S.C. and D.T.A. are numerous as are the applications of the techniques. Thermogravimetry¹⁸ (T.G.) involves the weight of the sample being recorded as a function of temperature or time. Hence when a chemical or physical change involving the loss of a volatile component or evaporation of the sample with temperature the corresponding weight change is recorded.

Since thermal decompositions reactions were being studied and were known to involve the loss of volatile components such as water, thermogravimetry was considered to be the most suitable method for following the reactions. D.T.A. and D.S.C. would enable chemical reactions to be observed but would also record enthalpy changes due to phase changes which might obscure the more important information of the chemical reactions in this case. Hence the initial study was by thermogravimetry supported by data obtained from compounds prepared separately corresponding to discrete stages in the decomposition reaction. The data obtained from the compounds established the chemical composition by chemical analysis. The co-existence of separate phases could be identified from Mössbauer spectra of the compounds. Infra-red spectroscopy was used to determine whether water was present and as a general method of identifying the species present. In addition, mass spectrometry was used to look at the volatile reaction products generated at various temperatures and the information used in establishing a reaction mechanism.

4.2 Experimental Method

The thermal decomposition was initially studied by thermogravimetry from which the temperature regions of interest were found. The thermogravimetric analyses were performed by Dr. I. McNeil¹⁹ using a DuPont 990 thermal analysis system. The sample weight was between 5 and 10mg and each analysis was carried out under nitrogen at a flow rate of 50ml/min. Samples corresponding to the temperatures of interest then prepared by heating the europium(III) halide hydrate to the chosen temperature as described in chapter III.

Mössbauer spectra were recorded on samples usually at 93K but occasionally at 273K for comparison. Spectra of the europium(III) halide hydrates and europium oxyhalides were recorded as references to aid the identification of intermediate compounds. The isomer shifts of the oxyhalides differed from those of the hydrates by about 1mms^{-1} . This difference is probably too small to allow resolution of spectra with components of a similar nature to those above. The observed resonant absorption is dependent upon the quantity of the species present and the recoil-free fraction. In general as previously discussed, the more rigid the lattice the higher the recoil free fraction, hence an apparent proportionally greater absorption. From consideration of the physical properties of the oxyhalides and hydrated trihalides of europium it may be assumed that the oxyhalides have a higher recoil-free fraction, as is found in practice. A spectrum containing both species would show a disproportionately large contribution

from the oxyhalide due to its recoil-free fraction. If the temperature is raised then the recoil-free fractions of both species will decrease but not necessarily at the same rate as the change in the recoil-free fraction of the oxyhalide is smaller. An unresolved spectrum of a mixture such as that described will show a single peak which at a higher temperature will appear to shift to an isomer shift closer to that of the oxyhalide. It is felt that this will aid the identification of any oxyhalide present in sufficient quantity in the sample; however this is a purely qualitative observation.

Infra-red spectra were run on some of the samples in an attempt to show the presence of water. The instrument used was a Perkin-Elmer 683 infra-red spectrophotometer operating in the range $4000-200\text{cm}^{-1}$. The samples were prepared by grinding with 'nujol' to form a mull and placing a small amount between two polished cesium iodide discs. The discs were mounted on a stainless steel holder outside of the instrument so that the preparation could be carried out inside the glove box. In practice even dried nujol was not considered free enough from water hence the presence of water in the samples could not be unequivocally proved. The infra-red spectra however, did show features which could be used as 'finger prints' for various components of the samples. Although as definite assignments could not be made to features some general regions of absorbance could be identified. Texts^{20,21} on the infra-red spectra of inorganic compounds

reveal that the components of interest can be grouped into categories shown in table 4.1. Using this data the presence of various species may be inferred.

Mass spectrometry enabled the identification of the volatile products of the thermal decomposition reactions and in doing so, provided evidence for a reaction mechanism. The mass spectra were obtained on an A.E.I. MS902 using standard techniques with a source temperature of 250°C. The instrument was operated by Mr. S.J. Smith of the University of Kent. The sample was heated to various temperatures between ambient and 250°C and the resultant volatile products were identified by their masses.

4.3 Results and Discussion

(a) Hydrated Europium(III) Chloride

The thermogram for the decomposition of europium(III) chloride hexahydrate is shown in figure 4.3. Some slight weight loss is observed at a temperature just above room temperature after which no further loss occurs until a temperature of about 75⁵⁰°C is reached. Then there is a reasonably steady weight loss until a horizontal plateau is reached at a temperature of 138°C and this continues to about 200°C. The total weight loss of the intermediate species corresponding to this region is 26.5 ± 0.5%. A further weight loss occurs until a second plateau region is encountered at a temperature of 230°C. The plateau is reasonably flat until 258°C after which a slight weight loss

is recorded up to a temperature of about ³²⁵310°C. Beyond this temperature a more rapid weight loss occurs. The total weight loss over the region 230°C to 310°C ranges from 32.5% to 34%. The third plateau region is encountered at 350°C. The corresponding weight loss is 44% and is indicative of EuOCl which decomposes to Eu₂O₃ at a temperature of about 900°C. 1.60
- 325
- 775

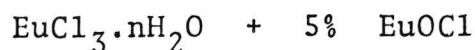
A

Chemical analyses of compounds corresponding to the regions of weight stability as determined from the thermogram give the compositions of the intermediate products. Typical results for the region between 138°C and 200°C are:

%Eu	%Cl	Ratio Eu:Cl
56.9 ± 0.7	38.6 ± 0.5	1: 2.91 ± 0.01
56.0 ± 0.7	38.1 ± 0.5	1: 2.90 ± 0.01

In all the samples the ratio of europium to chloride is found to be less than 1: 3.00 indicating the formation of EuOCl. The sum of the percentages of europium and chloride do not add up to 100%, the contribution of oxygen in EuOCl cannot account for this. The most likely explanations for this difference is the presence of water of hydration, this is also suspected from the infra-red spectra. Assuming europium oxychloride as an impurity and some water of hydration is present a composition for this intermediate can be prepared. The ratio of europium to chlorine is 1: 2.90 suggesting an impurity level of 5% for EuOCl. The B

difference in the sum of the percentages of europium, chloride and oxygen (from the oxychloride) from 100% indicates the number of waters of hydration to be about 0.5. The intermediate composition can be written



The calculated parameters for the composition with $n = 0.5$

%Eu	%Cl	Ratio Eu:Cl	% weight loss
57.5	38.9	1: 2.90	27.90

The calculated parameters are in good agreement with those found from experiment. The discrepancies might be accounted for if more water of hydration is present.

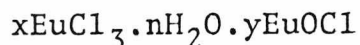
Therefore n can take the value

$$0.5 \leq n \leq 1$$

The compounds prepared to correspond to the temperature region 230°C to 310°C are further depleted in chloride and even higher depletion occurs beyond a temperature of 258°C . Typical analytical results are set out below

%Eu	%Cl	ratio Eu:Cl
$59.3^{\pm 0.7}$	$34.3^{\pm 0.5}$	$1: 2.48^{\pm 0.01}$
$62.1^{\pm 0.7}$	$31.2^{\pm 0.5}$	$1: 2.15^{\pm 0.01}$

Assuming EuOCl to be present in larger fractions as the temperature increases, it will be noticed that the sum of the percentages differs from 100% after the contribution of oxygen from EuOCl has been accounted for. Once again this can be attributed to water of hydration, this is also indicated on the infra-red spectrum. The proposed intermediate composition can be written



$$1 \leq x/y \leq 3; \quad 0.5 \leq n \leq 1$$

The calculated parameters are shown in table 4.2. The experimentally determined values fall within this range so supporting the suggested composition. There is wide agreement that in the final stages of the decomposition EuOCl is formed and decomposes to Eu_2O_3 . Data from the thermogram is seen to support this.

Mössbauer spectroscopy yields values for isomer shifts of the compounds in a sample. Preliminary spectra of europium(III) chloride hexahydrate and europium oxychloride were produced to serve as standards by which intermediate compounds could be identified. The isomer shifts and widths obtained from the spectra run at 93K are given in table 4.3. and the spectra are shown in figures 4.4 and 4.5 respectively.

Mössbauer spectra of samples in the temperature region

138°C to 200°C corresponding to the proposed composition $\text{EuCl}_3 \cdot n\text{H}_2\text{O} + 5\% \text{EuOCl}$ show only one peak with a reasonably narrow line width (figure 4.6). The relevant parameters are given in table 4.3. It was hoped that the spectra of samples corresponding to the temperature region 230°C to 310°C would identify two phases. However, the peaks could not be resolved. The spectra consist of a single broad peak which may be fitted to two lines with an improvement in the "goodness of fit". The isomer shifts obtained from the spectrum are close to those for $\text{EuCl}_3 \cdot n\text{H}_2\text{O}$ and EuOCl but do not coincide exactly. The parameters for a single and double peak fit are given in table 4.3 and the spectrum is presented in figure 4.7. In addition to recording the spectrum at 93K a second spectrum was recorded at 273K and fitted to a single peak giving a more positive isomer shift to that at 93K. This supports the proposed presence of EuOCl in the sample by the argument presented in section 4.2, the isomer shift is shown in table 4.3. The infra-red and mass spectra for the decomposition of europium(III) chloride hexahydrate will be presented with those of the europium(III) bromide system.

(b) Hydrated Europium(III) Bromide

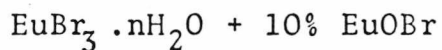
The thermogram for the decomposition of europium(III) bromide hexahydrate is shown in figure 4.8 and differs from that of the corresponding chloride in that definite horizontal regions are not observed except in the final stages. No weight loss is observed until a temperature of about 75°C is reached after which a steady weight loss occurs decreasing over a region between 160°C and 175°C. The

associated weight loss over this region ranges from $20.5 \pm 0.5\%$ to $21.5 \pm 0.5\%$. A second decrease in weight loss occurs between 195°C and 235°C at which temperature a more horizontal region is observed with an associated weight loss of between $25.5 \pm 0.5\%$ and $27.5 \pm 0.5\%$. A more rapid weight loss resumes but at a temperature of 305°C shallows to a reasonably horizontal plateau with a total weight loss of $49.5 \pm 0.5\%$. This weight loss corresponds to the formation of EuOBr (calculated weight loss, 50.4%). The EuOBr then decomposes at about 610°C to form europium(III) oxide. The lack of regions without weight loss make the characterization of the intermediate compounds difficult, hence the proposed intermediates are only approximate.

Compounds prepared to represent the products formed in the temperature region 160°C - 175°C have suffered a depletion of bromide. The results of chemical analysis suggests that water of hydration is present from arguments used in the corresponding chloride case. Typical results from the chemical analysis of such compounds for a decomposition temperature of 162°C

%Eu	%Br	ratio Eu:Br
39.8 ± 0.5	59.1 ± 0.7	$1: 2.82 \pm 0.01$

The ratio of europium to bromine suggests a europium oxybromide content of about 10% on that about 0.5 molecules of water is attached to each europium(III) bromide molecule. The proposed composition is then:



$$0 \leq n \leq 0.5$$

The calculated parameter for such a composition are:

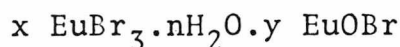
n	%Eu	%Br	ratio Eu:Br	weight loss %
0.5	39.4	58.1	1: 2.80	22.9
0	40.3	59.3	1: 2.80	24.5

These parameters are in reasonable agreement with those found experimentally but are only representative of one point in this region. It must be remembered that the temperature of decomposition which is recorded may vary over approximately 5°C and this represents a relatively large variation in composition.

Compounds corresponding to the second region of interest, the temperature region 195°C to 235°C have undergone a greater depletion of bromide but the presence of water of hydration is still suspected. Typical parameters for the compounds representing this region are presented below for decomposition temperatures of 198°C and 252°C

T(°C)	%Eu	%Br	ratio Eu:Br
198	40.6 ± 0.5	56.9 ± 0.7	1:2.66 ± 0.01
252	42.9 ± 0.5	53.1 ± 0.7	1:2.36 ± 0.01

The amount of EuOBr has clearly increased with temperature, shown by the second set of data. A composition may be proposed for this region.



$$2 \leq x/y \leq 4 \quad 0 \leq n \leq 0.5$$

Calculated parameters for $n = 0.5$ are given below

x/y	%Eu	%Br	ratio Eu:Br	weight loss%
4	41.1	56.1	1:2.60	25.9
2	43.5	53.3	1:2.83	30.0

Mössbauer results are similar to those for the chloride system and are summarised in table 4.4. The results do not provide very much information in this case, the isomer shifts do not show any pattern attributable to an increasing europium oxybromide content. Mössbauer Spectra of $\text{EuBr}_3 \cdot 6\text{H}_2\text{O}$ and EuOBr are shown in Figures 4.9 and 4.10 respectively. However, an increase in line width is associated with the sample containing the largest amount of europium oxybromide. The shallow region of the thermogram between 305°C and 390°C was investigated using the Mössbauer technique and yielded interesting results. Europium(II) is found in the sample which has not been previously reported. It demonstrates one useful aspect of Mössbauer spectroscopy, namely the ability to differentiate between oxidation states. The spectrum is presented in figure 4.11. In it both oxidation

states Eu(III) and Eu(II) are present. Mössbauer isomer shift and chemical analysis results are given for a sample in this range. The Mössbauer spectrum was recorded at 93K.

%Eu	%Br	ratio Eu:Br	δ (mms ⁻¹)	Γ (mms ⁻¹)
46.1 \pm 0.5	49.8 \pm 0.5	1:2.06 \pm 0.01	0.56 \pm 0.03	3.2 \pm 0.1
			-12.4 \pm 0.2	3.3 \pm 0.1

The isomer shift for the europium (III) species is in the region found for the mixed europium tribromide/europium oxybromide samples. The Eu(II) isomer shift is indicative of europium dibromide. The ratio of europium to bromine suggests that di and tri bromide species are present as well as europium oxybromide. No attempt will be made to suggest a composition for this sample; the important result is that europium dibromide is present. The shallow curve feature between 305°C and 390°C is not observed on the thermogram of Mayer and Zolotov (figure 4.3). Their thermogravimetric analysis was carried out in air. A second sample was prepared in the same way as that above, except the heating was carried out in an atmosphere of dry nitrogen and oxygen. Mossbauer isomer shift and chemical analysis data are given below.

%Eu	%Br	ratio Eu:Br	δ (mms ⁻¹)	Γ (mms ⁻¹)
52.25 \pm 0.5	41.65 \pm 0.5	1:1.52 \pm 0.01	0.76 \pm 0.05	2.7 \pm 0.1

Only one peak is observed in the Mössbauer spectrum (figure 4.12) and it yields an isomer shift tending towards that of EuOBr. The probable composition of the sample is 75% EuOBr with 25% EuBr₃.nH₂O; where $0 \leq n \leq \frac{1}{2}$. The formation of europium oxybromide

below 390°C is thus seen to be dependent on the oxygen available whether in the atmosphere or water present in the sample.

(c) Infra-red Spectra

The infra-red measurements previously mentioned could not effectively monitor the presence of water of hydration but gave an indication to its presence. Infra-red absorption is observed at low wave number and spectra for samples of the chloride and bromide systems are shown in figures 4.13 and 4.14 respectively. No assignments of the lines can be attempted as no suitable reference spectra are available. The respective europium oxyhalide species is most likely to be responsible for the absorbance as the europium halide absorbance occurs below 200cm^{-1} as in the case of europium(III) fluoride²²

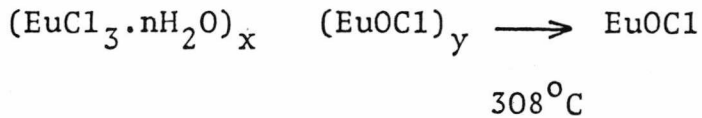
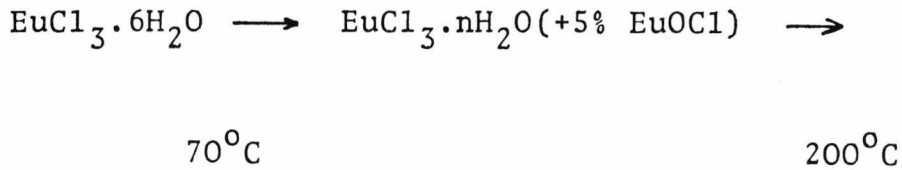
(d) Mass Spectrometry

The results for both halide systems are similar so will be treated together. The volatile products produced (with decomposition temperatures) are shown in table 4.5. In the initial stages of the decomposition water is the major volatile product with small amounts of the appropriate hydrogen halide gas being observed. At higher temperatures the hydrogen halide gas becomes the major product. No free halogen is observed up to the maximum obtainable decomposition temperature of 250°C on the instrument. Had higher temperatures been reached bromine might have been observed in the hydrated europium(II) bromide system corresponding to the formation of europium(II) bromide. The presence of the hydrogen halide gas and the absence of the free halogen gas indicates hydrolysis to be a mechanism for the reaction.

4.4 Conclusion

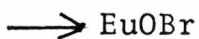
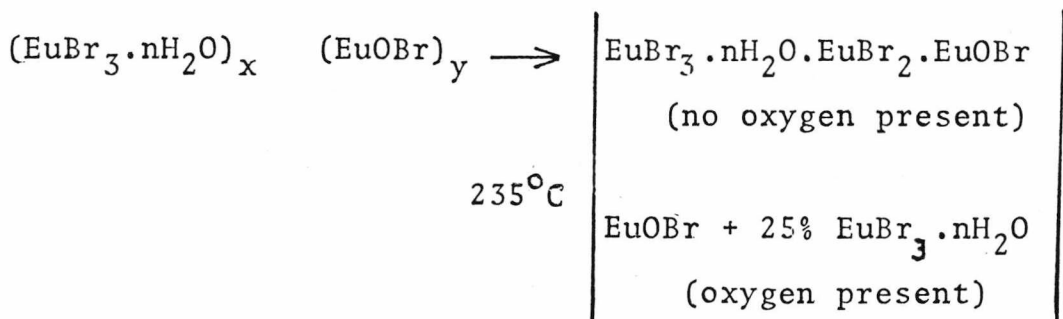
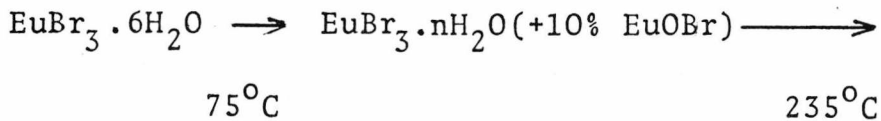
The results of the experiments performed lead to the following proposed reaction sequences for the decompositions:

For the chloride system.



$$\frac{1}{2} = \leq n \leq 1 \quad ; \quad 1 \leq x/y \leq 2$$

and for the bromide system.



390°C

The amount of water of hydration present can not be exactly quantified from the results presented here but they show that n is generally less than one. This would indicate more than one europium(III) halide is involved in the hydrolysis. The presence of europium(II) in the decomposition of hydrated europium(III) bromide in the absence of oxygen suggests that oxygen from the atmosphere is required. Some EuOBr is formed but at a slower rate than in the presence of oxygen suggesting another, less abundant source of oxygen is available namely the water of hydration. In both the halide systems, europium oxyhalide is seen to form at temperatures well below the temperature of complete conversion in small amounts. Mayer and Zolotov suggest this is due to the vapour pressure of water in the vicinity of the sample. When the bulk of **the** water has been removed (ie when $n \approx 0.5$) and has dispersed the water for hydrolysis is provided by the water of hydration remaining within the sample. The amount of water required is greater than that available for each europium(III) halide molecule to form the europium oxyhalide, hence there is a slowing down of the reaction rate leading to either stable or quasi stable points in the decomposition. In the case of hydrated europium(III) bromide decomposed in the absence of air a secondary reaction took place ²³ at temperatures between 235°C and 390°C , namely

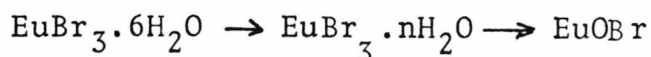


This is a secondary reaction occurring due to the lack of sufficient oxygen for the formation of europium oxybromide. It also shows anhydrous europium(III) bromide does occur but in



coexistence with large amounts of europium oxybromide. As the temperature increases the reaction goes to completion in both cases and the respective europium oxyhalide is formed. It is interesting to note that the behaviour of hydrated europium(III) bromide is intermediate between that of the corresponding chloride and iodide systems in that of the chloride does not give rise to measurable fractions of europium(II) species whereas the iodide probably goes entirely through divalent europium in its thermal decomposition²⁴.

It is hoped that the reported experimental results will clarify the discrepancies encountered in the literature for the thermal decompositions of hydrated europium(III) chloride and bromide. The conclusions drawn from the results from the chloride system are similar to those of Wendlandt but with water being present up to the final stage. The bromide system did not allow intermediate species to be clearly defined due to their quasi-stable nature as a function of temperature. A better but less detailed reaction sequence may be



$$0 \leq n \leq 0.5$$

as these were the only definable species. However, this investigation of other intermediate compounds did help in a comparison with the chloride system and enabled an overall view of both systems to be obtained.

Table 4.1

Characteristic Frequencies for Infra-red Spectra
of Inorganic Systems

Species	Mode	Frequency Range (cm^{-1})
Lattice water	antisymmetric and symmetric	3550-3200
	H-O-H bending	1630-1600
Co-ordinated water	Wagging, twisting rocking	about 750
	M-O rocking, wagging, stretching*	900-670
Metal halide	Stretching ⁺	300-100
Oxyhalides	M-O-X modes.	900-100

* the frequencies are dependent upon the strength of the co-ordinate bond and hydrogen bonding.

+ Frequencies are higher for chlorides than bromides.

Table 4.2

Calculated Parameters for Products in the Temperature
region 230 to 310°C



$$n = \frac{1}{2}$$

x/y	% Eu	% Cl	ratio Eu:Cl	% weight loss
3	60.62	35.07	1: 2.50	31.56%
2	61.81	33.60	1: 2.33	32.89%
1	64.50	35.76	1: 2.00	35.76%

Table 4.3

Mossbauer Parameters for Compounds in the Europium(III)
Chloride System

Composition + (proposed)	Temperature K	δ (mms ⁻¹)	Γ (mms ⁻¹)	remarks
EuCl ₃ ·6H ₂ O	93	0.54 ± 0.03	3.27 ± 0.06	
EuOCl	93	0.96 ± 0.02	3.16 ± 0.06	
EuCl ₃ ·½H ₂ O ⁺ + 5% EuOCl	93	0.39 ± 0.03	2.74 ± 0.03	decomposition temperature = 183°C
xEuCl ₃ ·nH ₂ O ⁺ .yEuOCl	93	-0.2 ± 0.1	2.3 ± 0.1	two peak fit
"	93	0.86 ± 0.08	2.2 ± 0.2	
"	93	0.48 ± 0.03	2.69 ± 0.05	x/y = 1.13 decomposition temperature =
"	273	0.60 ± 0.05	2.61 ± 0.2	252°C

* relative to EuF₃

Table 4.4

Mössbauer Parameters for Compounds
in the Europium(III) Bromide System.

Composition + proposed	Temperature (K)	δ (mms ⁻¹)	Γ (mms ⁻¹)	remarks
EuBr ₃ · H ₂ O	93	0.46 ± 0.05	3.1 ± 0.1	
EuOBr	93	1.18 ± 0.05	2.47 ± 0.07	
EuBr ₃ · nH ₂ O (+10% EuOBr)	93	0.60 ± 0.03	2.59 ± 0.08	Td = 178°C
xEuBr ₃ · nH ₂ O .yEuOBr	93	0.54 ± 0.03	3.06 ± 0.05	Td = 252°C

Table 4.5

Mass Spectral Data for the Volatile Decomposition Products
from Hydrated Europium(III) Chloride and Europium(III) bromide.

Decomposition Temperature °C	Products Detected	
	$\text{EuCl}_3 \cdot 6\text{H}_2\text{O}$	$\text{EuBr}_3 \cdot 6\text{H}_2\text{O}$
40	H_2O	H_2O
150°C	Mostly water plus some HCl	-
160°C	-	Mostly water plus some HBr
200°C	Mostly water with an increasing amount of HCl and HBr respectively.	
230°C	Mostly HCl with some water	-
250°C	-	Mostly HBr with some water.

Figure 4.1

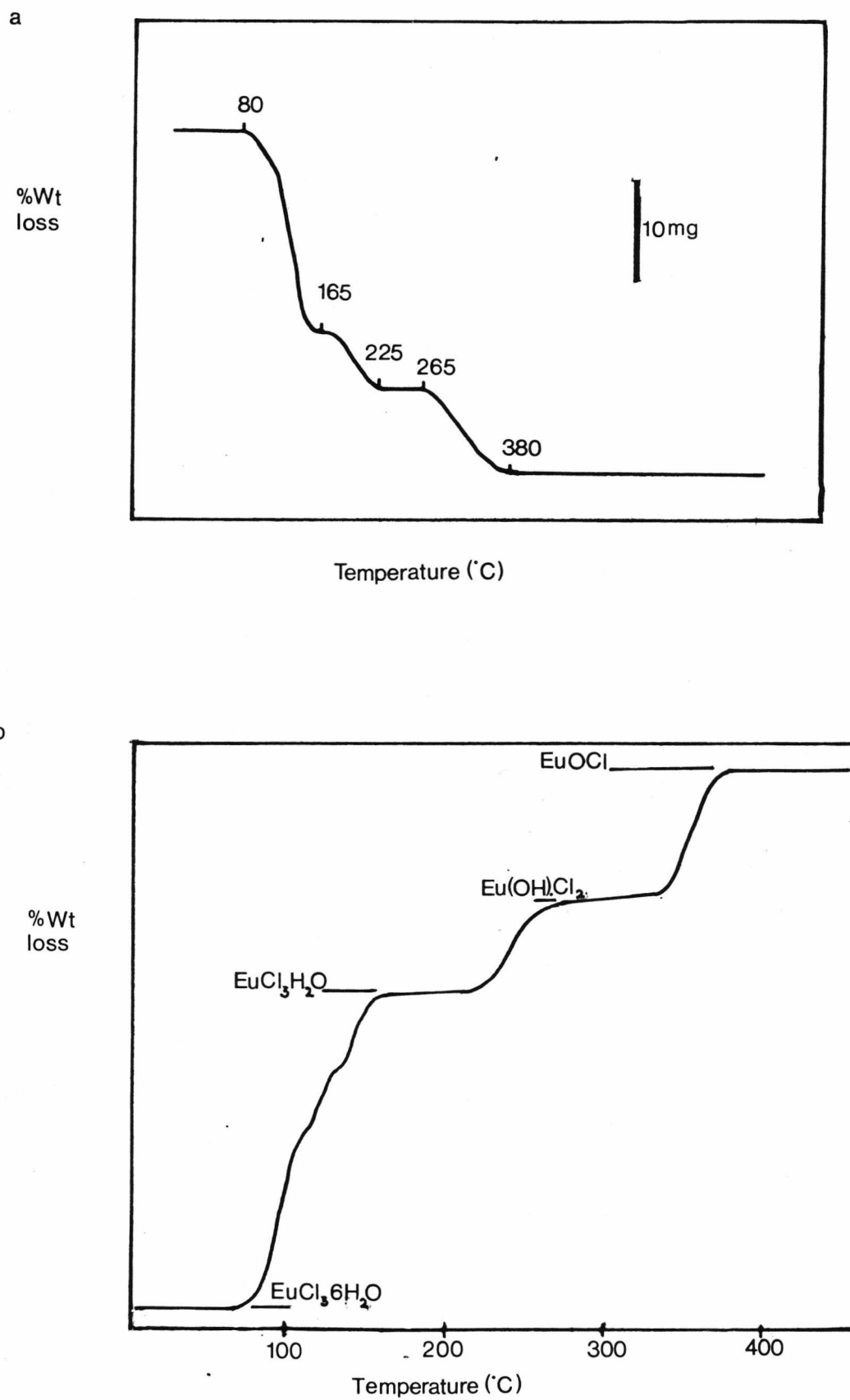
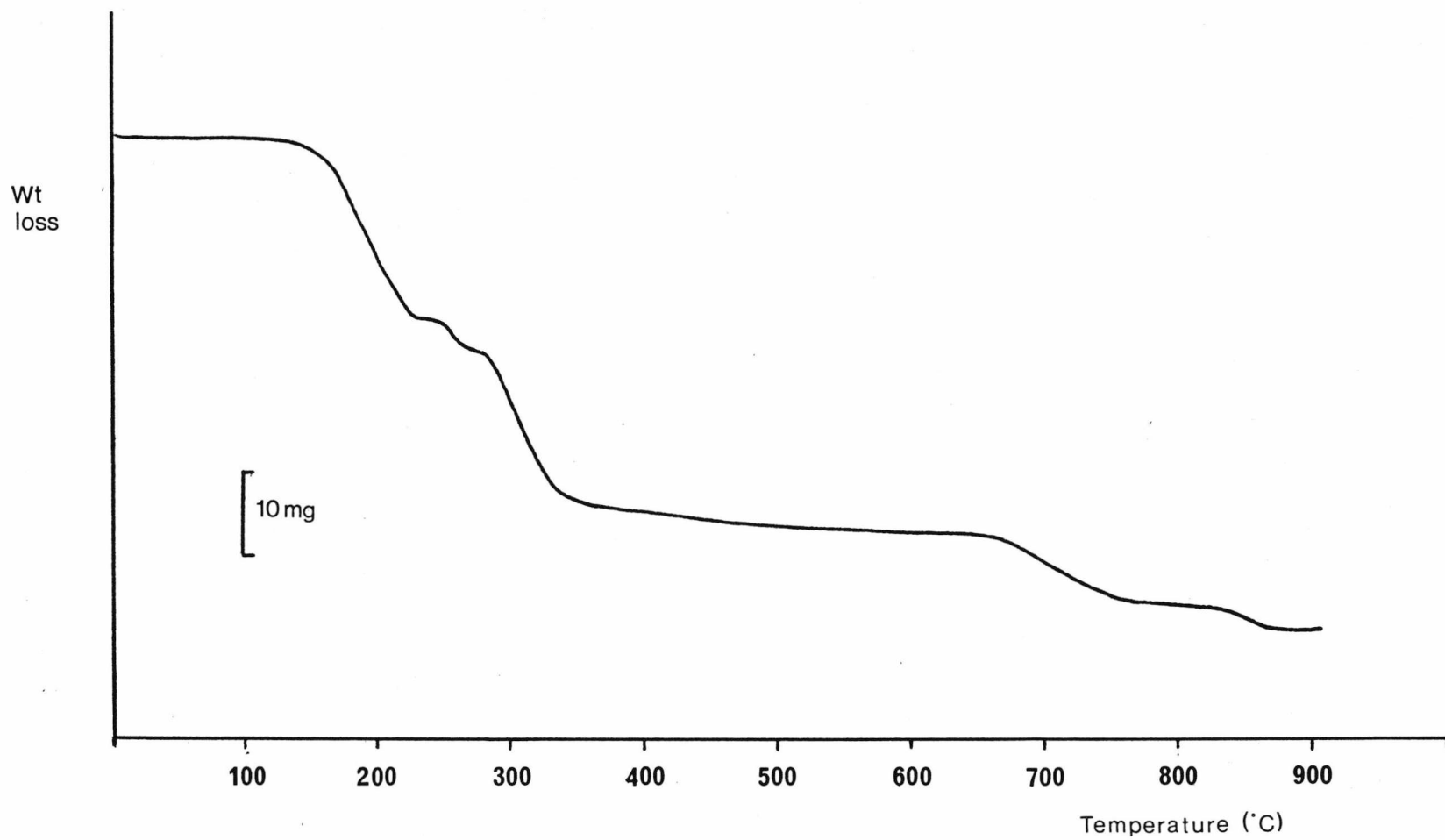
Thermograms for the Decomposition of Hydrated Europium(III) Chloride^{7,8}

Figure 4.2

Thermogram for the Decomposition of Hydrated Europium(III) Bromide¹⁰



Thermogram for the Decomposition of Hydrated Europium(III) Chloride

Figure 4.3

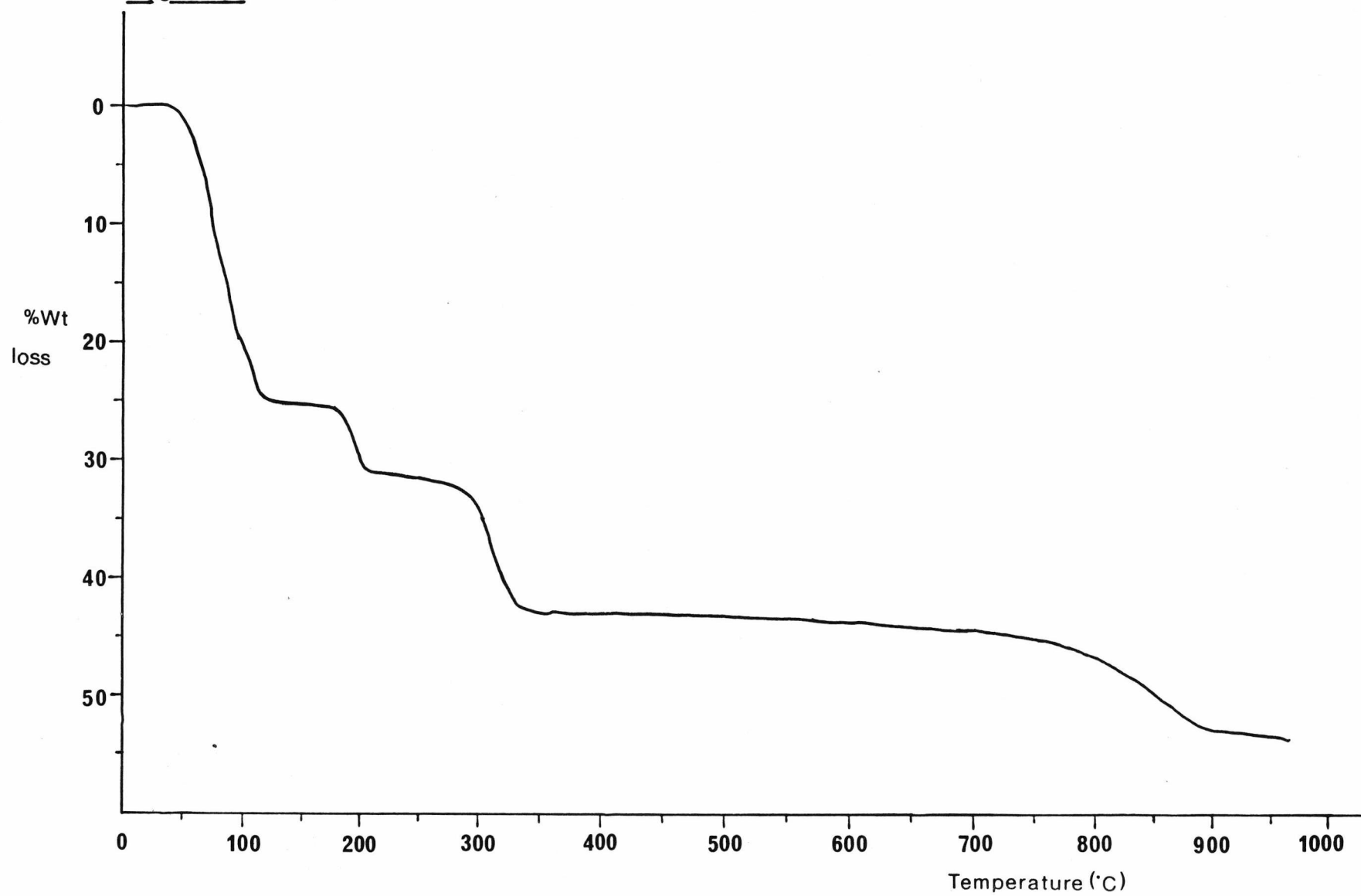


Figure 4.4

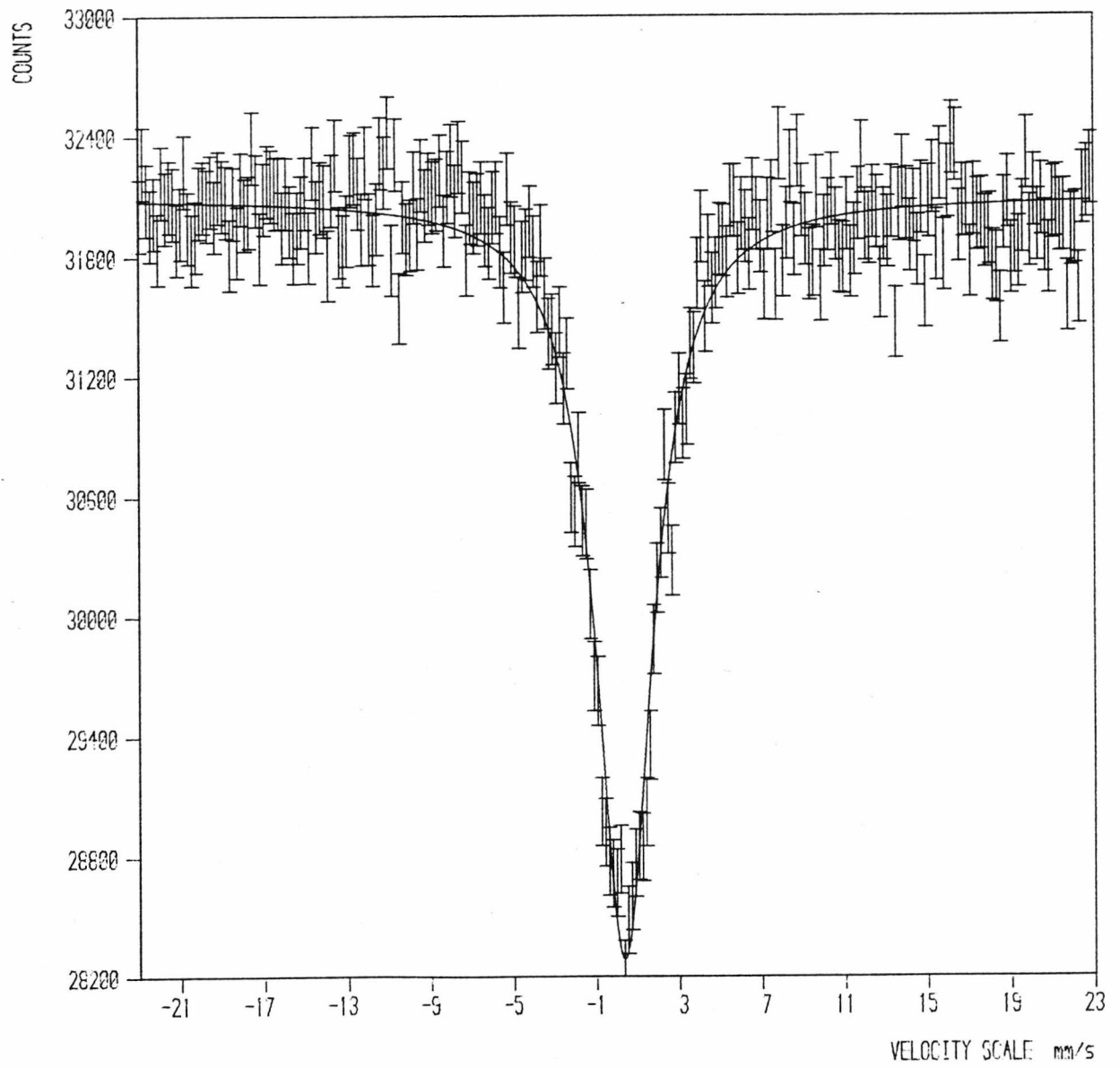
Mössbauer Spectrum of $\text{EuCl}_3 \cdot 6\text{H}_2\text{O}$ 

Figure 4.5

Mössbauer Spectrum of EuOC1

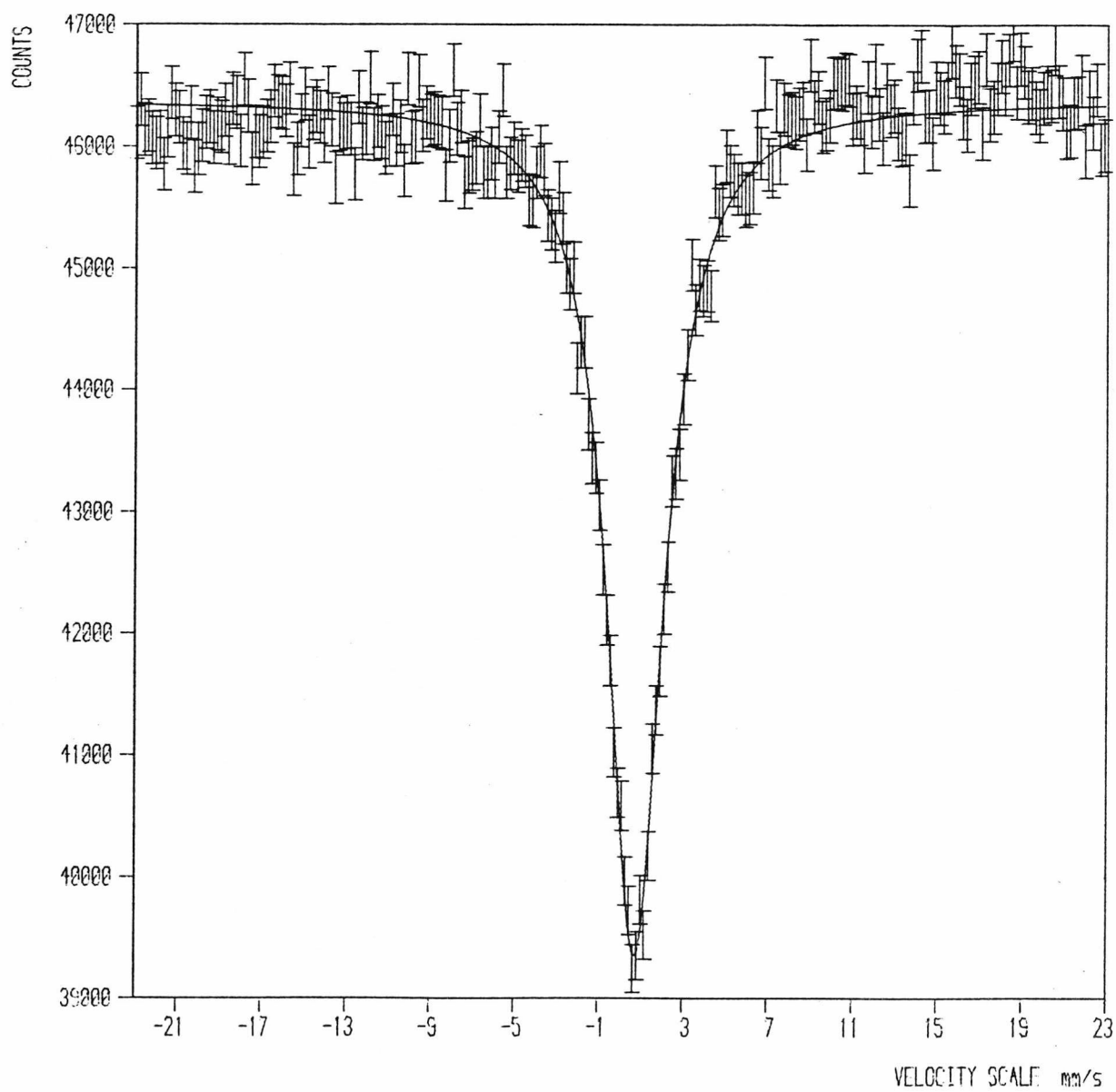


Figure 4.6

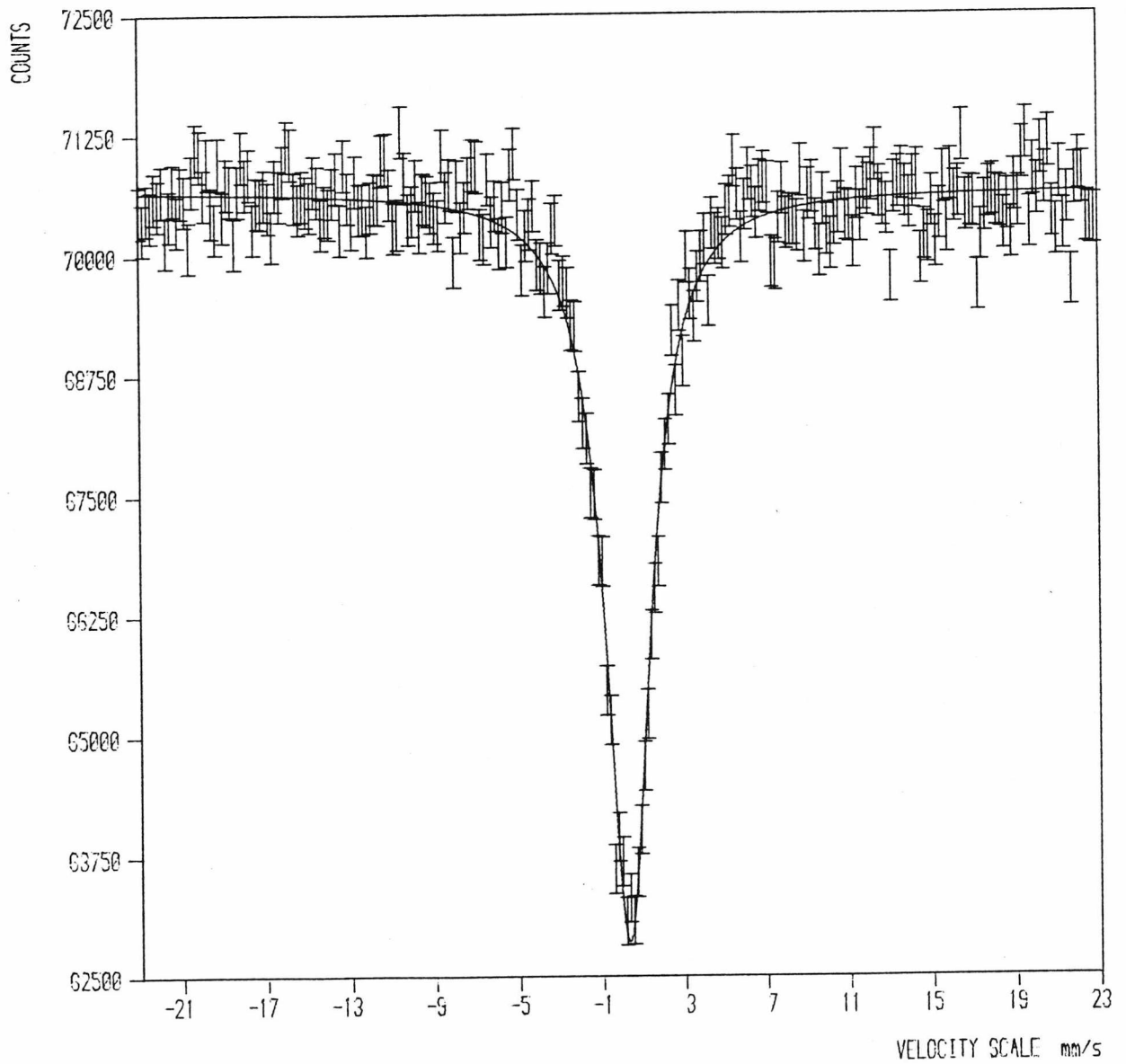
Mössbauer Spectrum of $\text{EuCl}_3 \cdot n\text{H}_2\text{O} + 5\% \text{EuOCl}$ 

Figure 4.7

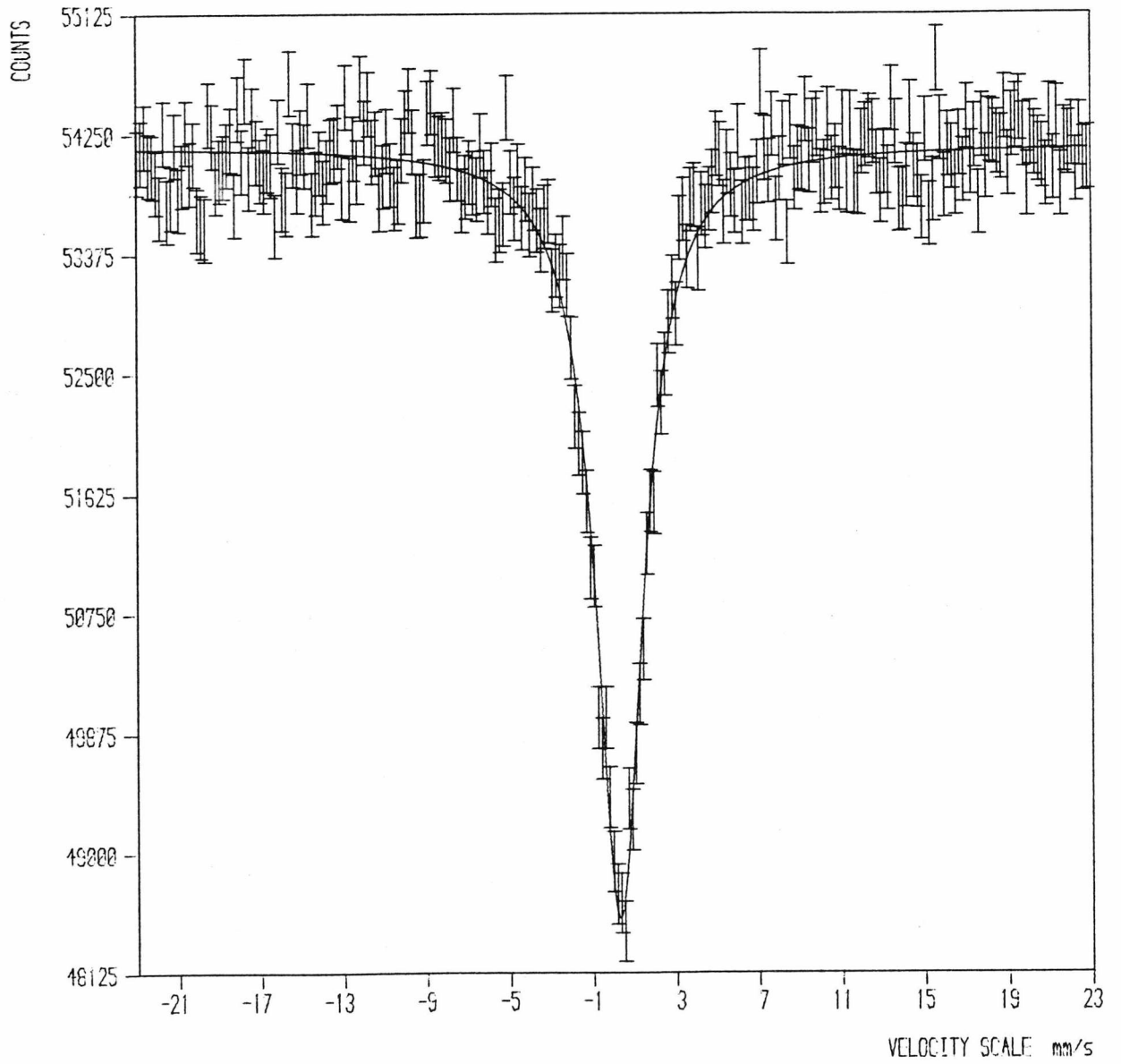
Mössbauer Spectrum of the Mixed $\text{EuCl}_3 \cdot n\text{H}_2\text{O} \cdot \text{EuOCl}$ Phase

Figure 4.8

Thermogram for the Decomposition of Europium(III) Bromide

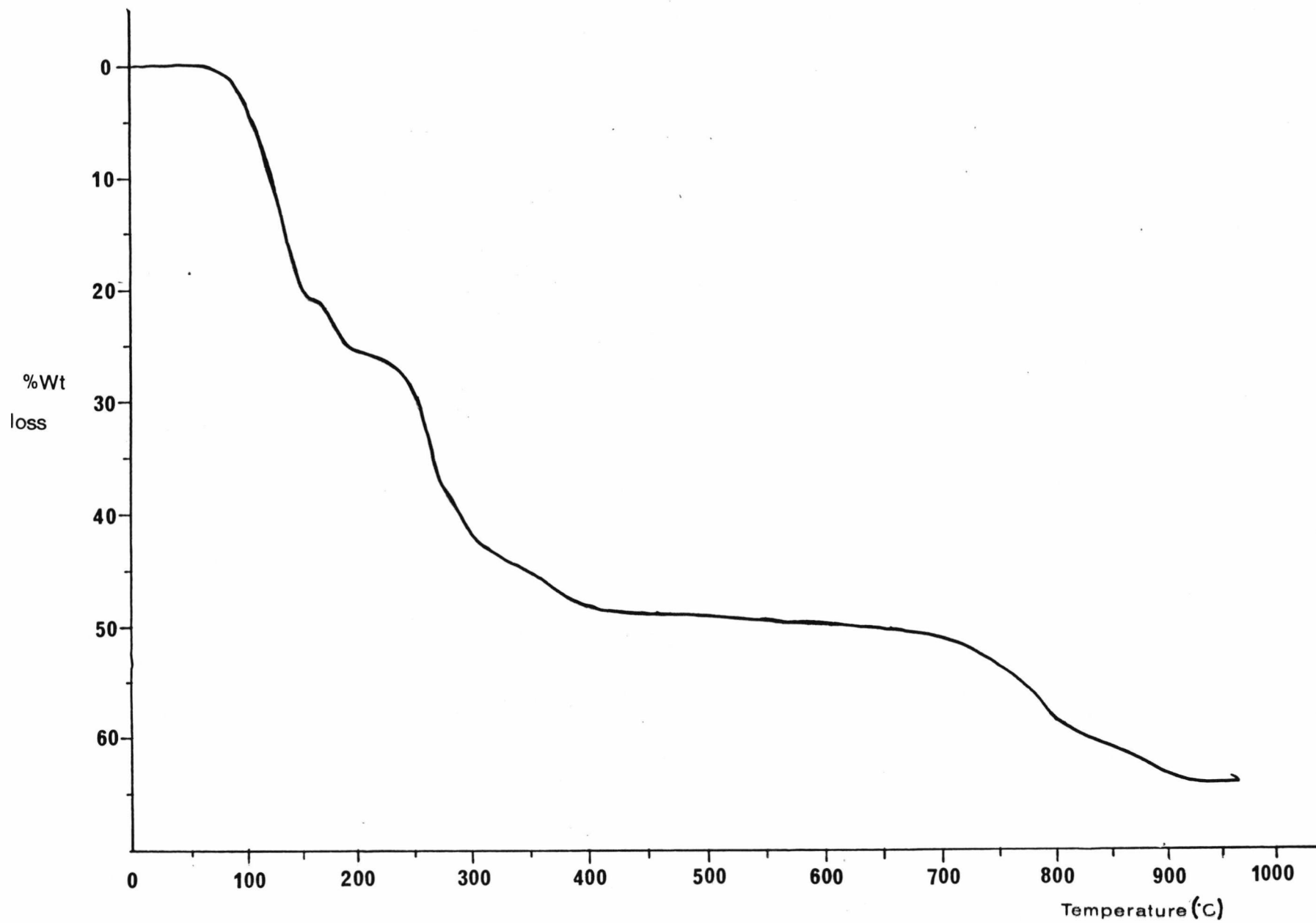


Figure 4.9

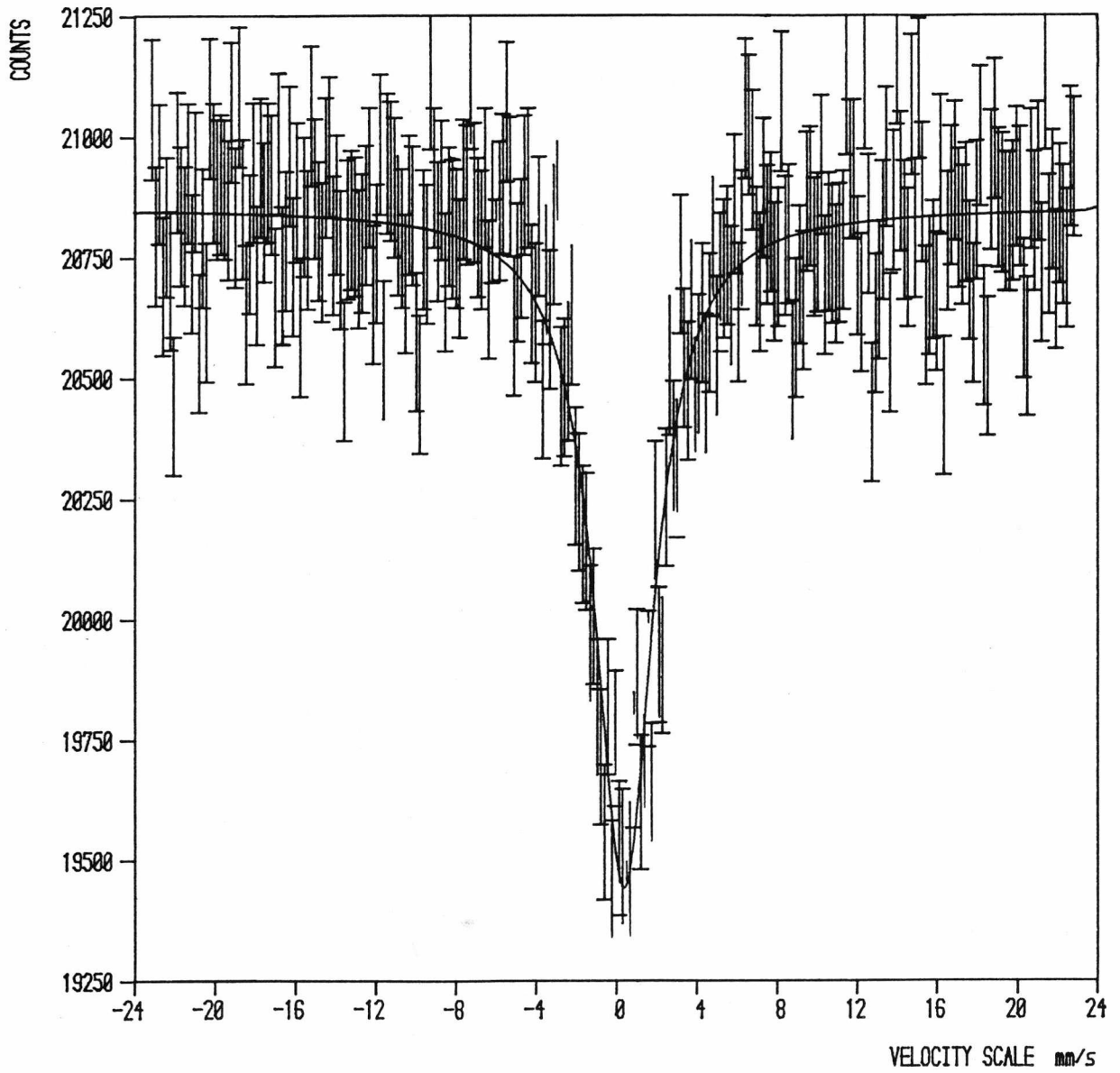
Mössbauer Spectrum of $\text{EuBr}_3 \cdot 6\text{H}_2\text{O}$ 

Figure 4.10

Mössbauer Spectrum of EuOBr

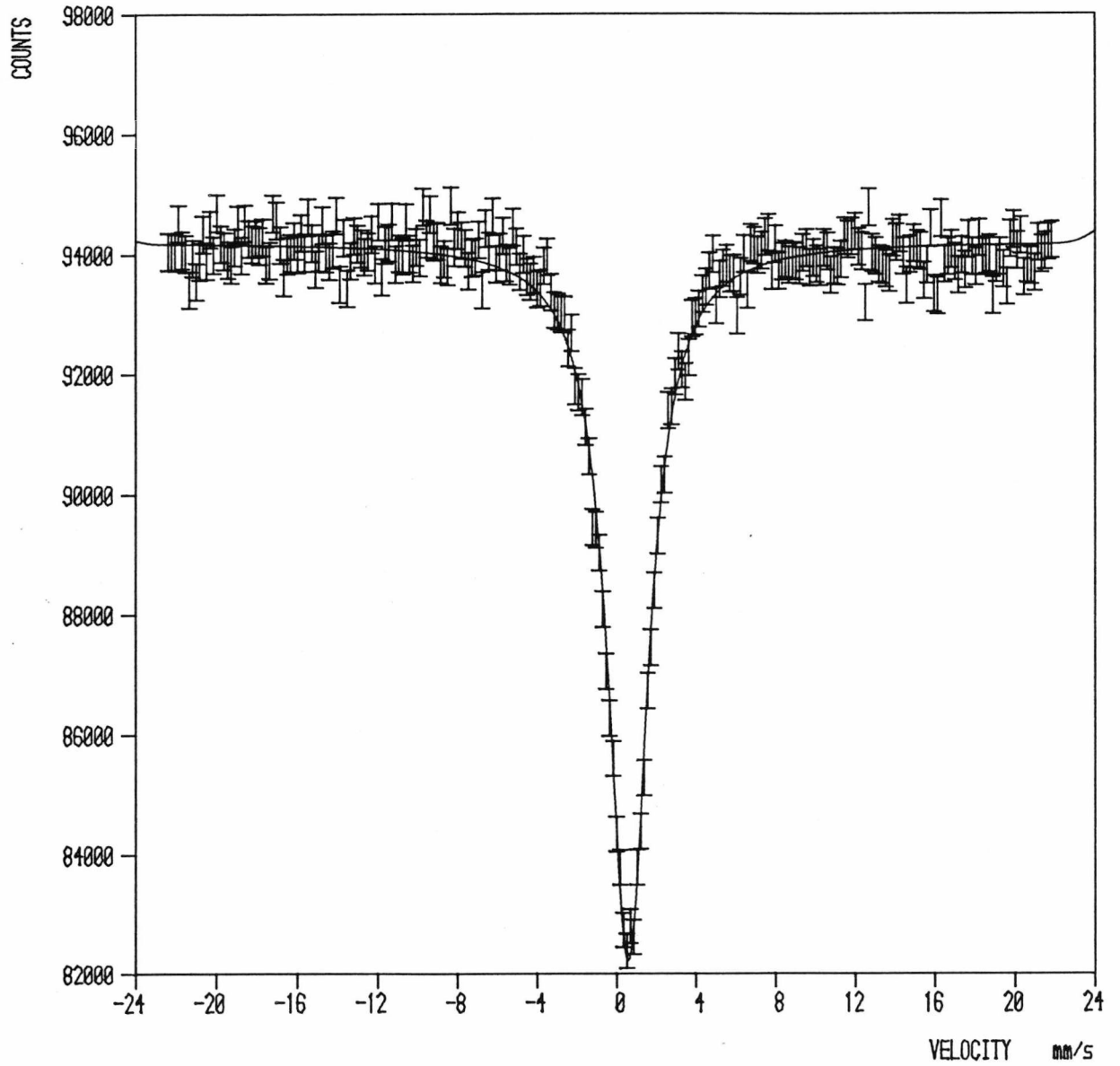


Figure 4.11 Mössbauer Spectrum of an Intermediate Compound Prepared at a Temperature between 305°C and 390°C in the Absence of Oxygen

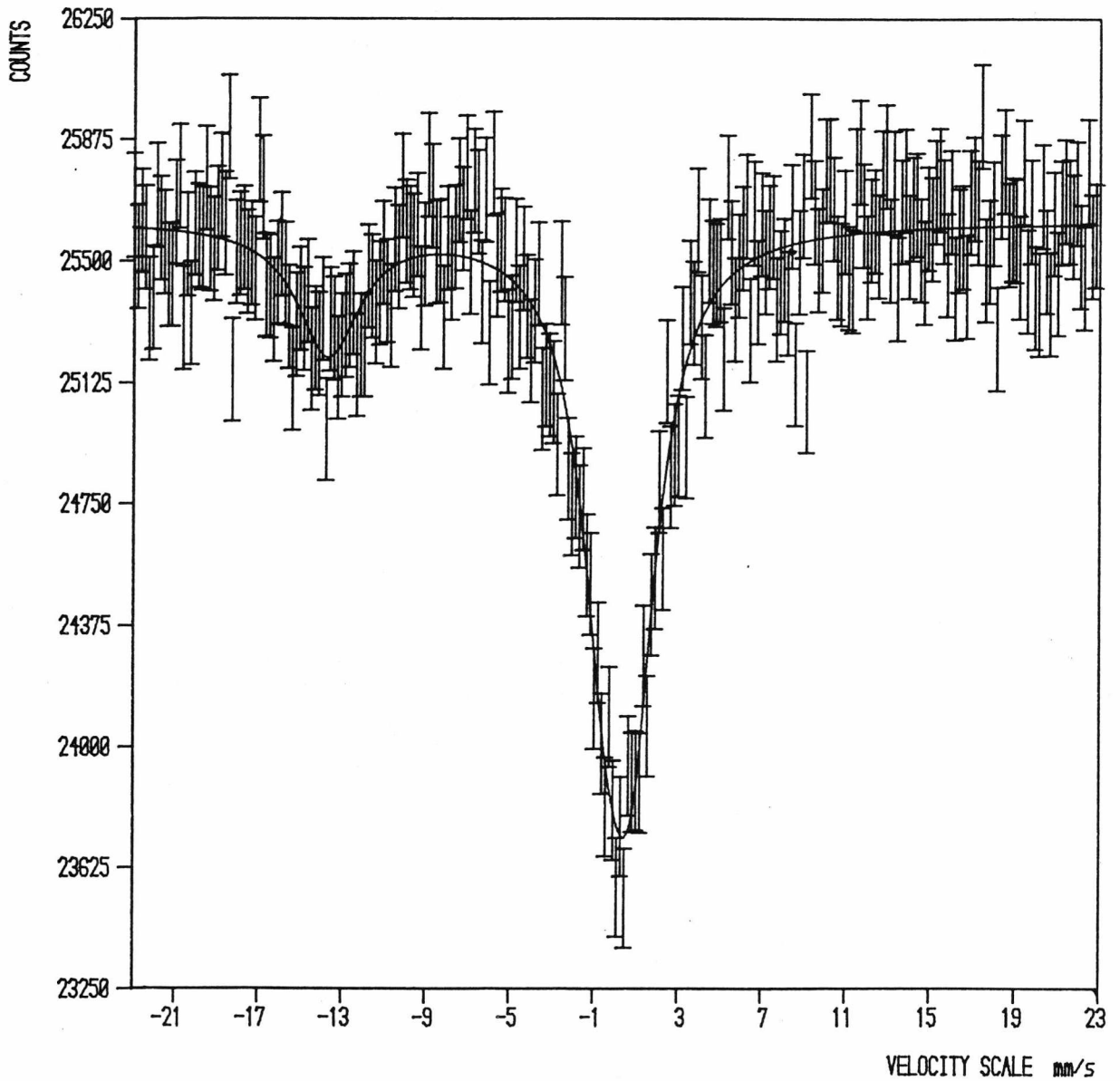


Figure 4.12

Mössbauer Spectrum of an Intermediate Compound Prepared at a temperature between 305°C and 390°C in the Presence of Oxygen.

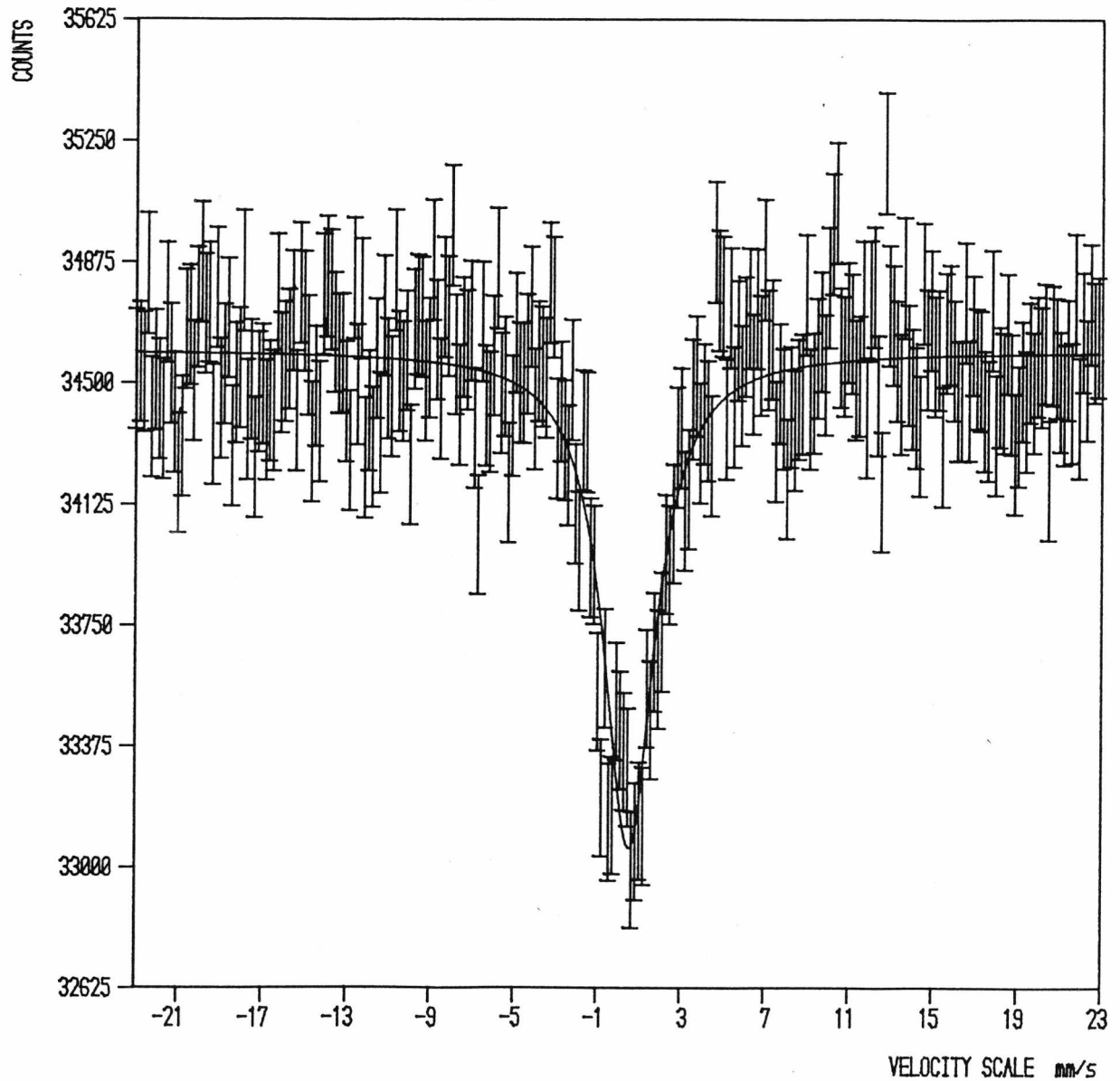


Figure 4.13

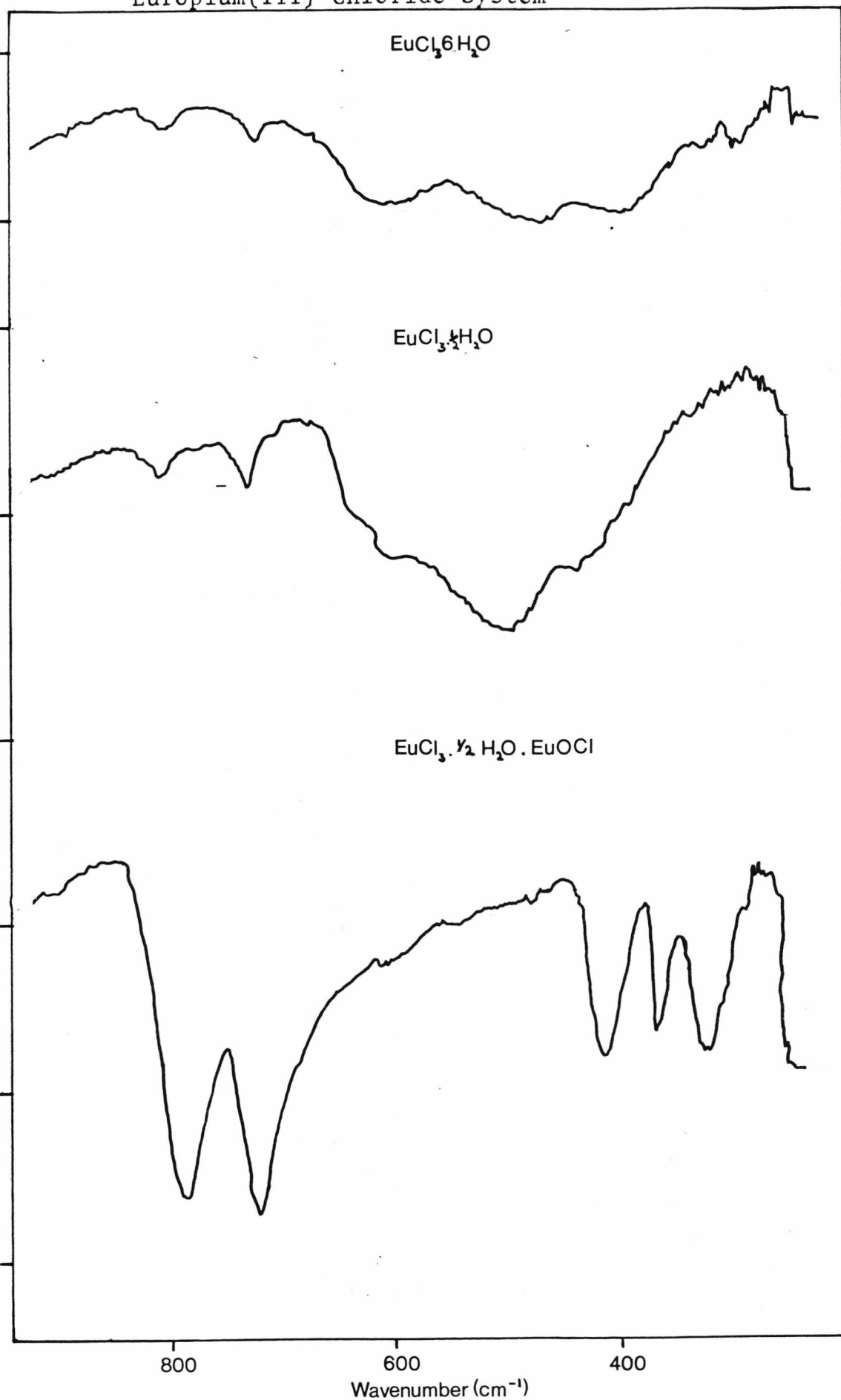
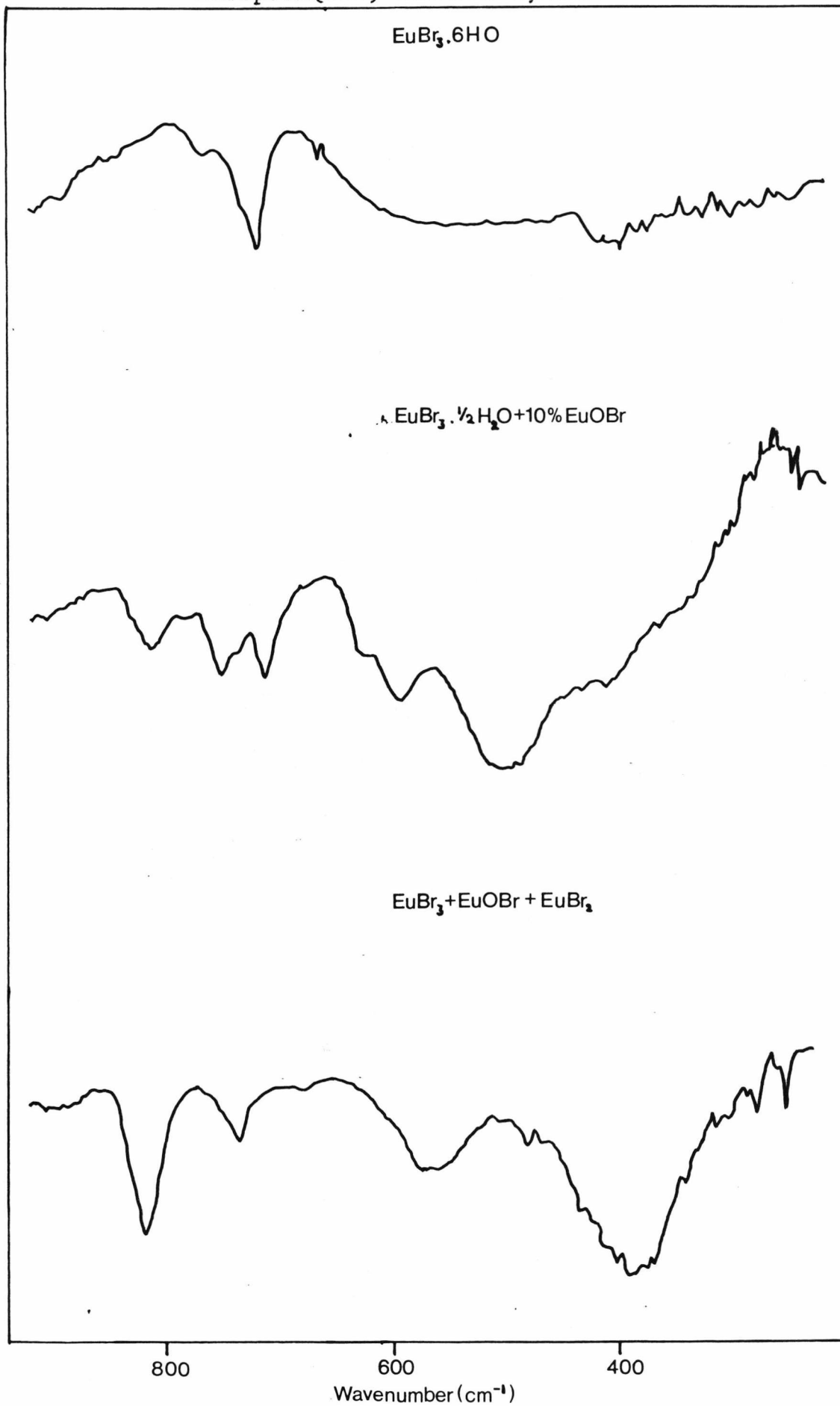
Infra-red Spectra of Compounds from the
Europium(III) Chloride System

Figure 4 14

Infra-red Spectra of Compounds from the
Europium(III) Bromide System

References

Chapter 4.

1. S.J. Ashcroft and G.T. Mortimer. J. Less Common Metals, 1968, 14, 403.
2. B.S. Mathur and T.R. Bhat, Z. Anorg. Allgem. Chemie, 1966, 343 220.
3. D. Brown, S. Fletcher and D.G. Holah, J. Chem. Soc. (A), 1968 (in press).
4. W.W. Wendlandt, J. Inorg. Nucl. Chem., 1957, 5, 118.
5. W.W. Wendlandt, J. Inorg. Nucl. Chem., 1959, 9, 136.
6. W.W. Wendlandt and J.L. Bear, Anal. Chim. Acta, 1959, 21, 439.
7. J.E. Powell and H.R. Burkholder, J. Inorg. Nucl. Chem. 1963, 14, 165.
8. F. Mathes and G. Haeseler, Z. Chem. 3 Jg. 1963, 2, 72.
9. F. Mathes and G. Haeseler, J. Less Common Metals, 1965, 9, 133.
10. I. Mayer and S. Zolotov, J. Inorg. Nucl. Chem., 1965, 27, 1905.
11. H. Uchida, M. Momota and T. Sugiyama, Shikizai kyokaishi, 1970, 43, 304.
12. W. Adam, Rev. Col. Quim. P.R. 1969, 28, 2.
13. R. Kind, Wiss. Z. Tech. Hochsch, Chem. Leuna, Merseburg, 1969, 11, 225.
14. H. Uchida, Nendo Kagaku, 1971, 11, 126.
15. Soloway and S. Jarnell, Indust. Res., 1970, 12, 52.
16. P.F. Levey, Amer. Lab., 1970, 46, 50, 52.
17. H. Kanetsuma, Sen-iTo Kogyo, 1970, 3, 670.
18. P.D. Goarn, "Thermoanalytical Method of Investigation" Academic Press, New York, 1965 (Chapters IX and X).

19. I. McNeil, University of Glasgow, Scotland.
20. K. Nakamoto, "Infra-red Spectra of Inorganic and Coordination Compounds" John Wiley and Sons, New York, 1963.
21. P.M. Adams "Metal-ligand and Related Vibrations", Edward Arnold Ltd, London, 1966.
22. R.H. Hauge, J.W. Hastie and J.L. Margrave, J. Less Common Metals, 1971, 23, 359.
23. D.G. Polyachenok and I.G. Novikov, Russ. Inorg. Chem., 1964, 9, 429.
24. C.M. Jenden and S.J. Lyle, J. Chem. Soc., Dalton, 1982, 2409.

Chapter 5Electron Hopping in Anhydrous EuropiumHalides.5.1 Introduction

A very elegant demonstration of electron hopping has been reported by Berkhoos et al¹ using the Mössbauer effect. The system chosen was Eu_3S_4 in which Eu(III) and Eu(II) ions occur on identical lattice sites and electron exchange occurs between them. Work has been carried out in this laboratory on electron hopping in non-stoichiometric europium(III) chloride by Ball² and Jenden³; this chapter describes the continuation of the work on the chlorides and the extension to non-stoichiometric europium(III) bromide.

Berkhoos's experiment showed the effect of temperature on the Mössbauer spectrum of Eu_3S_4 . At low temperatures a peak was present for each oxidation state in a ratio of 2:1 for Eu(III) and Eu(II) respectively. As the temperature was increased the peaks widened and merged into one forming a single peak at the centre of gravity of the low temperature peaks. The effect was so well demonstrated because of the large populations of each oxidation state and the large separation in isomer shift of the Eu(III) and Eu(II) oxidation states. The model used to explain the behaviour

postulates that the extra electron at an Eu(II) site is localized but that it may move through the lattice via the Eu(III) sites. In order for the electron to move from one lattice site to another it has to overcome an energy barrier. The electron is bound to a site for a time τ ; increasing the temperature increases the jump probability and decreases the relaxation time τ . The Mössbauer effect senses the change in τ by its relationship with the life time of the γ -ray excited ^{151}Eu nucleus. If the relaxation time τ is very much shorter than the life time of the nuclear excited state then the electron will have made many jumps in the time of a single nuclear relaxation, the environment the nucleus 'sees' will be that of an average oxidation state and this is reflected in the intermediate isomer shift at high temperatures. If the relaxation time is approximately equal to the time of a nuclear decay then intermediate behaviour is observed and a variation in environments is observed. The relaxation time may increase further so that few jumps are made in the nuclear life time and the excited nucleus mainly 'sees' the discrete Eu(III) or Eu(II) oxidation state so leading to the two corresponding peaks of the Mössbauer spectrums. Detailed mechanisms for the effect are not provided in Berkooz's paper but the analysis used in the interpretation did not require them as this follows from a general treatment by Wickman et al^{4,5}. The Mössbauer spectra at various temperatures could be fitted to a theoretical curve dependent on τ . Since τ is temperature

dependent, the shapes of the theoretical curves could be made to fit the temperature dependent experimental data by finding suitable values of τ . Thus the relationship between τ and temperature can be found. Not surprisingly the dependence is Boltzmann like and could be represented by the equation

$$\tau = \tau_0 \exp \left(-E_a/kT \right) \quad (5.1)$$

from which E_a the activation energy can be determined.

A preliminary investigation was carried out by Ball² in this laboratory to see if a similar effect could be observed in non-stoichiometric compounds. In this case a second oxidation state would have to be produced such that it occupied an identical lattice site to that of the original oxidation state. The system chosen was anhydrous europium(III) chloride which had been depleted in chloride so that it contained Eu(II) in a host Eu(III) lattice. Care had to be taken to ensure the lattice did not break down and the Eu(II) form a separate phase. It was found that this system would only tolerate a small deviation from stoichiometry so that a large Eu(II) population was not observed as in the previous example; however a change in isomer shift was observed and this seemed likely to be due to electron hopping. Jenden³ examined the system in more detail and found values of τ using the theoretical model hence evaluating the activation energy for electron hopping in the system.

The method used to find the values of τ lacks precision as the goodness of fit of the theoretical curve to the experimental data was determined by superimposing one on to the other. Hence this method can only give the order of magnitude of the activation energy, but nevertheless it showed very clearly the electron hopping effect. Berkooz et al¹ found that the electrical conductivity followed the same relationship with temperature as the relaxation time and that both lead to the same activation energy, the activation energy can be determined from the electrical conductivity measurements with greater precision. The work described here consists of supporting conductivity data for the Mössbauer studies on the chloride system and the extension of the system to include Mössbauer and conductivity data for non-stoichiometric europium bromide. Comparisons can be made between the systems due to their broad similarity and slight differences.

5.2 Mechanisms by which Non-stoichiometric Phases Arise

Much of the work carried out in this laboratory and described in this and previous theses was performed on non-stoichiometric phases. A description of the formation of these phases will give a better understanding of the conditions leading to the observations of electron hopping.

Consider a stoichiometric compound MX in equilibrium with the vapours of its constituents at pressures $P_x(0)$ and $P_y(0)$. The formation of a non-stoichiometric phase can occur by several mechanisms. If the vapour pressure of one of the constituents, X is raised then X^- will be incorporated into the lattice in either interstitial positions leading to M being oxidised to maintain overall charge neutrality or excess X^- can be considered to build up on the surface of the solid creating cation vacancies which may diffuse into the crystal. If the vapour pressure of X is reduced the X^- will leave the lattice creating anion vacancies and usually an equivalent amount of reduced cations to maintain overall charge neutrality. Alternatively the reduced cation may move into a interstitial site and the cation vacancy produced together with the anion vacancy may diffuse to the surface leading to the surface retreating. These processes can be described thermodynamically by a treatment adapted for Frenkel and Schottky defects in a stoichiometric compound. For the Frenkel⁶ case the ratio of the pressure of the vapour described as a function of the deviation from stoichiometry $P_x(x)$ to the equilibrium pressure for stoichiometry $P_x(0)$ is given by:

$$\frac{P_x(x)}{P_x(0)} = \frac{1 + x^2 + x(x^2 + 4d^2)^{\frac{1}{2}}}{2d^2} \quad (5.2)$$

where d is the intrinsic disorder of the crystal given by:

$$\frac{n_F}{N}$$

the ratio of Frenkel defects to the total number of cation sites. The deviation from stoichiometry is given by x where

$$x = \frac{n_v - n_i}{N}$$

n_v = the number of vacancies

n_i = the number of interstitial sites.

The equation shows that the greater the intrinsic disorder the smaller the pressure change required to produce a deviation from stoichiometry. This treatment only considers the non-stoichiometric defect to be confined to one site. A real system would be far more complex requiring a more sophisticated treatment. However if one defect predominates then some useful conclusions may be drawn from the model. The range of non-stoichiometry will be limited by the energy required to form a defect; by the difference in energy between the two oxidation states of the cation involved in the defect formation. Furthermore the difference in the ionic radii of these two oxidation states must be small to reduce strain in the lattice and reduce the tendency for two separate phases to form. Deviations from stoichiometry involving excess cation, from a qualitative view, would tend to destabilize the non-stoichiometric compound so reducing the range. Excess anion would tend to stabilize the compound as the oxidation of the cation will increase the Coulombic attraction between the ions as well as reducing the cationic size. The limit to the range of non-stoichiometry is governed by the interactions between defects. For excess cation it has been shown that

$$\frac{P_x(x)^{\frac{1}{2}}}{P_x(0)} = \frac{\theta_i}{(1-\theta_i)} \frac{(1-d)}{d} \exp \left\{ \frac{-2(d-\theta_i)W_{ii}}{kT} \right\} \quad (5.3)$$

θ_i is the ratio of interstitial cation to anion sites and W_{ii} is the energy of interaction between one interstitial cation and another. A critical temperature, T_c , can be associated with this energy of interaction such that

$$T_c = \frac{W_{ii}}{2k}$$

Above T_c there is only one composition for each value of vapour pressure which produces a single non-stoichiometric phase. Below T_c there are three solutions only one of which is physically meaningful. The range of non-stoichiometry is seen to be determined by the intrinsic disorder, the defect interaction energy and the temperature.

5.3 The Observation of Electron Hopping using the Mössbauer Effect and the Choice of System.

The phenomenon of 'electron hopping' is observed through the behaviour of the relaxation time τ with temperature. The relaxation time can be observed by the Mössbauer effect because of the difference between τ and the life time of the nuclear excited state as stated in section 5.1. Electron hopping is observed when τ is approximately equal to or longer than the life time of the excited ^{151}Eu nucleus. If τ is shorter this corresponds to the situation in which the Mössbauer atom 'sees' an average

environment leading to a single peak being observed in the Mössbauer spectrum. The isomer shift of this single peak in this case is a weighted average of the isomer shifts of the peaks in the low temperature spectrum, this is different from other relaxation processes where the isomer shift of the high temperature spectrum would be a weighted average of the areas of the low temperature peaks. The areas of the peaks would depend upon the recoil-free fractions of the ions in each oxidation state at low temperatures which would be different. However at high temperatures where the nucleus experiences an average environment there would only be one type of ion with an intermediate oxidation state or valence. The isomer shift should show a dependency on this valence since it reflects the electronic environment of the nucleus. The ions in the high and low temperature cases must all occupy identical lattice sites otherwise this change in environment will have to be taken into account. To observe electron hopping by Mössbauer spectroscopy several factors must be taken into account. The temperature range for observation is determined by the life time of the excited nucleus ie the relaxation time must be equal or greater than this time. For electron hopping to take place the electron must surmount an energy barrier; the energy required to do this is from the thermal energy in the system. Hence for a given nucleus the observation of electron hopping is largely dependent upon the chemical compound in allowing the process to occur in a convenient temperature range. Observation of electron hopping in a non-stoichiometric phase imposes more conditions, the general conditions are set out below

1. For observation using the Mössbauer effect, the usual constraints are required, especially a high bulk modulus so that measurements can be made over a large temperature range.
2. The range of non-stoichiometry of the crystal must be suitably large to allow adequate population of the minority state without the occurrence of phase separation. The minority ions must remain on identical lattice sites to those of the host ion.
3. In order to fulfil condition 2 the difference in size of the ion in the two oxidation states must be small, causing as little strain to the lattice as possible.
4. The energy difference between the two oxidation states must be small to minimise the activation energy for hopping and that for the formation of defects associated with the non-stoichiometric phase.
5. If the non-stoichiometric phases is formed by thermal decomposition as it is in the present case, the decomposition must occur at a higher temperature than the high temperature limit at which the electron hopping is observed.
6. The isomer shifts of each oxidation state in the low temperature regime must be well separated compared with the resonance line widths, allowing good resolution of the spectrum.

The non-stoichiometric europium halides appear to fulfil these conditions. Europium seems a suitable cation as the ionic radii for the two oxidation states are similar ($\text{Eu}^{3+} / \text{Eu}^{2+} = 0.95\text{\AA} / 1.09\text{\AA}$) and the energy difference between each oxidation state is small. The latter is seen from the small electrode potential $E_0(\text{Eu}^{3+} / \text{Eu}^{2+}) = -0.43\text{V}$. The isomer shift difference between Eu(III) and Eu(II) is large compared with the natural line width. The non-stoichiometric europium chloride system was chosen² as it was known that thermal decomposition occurred at temperatures of about 600K; this is well below the decomposition temperature for the europium fluoride system⁷. Non-stoichiometric europium fluoride compounds do not show electron hopping i.e. Mössbauer measurements did not show a time averaged spectrum. It was considered that if europium(III) chloride is more easily decomposed (implying that the energy difference between the two types of ions in the lattice is lower in the chloride case) then the activation energy for electron hopping will follow suit. Non-stoichiometric europium bromide should also be suitable if the reasoning is correct and so might the iodide system if anhydrous europium(III) iodide exists.

5.4 Relaxation Effects and Mössbauer Spectra

A relaxation model is used to quantify the temperature dependence of the Mössbauer spectra. It will be useful to describe some of the theoretical principles behind the interpretation of relaxation effects especially with respect to the Mössbauer effect. Mössbauer studies have centred

around investigations of electric and magnetic hyperfine interactions and the electron-nucleus interaction leading to the isomer shift. In many cases the time independent-features have been emphasized. However, many systems such as paramagnetic hyperfine interactions are time dependent. Models for calculating relaxation in Mössbauer spectra have been developed and all require simplifying procedures. Two of interest are the stochastic spin flip relaxation model and the perturbation theory. The former is used by Wickman et al^{4,5}; Blume and Tjon⁸; and Van der Woude and Dekker⁹ whilst the latter is associated with Kagan and Affanas'ev¹⁰; Bradford and Marshal¹¹ and Gabriel et al¹². The stochastic spin flip model of Wickman et al is used to describe the temperature dependence of the spectra reported in this thesis. The method is general and has the advantage that no detailed description of a mechanism is required as we are only considering the effect of the nucleus on an electronic transition.

The model considers the relaxation of electronic spin of a paramagnetic ion. This may proceed via two mechanisms, namely a spin-spin interaction which is temperature independent or a spin-lattice interaction which is temperature dependent. A

Boyle and Hall¹³ suggested that under certain conditions magnetic hyperfine effects could be observed in paramagnetic crystals. Later such effects were found

experimentally by Wertheim et al¹⁴ in Fe³⁺ ions in corundum (Al₂O₃). Such effects are time dependent since in a paramagnetic ion the orientation of each individual electronic spin may vary but the total spin expectation value will be zero. If the relaxation time becomes long with respect to the nuclear Larmor precession frequency then the effective spin will no longer be zero and magnetic hyperfine effects will be observed.

The Hamiltonian for a paramagnet may be written as a sum of operators

$$H_{\text{eff}} = H_z + H_{\text{CR}} + H_{\text{mhf}} + H_Q + H_N \quad (5.4)$$

where the terms represent the Zeeman, crystal field, magnetic hyperfine, Quadrupole and nuclear interactions respectively. The first two terms H_z and H_{CR} dominate so they may be 'diagonalized' and the remaining terms treated as perturbation. A system with a number of electronic levels represented by the quantum number J is produced. If $J = 0$ then for a non-degenerate system there is no hyperfine field; if $J \neq 0$ then an effective spin S is defined and the degeneracy of the level is given by $2S + 1$. The magnetic hyperfine interaction can be written

$$m_{\text{hf}} = A'_x S'_x I_x + A'_y S'_y I_y + A'_z S'_z I_z \quad (5.5)$$

where A'_i is the effective hyperfine tensor

S'_i is the effective spin

I_i is the nuclear spin operator

This may be simplified further by considering uni-axial symmetry where $A_z \gg A_x, A_y$

$$\begin{aligned} H_{\text{mf}} &= A_z^1 S_z^1 I_z \\ &= g_N \beta_N H_{\text{eff}} I_z \end{aligned} \quad (5.6)$$

where g_N , β_N and H_{CH} are the Lande¹ g factor the Bohr magneton and effective magnetic field at the nucleus can be written

$$H_{\text{eff}} = \frac{A_z S_z}{g_N \beta_N} \quad (5.7)$$

and in this system $S_z = \pm \frac{1}{2}$

so

$$H_{\text{eff}} = \frac{\pm A_z}{2g_N \beta_N} \quad (5.8)$$

The electron in this system has an equal probability of being in either orientation ie a two fold degeneracy.

$$\langle + | S_z | - \rangle = - \langle - | S_z | + \rangle$$

or

$$\text{or } \langle S_z \rangle = 0$$

unlike the case for ferromagnetism where

$$\langle S_z \rangle \neq 0.$$

Relaxation between $\langle + |$ and $| - \rangle$ leads to a reversal in the direction of the effective magnetic field as seen from equation (5.8). During the life time of the excited nuclear state these transitions may occur many times so that $\langle S_z \rangle = 0$. No net internal field is experienced so the Mössbauer spectrum records a single line for that transition. If the relaxation time is long with respect to the excited state nuclear life time then $\langle S_z \rangle \neq 0$ so a magnetic hyperfine interaction is experienced by the nucleus. This is known as the static case. Wickmann et al^{4,5} develop the model and show that the conditions outlined are the same for proton exchange in N.M.R. Modified Bloch equations are used as in a theory developed by Gutowsky, McCall and Slichter¹⁵ (G.N.S. theory) for which the solutions are well known. In the context of Mössbauer spectroscopy the solution to the equation is :

$$I(w) = -C [(1 + \tau \Gamma) P + QR] / (P^2 + R^2) \quad (5.9)$$

$$P = \tau \left\{ \Gamma^2 - (\Delta - w)^2 + \delta^2 \right\} + \Gamma$$

$$Q = \tau \left\{ \Delta - w - (p_1 - p_2) \delta \right\}$$

$$R = (\Delta - w) (1 + 2\tau\Gamma) + (p_1 - p_2) \delta$$

$$\Delta = \frac{1}{2} (w_A + w_B)$$

$$\delta = \frac{1}{2} (w_A - w_B)$$

C is the relative intensity of the Mössbauer transition

w_A and w_B are the frequencies of the two lines.

Γ is the natural line width.

τ is the relaxation time.

p_A and p_B are the relative populations of the two states A and B such that $p_A + p_B = 1$.

5.5 Experimental

Non-stoichiometric europium chloride and europium bromide phases were prepared and chemically analysed as described in chapter 3. Further characterization was obtained from running x-ray powder diffraction experiments on the samples. Mössbauer spectra were recorded on successful samples between 77K and room temperature. The experimental data obtained from the spectra were compared with spectra generated from the theoretical model (Equation 5.9) by superimposing the experimental and theoretical spectra. From this the relaxation time τ could be determined for a given sample at a given temperature. Electrical conductivity measurements were made on pellets as described in chapter two. The activation energies derived from the Mössbauer and electrical conductivity experiments were compared.

5.6 Results and Discussion

The work described in this chapter is chiefly concerned with the non-stoichiometric europium bromide system since the non-stoichiometric chloride system has been the subject of a previous study^{2,3}. However, the electrical conductivity experiments on non-stoichiometric europium chloride carried out during the course of this work have revealed a transition not encountered in previous work. Therefore Mössbauer data has been accumulated on the chloride system for comparison with that previously reported³.

The structures of anhydrous europium(III) chloride and europium(III) bromide are similar. Both share the same type of molecular unit but differ in packing. The crystal structures are shown in figure 5.1, the molecular unit in (A) with the packing diagrams for EuBr_3 and EuCl_3 in figures 5.1 (B) and 5.1 (C) respectively. (Note that similarly shaded circles lie in the same plane). The EuCl_3 structure is of the Y(OH)_3 or UCl_3 - type with the space group $P6_3/m$ in Herman Manguin notation. The cell is hexagonal consisting of bimolecular units. Each europium is surrounded by nine chloride ions, six at $2.7 \overset{\circ}{\text{Å}}$ and three at $3.0 \overset{\circ}{\text{Å}}$, the closest Eu-Eu distance is $3.75 \overset{\circ}{\text{Å}}$ all distances being approximate.

The EuBr_3 structure is of the PuBr_3 type with a space group Cmmm . The orthorhombic structure consists of tetramolecular units with each europium surrounded by nine bromide ions, six at $3.1 \overset{\circ}{\text{Å}}$ and three at $4.6 \overset{\circ}{\text{Å}}$, the closest Eu-Eu distance is $6.7 \overset{\circ}{\text{Å}}$, all distances are approximate.

Lattice parameters are presented in tables 5.1 and 5.2; these consist of previously published results as well as those found from the present work. Few parameters are available for EuBr_3 as little work has been recorded since the successful preparation by Haschke and Eick¹⁶. The parameters found in the present work are slightly in error as europium absorbs the $\text{CuK}\alpha$ radiation used to produce the

x-ray diffraction patterns. Corrections can be made¹⁷ but as the quality of the diffraction patterns is poor and the intensities of the lines are such that only low diffraction angles can be measured no corrections were made. A more suitable radiation is the MoK α line but a Mo target was not available to the author. A

The diffraction patterns can be used to establish the authenticity of the samples and to ensure single phases are present. Jenden³ and Ball² claim that an increase in cell volume occurs with increasing defect concentration, this can be expected as the Coulombic forces within the lattice will decrease as Eu(III) is reduced to Eu(II) as a result of halide depletion. Similar trends have been observed in the present work but no quantitative analysis can be offered due to the lack of precision of the lattice parameters. D

The Mössbauer data for stoichiometric EuCl₃ and EuBr₃ are shown in tables 5.3 and 5.4 respectively. Many previously reported results used monoclinic Eu₂O₃ as a reference. However since anhydrous EuF₃ has been used as the reference material for isomer shift values reported in this thesis, isomer shifts will be reported relative to both for comparison. The isomer shift difference between monoclinic Eu₂O₃ and EuF₃ used is that determined by Gerth et al¹⁸ and is -0.59 ± 0.02 mms⁻¹. Later work by Large et al¹⁹ finds the isomer shift of EuF₃ relative to Eu₂O₃ to be -1.060 ± 0.003 mms⁻¹ C

and the authors experience supports this figure. However since Jenden has used Gerth's result to convert isomer shifts found relative to EuF_3 to shifts relative to Eu_2O_3 the same practice will be continued here.

The agreement found between isomer shifts of 'stoichiometric' europium(III) chloride samples is generally poor. This is because chlorine deficient samples are known to have a different isomer shift to the stoichiometric sample; this will account for small differences in the isomer shifts. The results found in the present work are in reasonable agreement with those of Jenden³, both being obtained in the same laboratory. However good agreement is not found with the result reported by Gerth et al¹⁸ probably due to the different reference materials used. Similar disagreement is found with the isomer shifts of europium(III) bromide, those found of the course of the present work are in good agreement with each other. The isomer shift reported by Gerth et al differs; this is possibly due to the different reference material or the sample preparation. The isomer shift reported is similar to that for $\text{EuBr}_3 \cdot n\text{H}_2\text{O}$ reported in chapter 4.

A
B

Isomer shifts for depleted europium chloride and europium bromide samples are shown in tables 5.5 and 5.6 respectively. The chloride data are mainly from previous work and are shown for comparison. The isomer shifts for each sample are given

at low and high temperatures, the isomer shift is seen to increase with decreasing temperature. A large variation in absolute values of isomer shifts is evident for the chloride samples, this is possibly due to more than one non-stoichiometric phase being formed. The bromide data is presented in the same way although good agreement is observed for isomer shifts of different samples at a given temperature. Figure 5.2 shows the isomer shifts for two non-stoichiometric europium bromide samples plotted against temperature. The average isomer shift for stoichiometric europium(III) bromide is presented as a straight line bounded by limits shown as dotted lines. The data show there is good correlation of isomer shifts for different samples with temperature. Although the errors associated with each measurement are relatively large there is a definite change in isomer shift with temperature the magnitude of which is larger than the experimental error over the temperature range studied. The second order Doppler shift will lead to an increase in isomer shift with a decrease in temperature as shown in chapter 2. However this effect will occur with stoichiometric samples and on consideration of the data presented in table 5.4 no such trend is observed. It may be concluded that the second order Doppler shift is smaller than the experimental error associated with the isomer shifts and that the temperature dependence of the isomer shifts is not due to this effect; this is not surprising as the cryostat is designed to minimise the effect.

ie
scal
sample -
heterogeneity
of phases

Mössbauer spectra of stoichiometric and depleted europium(III) chlorides and bromides are presented in figures 5.3 - 5.10 at ambient and approximately liquid nitrogen temperatures. For samples where electron hopping is observed the absorption peak profiles will be slightly distorted from true Lorentzian profiles. This is reflected in the goodness of fit parameter χ^2 being in the region of 1.1 to 1.2 as opposed to 1.0 for stoichiometric samples. The distortion of the profiles should be similar for all samples thus allowing the comparison of isomer shifts at various temperatures as in figure 5.2. The sample having the largest depletion in bromine is $\text{EuBr}_{2.84}$, the spectrum at 77K (figure 5.10) shows a peak due to Eu(II) but the spectrum recorded at 273K (figure 5.9) does not. The recoil-free fractions for the europium bromide species are significantly lower than those for the equivalent chlorides and observation of the minority europium(II) bromide species is difficult. The accumulation time for the $\text{EuBr}_{2.84}$ spectrum at 77K was four days. Isomer shifts of europium(II) bromide are presented in table 5.7 and it is seen that the isomer shift for the Eu(II) species in $\text{Eu Br}_{2.84}$ is more positive than for the other samples. This is to be expected for samples exhibiting electron hopping. Samples with a gross deviation from stoichiometry were prepared to find a lower limit to the non-stoichiometric range for the bromide system. An example of such a sample is $\text{EuBr}_{2.47}$ with isomer shifts for Eu(III) and Eu(II) of 0.29 ± 0.05 mms and -13.3 ± 0.1 mms⁻¹

respectively. The Eu(III) isomer shift is not the same as that for stoichiometric EuBr_3 and does not lie in the range of isomer shifts of samples exhibiting electron hopping. This would indicate a different non-stoichiometric range or maybe more than one. The europium(III) chloride sample $\text{EuCl}_{2.96}$ although depleted does not exhibit a temperature dependent isomer shift; this is thought to be due to traces of EuOCl as a separate phase to the bulk sample of EuCl_3 . A

The relaxation times for electron hopping can be determined from the Mössbauer spectra of the samples obtained at various temperatures. Theoretical spectra were generated using the equation 5.9 and compared with the variable temperature spectra obtained from the samples. One europium chloride sample $\text{EuCl}_{2.89}$ was treated in such a way to compare the calculated activation energies with those found by Jenden. More attention was paid to the low temperature region following the results obtained from electrical conductivity measurements. Figure 5.11 shows the experimental data (error bars) and the theoretically generated spectra (solid curve). The goodness of fit is judged by eye. From these spectra the relaxation times were determined for various temperatures. Figure 12 shows spectra for $\text{EuBr}_{2.95}$ treated in the same way. The values of τ were then used to find the activation energies for hopping using equation 5.1. Plots of $\log_{10} \tau$ against reciprocal temperature were made and the activation energies determined from the gradients of the lines. Figures 5.13 and 5.14 show the $\log_{10} \tau$ versus reciprocal temperature for B

$\text{EuCl}_{2.96}$ and $\text{EuBr}_{2.95}$ respectively. Only one europium bromide sample was used to determine the activation energy for electron hopping as the consistency of isomer shift with temperature between bromide samples indicated that similar activation energies would be found for each sample.

The $\log_{10} \tau$ versus reciprocal temperature plots for the chloride and bromide systems are similar. The plots show two regions separated at a temperature T_k ; two activation energies for each sample may be determined one above this temperature and one below. The data derived from these plots are shown in table 5.8 and show the activation energies for both systems below the temperature T_k to be much lower than those above. The errors associated with the results are large and the activation energies may be obtained with greater precision from electrical conductivity measurements. The treatment of the data from the Mössbauer spectra enables the temperature dependence to be quantified and provides information which may be compared with that found from other sources.

Electrical conductivity measurements, as has already been mentioned, provide a method for determining the activation energies. Berkooz' noted the similarity of the temperature dependence with that of the relaxation time which may be written

$$\sigma = \sigma_0 \exp \left\{ -E_a / kT \right\} \quad (5.10)$$

where σ is the electrical conductivity at a temperature T and E_a is the activation energy. Figures 5.15 and 5.16 show plots of $\log_{10} \sigma$ versus reciprocal temperature for europium chlorides and bromides respectively. They are similar to the $\log_{10} \tau$ vs reciprocal temperature plots and show two regions separated by a temperature T_k . The activation energies are found in the same way as for the relaxation time results and are presented in table 5.9. The conductivity is seen to decrease with decreasing temperature and the absolute values are reasonably high; this suggests semiconductor like properties for the compounds. The data derived from the electrical conductivity measurements are comparable to that derived from the Mössbauer data. All the activation energies below T_k are similar for both the chlorides and bromides, but more variation exists with those found above T_k . Jenden's³ values for the activation energies for europium chloride samples found from Mössbauer spectra are 0.07 ± 0.03 eV and 0.04 ± 0.03 eV. Both values refer to the high temperature regime as insufficient data were available to observe the low temperature region.

The results may be summarized as follows

Depleted europium chloride and europium bromide retain the crystal structure of the appropriate stoichiometric anhydrous europium(III) halide. The crystal structures of europium(III) chloride and europium(III) bromide are similar.

Electron hopping is observed in depleted europium halide compounds by Mössbauer spectroscopy and the activation energies are derived from $\log_{10} \tau$ vs reciprocal temperature plots. Electrical conductivity measurements confirm the activation energies determined from the Mössbauer data and a change in behaviour at a characteristic temperature T_k . The activation energies for both the chloride and bromide system are similar while the characteristic temperature T_k is approximately 20K higher in the bromide case than that for the chloride system.

The change in activation energy at the characteristic temperature T_k has been studied in other rare earth systems exhibiting electron hopping^{22,23,24} and has been attributed to the formation of long range charge ordering as proposed by Carter²⁵. No evidence of magnetic structure can be found from the Mossbauer spectra of the compounds in the temperature region studied although at lower temperatures this might occur. Electron hopping appears to continue below the ordering temperature with the activation energy being reduced considerably. The higher transition temperature and lower thermal decomposition temperature for the bromide system when compared with the chloride system indicates the higher intrinsic disorder of the former.

The activation energies for both the chloride and bromide systems are similar this indicates that the anions have little to do with the effect directly but might indirectly through lattice effects. In the electron hopping model an electron

from a Eu^{2+} 'hops' to a Eu^{3+} site, the Coulombic energy of each site will change but the associated energy of the pair of sites remains the same. When an ion changes its oxidation state the lattice undergoes modification to accommodate the change in ionic radii and charge density; in this case the lattice will expand to accommodate an Eu^{2+} . The valence change is strongly coupled to lattice phonons so that the electron hopping process is temperature driven, random and will involve all cation sites. One might expect that the differences between the europium chloride and bromide lattices will lead to a difference in activation energy between the two systems, this is not the case so it will be fruitful to consider what happens to the electron once it has left a Eu^{2+} site. In recent years the so called mixed valence compounds have received much attention, they are a general set of compounds where an element can exist in two oxidation states. Varma²⁶ and Batlogg et al²⁷ have placed mixed valence compounds into three categories.

- i Homogeneous mixed valence compounds where all the cation sites are equivalent and there are localized band states at the Fermi energy. Such compounds exhibit metallic conductivity and the valence fluctuations are temperature independent with relaxation times in the range $10^9 - 10^{15} \text{ Hz}$. Examples are SmB_6 ²⁸ where an intermediate valence is observed at all temperatures and SmS ²⁹ undergoes a first order phase transition under pressure at 6Kbar where an intermediate valence is observed.

- ii Inhomogeneous mixed valence compounds with equivalent cation sites. Here there are no localized states at the Fermi energy and semiconductor like behaviour is observed. The valence fluctuations are temperature driven with relaxation times in the range of $0-10^{11} \text{H}_z$ at 300K. Two distinct valencies may be observed at sufficiently low temperatures but also an intermediate valence at sufficiently high temperatures. The terms mixed valence and intermediate valence depend on the time scale of the measurement technique being used. Examples are Eu_3S_4 and $\text{Sm}_3\text{S}_4^{22}$ where electron hopping similar to that proposed for the europium halide samples is observed. A
- iii Inhomogeneous mixed valence compound within equivalent cation lattice sites. These compounds have a static and regular distribution of cations of different valence. An example of such a compound is Eu_3O_4 where Eu^{2+} and Eu^{3+} occupy different lattice sites, no fluctuating valence is observed for this category. D

The compounds studied in this work clearly belong to category (ii) as can be seen from the temperature dependent Mössbauer spectra. C

The requirement for valence fluctuation is that the two bonding states are nearly degenerate. In this case the states are $\text{Eu}^{2+} (4f^7)$ and $\text{Eu}^{3+} + e (4f^6 + e)$ and the electron is considered to be promoted into a 5d6s conduction band. The D

activation energy is dependent upon the energy gap between the 4f shell and the 5d6s conduction band and so will be similar for all systems with the same cation. The energy gap between the highest 4f electron energy and the bottom of the conduction band may be varied by either the crystal field splitting of the 5d electron energies or the density of states in the 4f shell. The crystal field splittings associated with the rare earths are small and in general spherical symmetry is assumed³⁰. The density of states will be directly affected by the crystal lattice as it is determined by the valence electron concentration in the lattice³¹. The europium concentration in the lattice is proportional to the valence electron concentration and will give an average value due to two oxidation states of europium being present. The anions play no part in the valence electron concentration since the $3s^2 3p^6$ and $4s^2 4p^6$ electrons for chloride and bromide respectively are much too low in energy. If the europium concentration in the chloride and bromide lattices are calculated they are found to be approximately equal as the values are $(8.95 \pm 0.05) \times 10^{-30} \text{ \AA}^{-3}$ and $(8.20 \pm 0.04) \times 10^{-30} \text{ \AA}^{-3}$ respectively; the difference is about 9%. These values may be compared with those of Eu_3S_4 and Sm_3S_4 ; they are $3.24 \times 10^{-30} \text{ \AA}^{-3}$ and $3.19 \times 10^{-30} \text{ \AA}^{-3}$ respectively. The activation energies for Eu_3S_4 and Sm_3S_4 (0.163 and 0.142eV respectively) above the transition temperature are much higher than those associated with depleted EuCl_3 and EuBr_3 (approximately 0.08eV) as could be predicted by the lower europium concentrations in the lattice.

The similarity between the activation energy values for Eu_3S_4 and Sm_3S_4 is due to both compounds having the same crystal structure with almost identical lattice parameters. The valence electron density for Sm will be lower than that for Eu but the conduction band edge will also be expected to be lower in energy.

In conclusion the non-stoichiometric phases of europium chloride and europium bromide are category (ii) mixed valence compounds. The valence fluctuations have been observed by variable temperature Mossbauer spectroscopy with activation energies being derived from this and electrical conductivity data. The process is temperature driven involving all cation sites so that the conductivity depends upon the mobility of the electron rather than the charge carrier concentration which remains constant. A

The activation energy is largely dependent upon the valence electron density in the lattice, the higher the concentration the lower the activation energy. Differences exist between the electron concentrations of the chloride and bromide systems which have not been detected in the calculated activation energies. The data presented in table 5.10 is generally consistent but includes some spurious results, the cause of the variation is not known but the associated errors for the values are high. More precise measurements might well reveal the small difference but more precise measurement will require more careful control of the purity S

of the samples. The electrical conductivity measurements are more precise than those by the Mössbauer technique but will be affected by impurities to a greater extent. Comparison of the depleted samples with stoichiometric samples is difficult since extrinsic, thermally generated, crystal defects will always be present leading to the effects reported here. While these effects will be greatest in electrical conductivity measurements they will be less noticeable to Mössbauer spectroscopy as a larger concentration of minority ions are required for their detection. The exact nature of the charge ordering and the part played by the anion vacancies in the process are not known. Low temperature x-ray diffraction measurements would be helpful to determine whether any change in symmetry has occurred or any large contraction of the lattice. Some explanation of the temperature dependent behaviour of the europium chloride and bromide compounds has been possible but there are still more properties to be examined.

Table 5.1

Lattice Parameters for Europium(III) Chloride

Material	$\overset{\circ}{a}$ (Å)	$\overset{\circ}{c}$ (Å)	reference
EuCl ₃	7.375 ± 0.001	4.1323 ± 0.0005	20
EuCl ₃	7.370 ± 0.002	4.137 ± 0.004	21
EuCl ₃	7.287 ± 0.002	4.071 ± 0.003	2
EuCl _{2.945}	7.38 ± 0.002	4.102 ± 0.002	2
EuCl _{2.95}	7.319 ± 0.005	4.010 ± 0.007	3
EuCl _{2.85}	7.367 ± 0.005	4.050 ± 0.005	3
EuCl _{2.99}	7.45 ± 0.01	4.304 ± 0.008	} present work
EuCl _{2.89}	7.35 ± 0.01	4.133 ± 0.005	

Lattice parameters for Europium(III) Bromide

Table 5.2

Material	$\overset{\circ}{a}$ (Å)	$\overset{\circ}{b}$ (Å)	$\overset{\circ}{c}$ (Å)	reference
EuBr ₃	12.66 ± 0.02	4.013 ± 0.005	9.12 ± 0.01	16
EuBr _{2.99}	12.86 ± 0.02	4.045 ± 0.003	9.17 ± 0.01	} present work
EuBr _{2.97}	12.99 ± 0.02	4.057 ± 0.003	9.20 ± 0.01	
EuBr _{2.95}	12.96 ± 0.02	4.096 ± 0.005	9.19 ± 0.07	

Table 5.3

Mössbauer Isomer Shifts for Europium(III) Chloride

Sample	Temperature (K)	Isomer Shift (mms^{-1})		Reference
		Relative to Eu_2O_3	Relative to EuF_3	
EuCl_3	293	-0.29 ± 0.09	0.30	18
EuCl_3	293	-0.34 ± 0.08	0.25	2
$\text{EuCl}_{2.99}$	293	-0.41	0.18 ± 0.01	present
	77	-0.39	0.20 ± 0.01	
$\text{EuCl}_{2.96}$	293	-0.34	0.25 ± 0.02	work
	77	-0.37	0.22 ± 0.01	

Table 5.4

Mössbauer Isomer Shifts for Europium(III) Bromide

Sample	Temperature (K)	Isomer Shift (mms^{-1})		Reference
		Relative to EuF_3		
EuBr_3	293	0.53 ± 0.05		18
EuBr_3	223	0.36 ± 0.02		present
	77	0.35 ± 0.03		
$\text{EuBr}_{2.99}$	293	0.34 ± 0.06		work
	77	0.31 ± 0.03		

Table 5.5

Mössbauer Isomer Shifts for Depleted Europium(III)
Chloride Samples

Sample	T(K)	Isomer Shift (mms^{-1})		reference
		relative to Eu_2O_3	relative to EuF_3	
$\text{EuCl}_{2.85}$	298	-0.45 ± 0.05	0.14	3
	78	-0.44 ± 0.05	0.15	
$\text{EuCl}_{2.95}$	298	-0.42 ± 0.06	0.17	3
	78	-0.24 ± 0.02	0.35	
$\text{EuCl}_{2.89}$	273	-0.53	0.06 ± 0.02	present work
	93	-0.36	0.23 ± 0.03	

Table 5.6

Mössbauer Isomer Shifts for Depleted Europium(III)
Bromide Samples (present work)

Sample	T(K)	Isomer Shift (rel. EuF_3) (mms^{-1})
$\text{EuBr}_{2.97}$	273	0.24 ± 0.05
	83	0.31 ± 0.03
$\text{EuBr}_{2.96}$	291	0.26 ± 0.05
	235	0.23 ± 0.04
$\text{EuBr}_{2.95}$	291	0.24 ± 0.05
	83	0.32 ± 0.04
$\text{EuBr}_{2.84}$	273	0.23 ± 0.04
	77	0.34 ± 0.02

Table 5.7

Mössbauer Isomer Shifts for Europium(III) Bromide Samples

Sample	Temperature (K)	Isomer Shift (rel. EuF_3) (mms^{-1})
EuBr_2	77	-13.17 ± 0.03
$\text{EuBr}_{1.93}$	77	-13.19 ± 0.03
$\text{EuBr}_{1.99}$	223	-13.4 ± 0.1
	93	-13.42 ± 0.03
$\text{EuBr}_{2.84}$	77	-13.0 ± 0.1

Table 5.8

Activation Energies and Transition

Temperatures (T_k) determined from the Mössbauer Spectra

Sample	T_k (K)	Activation Energy (ev)	
		$T > T_k$	$T < T_k$
$\text{EuCl}_{2.89}$	198 ± 2	0.08 ± 0.02	0.007 ± 0.004
$\text{EuBr}_{2.95}$	222 ± 2	0.04 ± 0.02	0.002 ± 0.002

Table 5.9

Activation Energies and Transition Temperatures.

 (T_k) Determined from the Electrical Conductivity Data.

Sample	T_k (K)	Activation		Energy (eV)	
		$T > T_k$		$T < T_k$	
$\text{EuCl}_{2.99}$	197 ± 1	0.048 ± 0.003		0.007 ± 0.005	
$\text{EuCl}_{2.96}$	221 ± 2	0.083 ± 0.006		0.007 ± 0.005	
$\text{EuBr}_{2.99}$	225 ± 2	0.076 ± 0.005		0.008 ± 0.005	
$\text{EuBr}_{2.95}$	223 ± 2	0.086 ± 0.006		0.008 ± 0.005	

Table 5.10

Collected Activation Energies and Transition Temperatures found from Mössbauer Effect and Electrical Conductivity Measurements.

Sample	T_k (K)	Activation		Energy (eV)		Method
		$T > T_k$		$T < T_k$		
$\text{EuCl}_{2.85}^3$	-	0.07 ± 0.03		-		M.E
$\text{EuCl}_{2.89}$	198 ± 2	0.08 ± 0.02		0.007 ± 0.004		M.E
$\text{EuCl}_{2.95}^3$	-	0.04 ± 0.03		-		M.E
$\text{EuCl}_{2.96}^5$	221 ± 2	0.083 ± 0.006		0.007 ± 0.005		E.C
$\text{EuCl}_{2.99}$	197 ± 1	0.048 ± 0.003		0.007 ± 0.005		E.C
$\text{EuBr}_{2.95}$	223 ± 2	0.086 ± 0.006		0.008 ± 0.005		E.C
$\text{EuBr}_{2.95}$	222 ± 2	0.04 ± 0.02		0.002 ± 0.002		M.E
$\text{EuBr}_{2.99}$	225 ± 2	0.076 ± 0.005		0.008 ± 0.005		E.C

Figure 5.1

Crystal Structures of Europium(III)
Chloride and Europium(III) Bromide

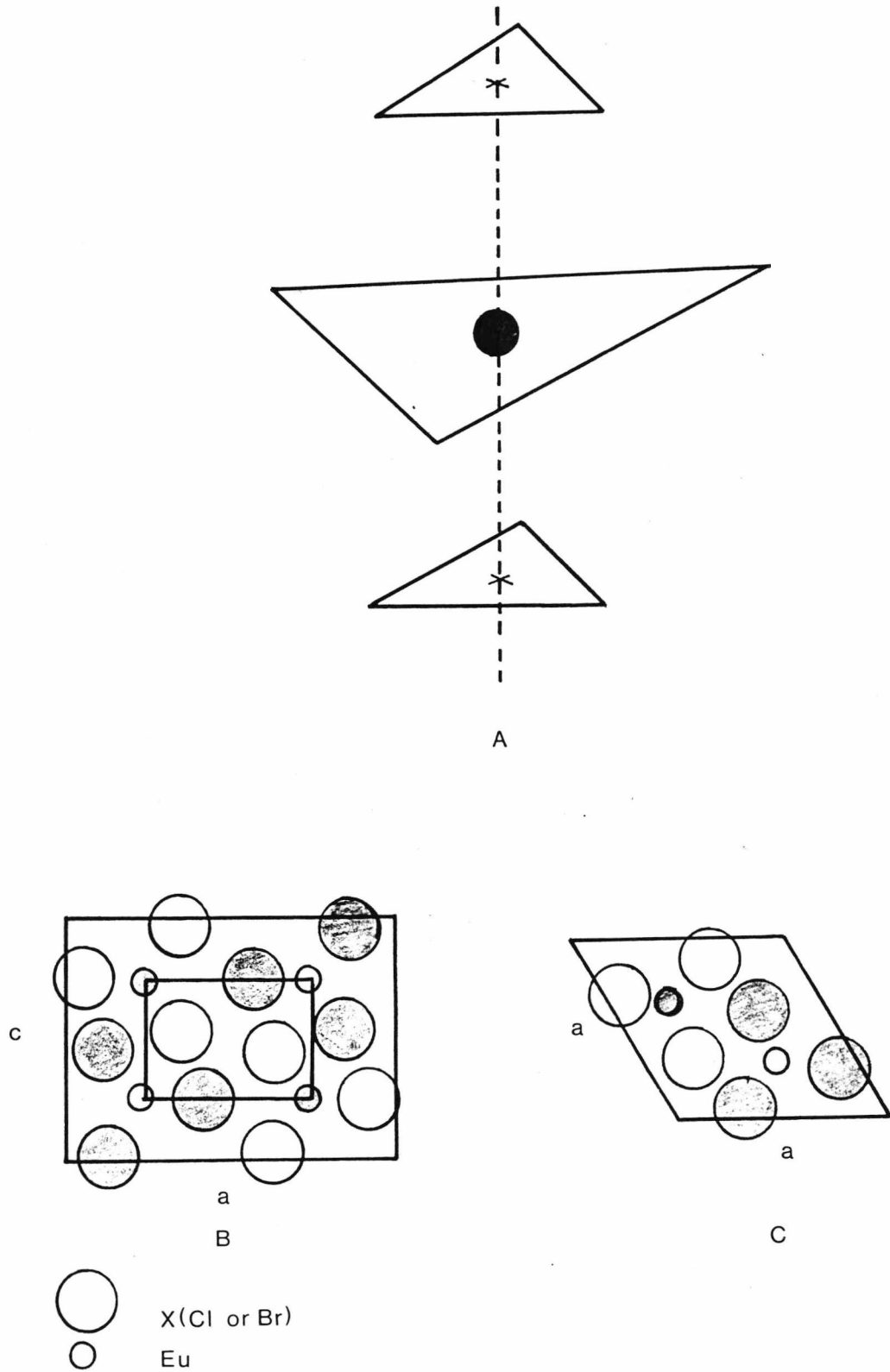


Figure 5.2

Isomer Shift Values with Temperature for two Non-Stoichiometric Europium Bromide Samples.

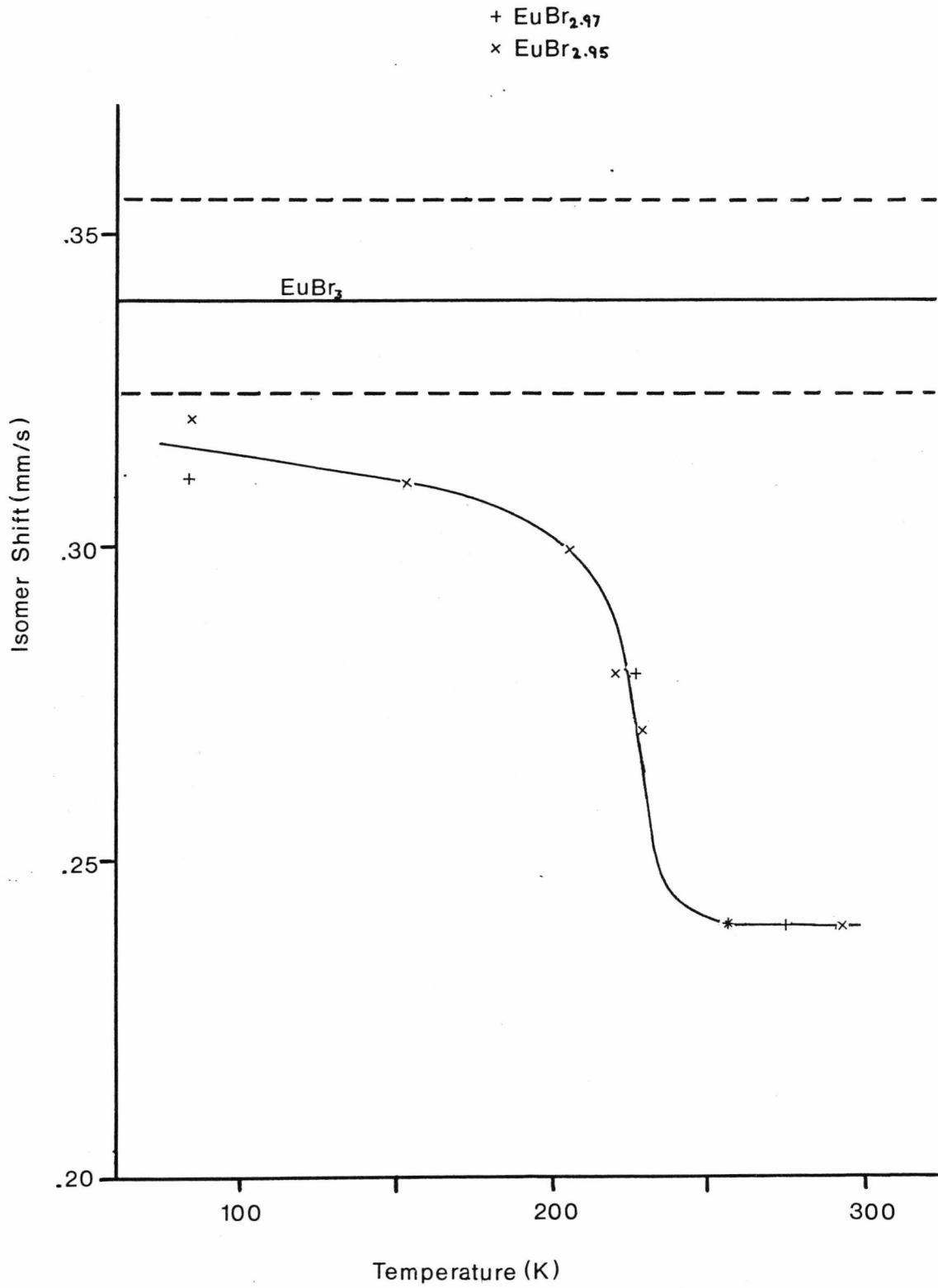


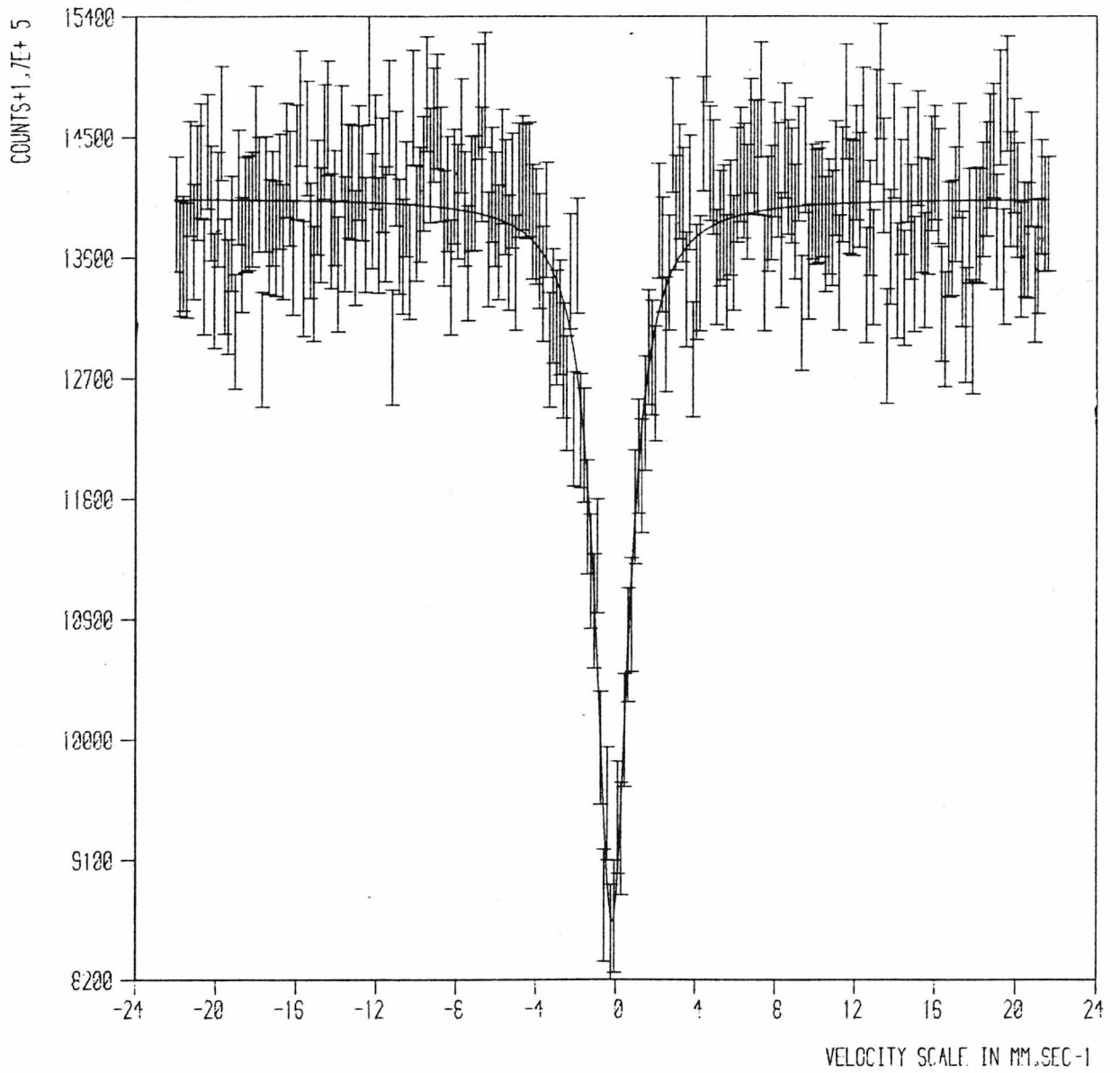
Figure 5.3Mössbauer Spectrum of $\text{EuCl}_{2.89}$ at 273K

Figure 5.4

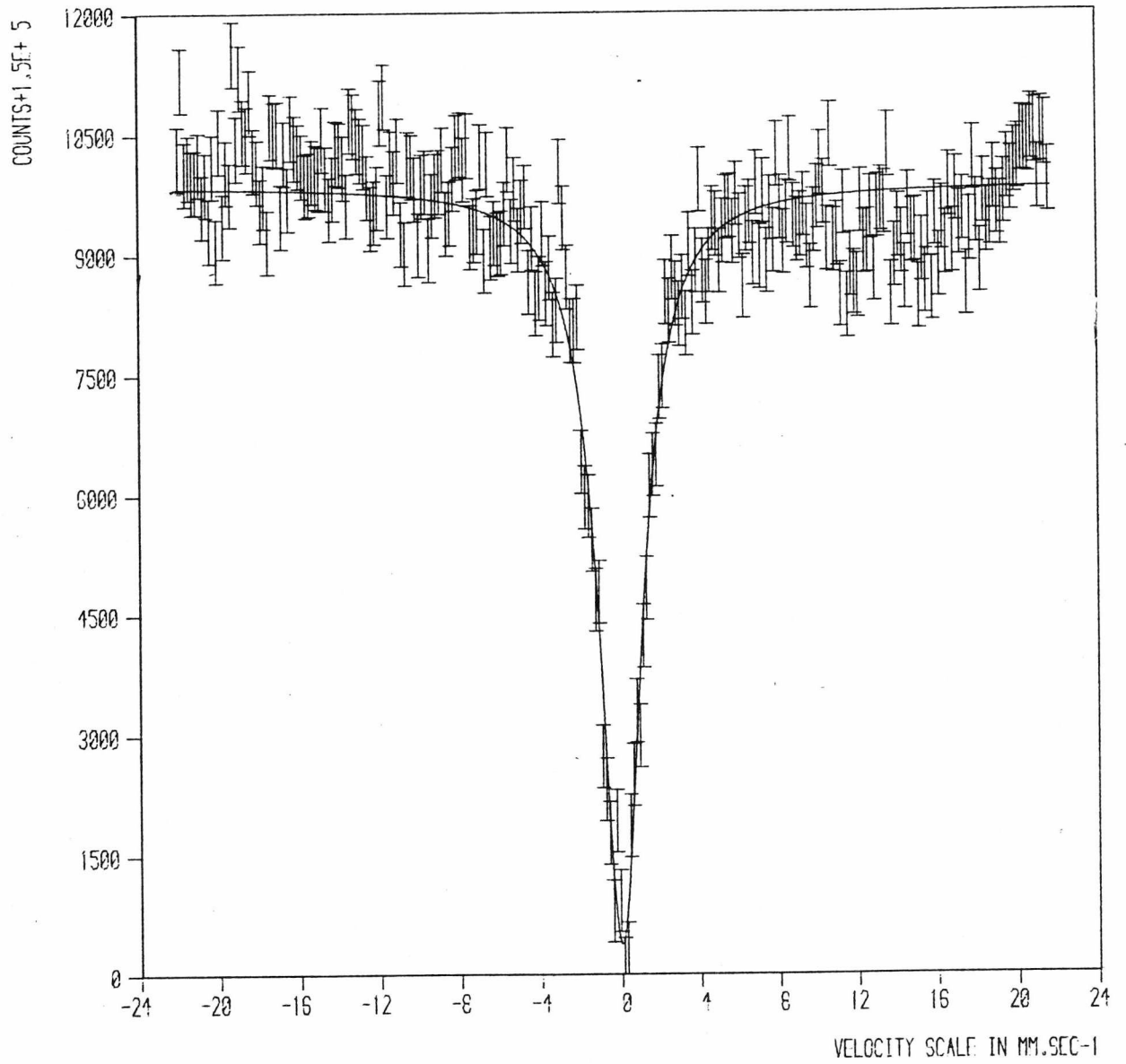
Mössbauer Spectrum of $\text{EuCl}_{2.89}$ at 97K

Figure 5.5

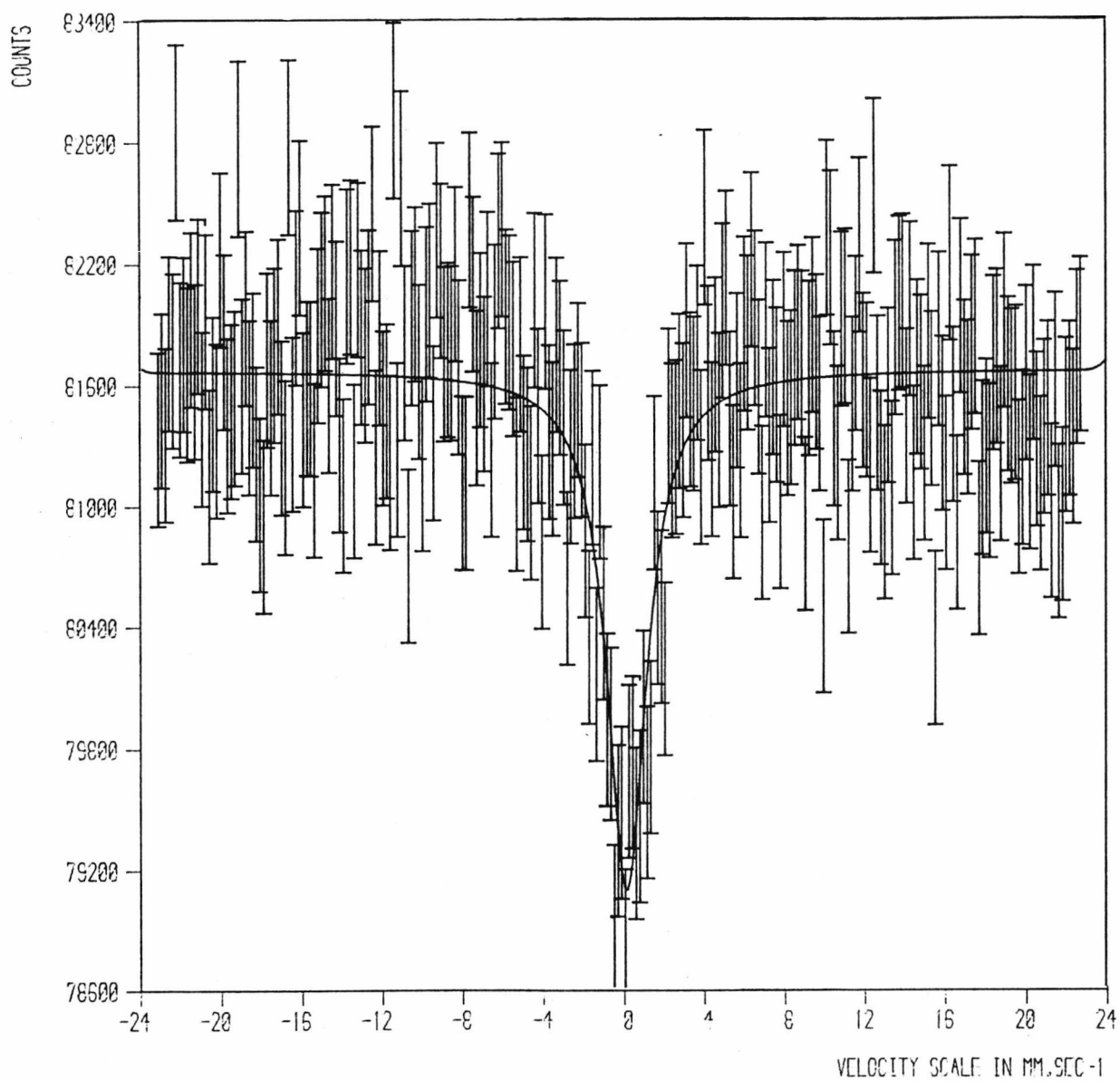
Mössbauer Spectrum of $\text{EuBr}_{2.99}$ at 253K

Figure 5.6

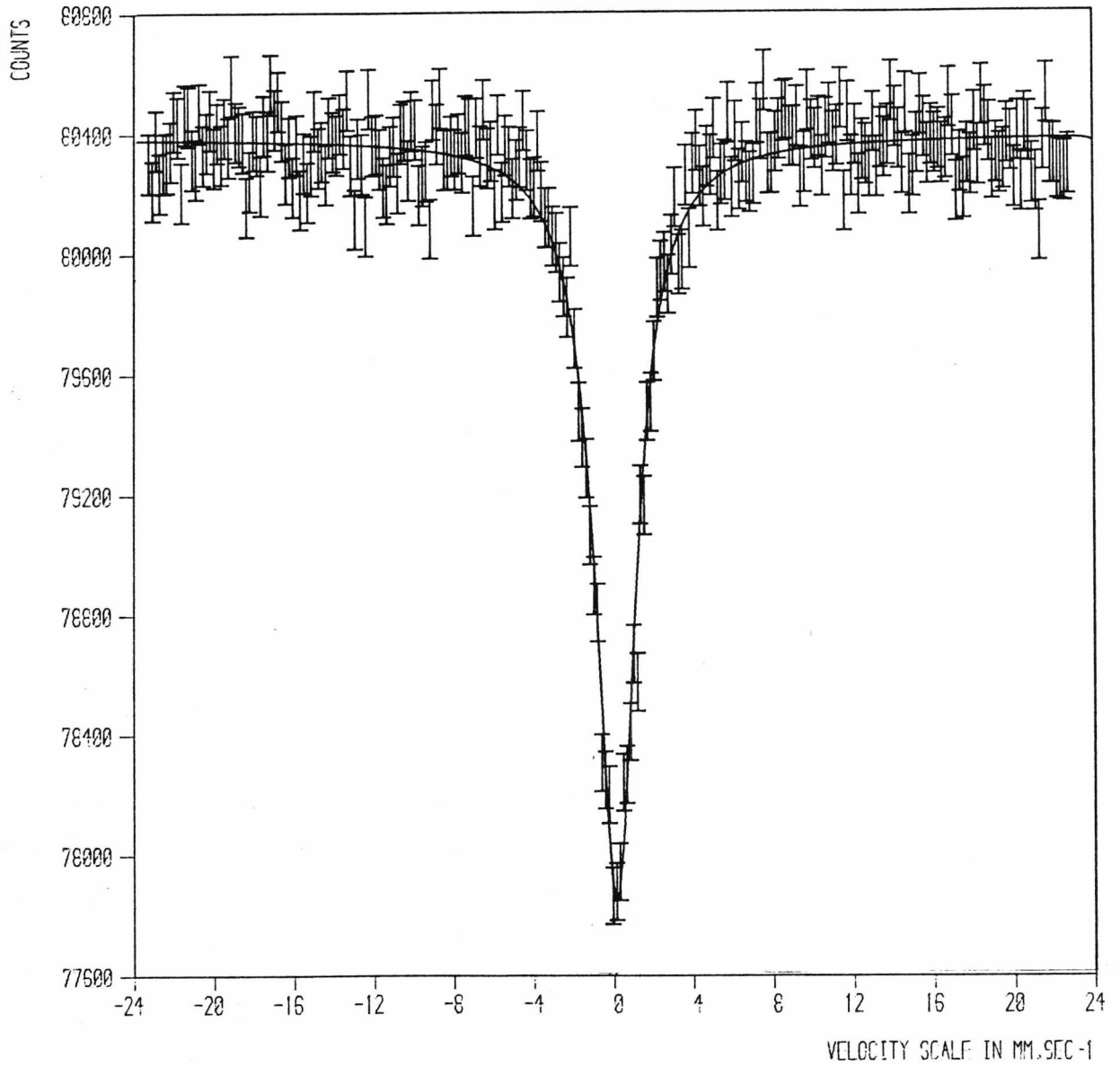
Mössbauer Spectrum of $\text{EuBr}_{2.99}$ at 78K

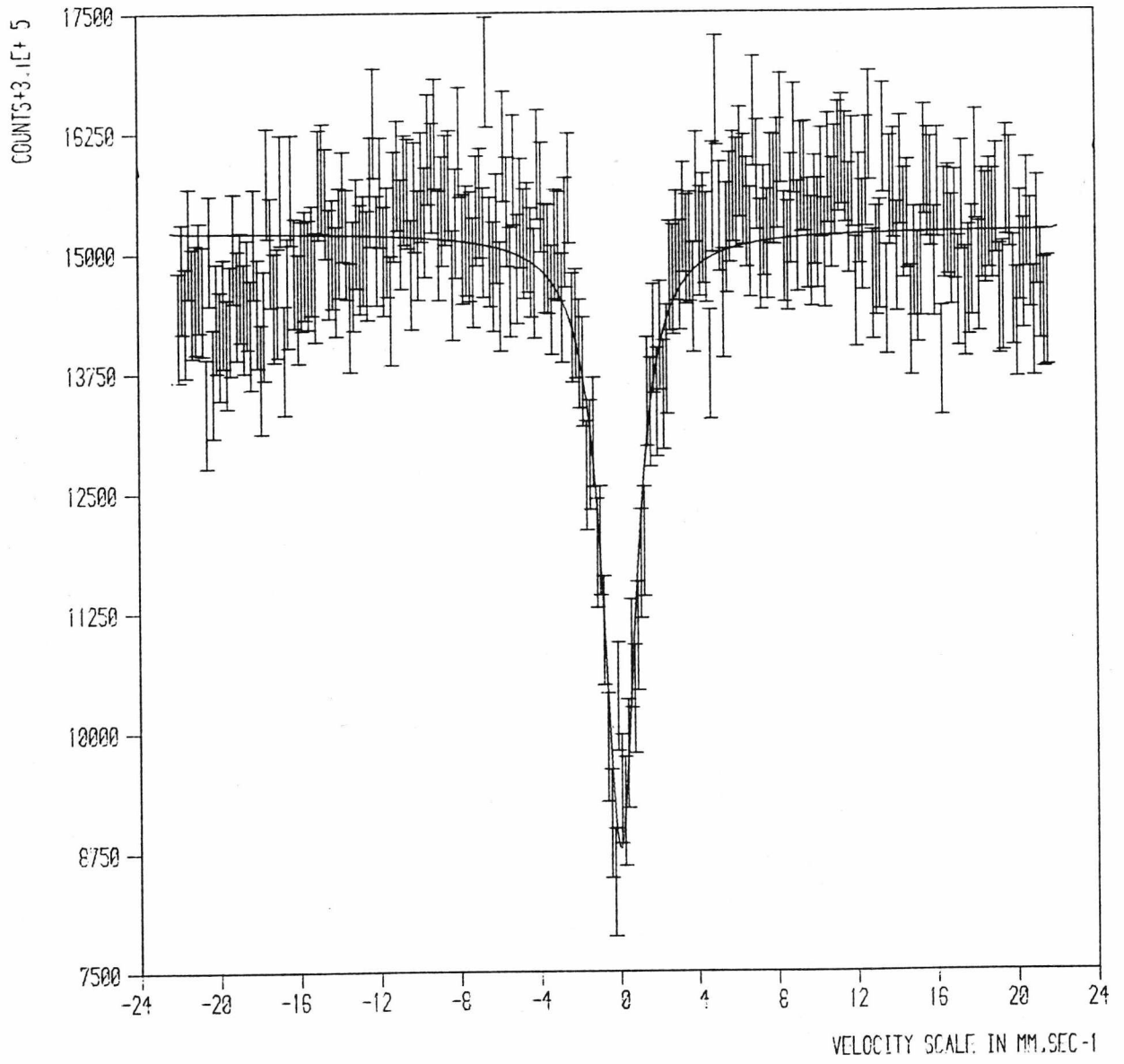
Figure 5.7Mössbauer Spectrum of $\text{EuBr}_{2.95}$ at 291 K

Figure 5.8

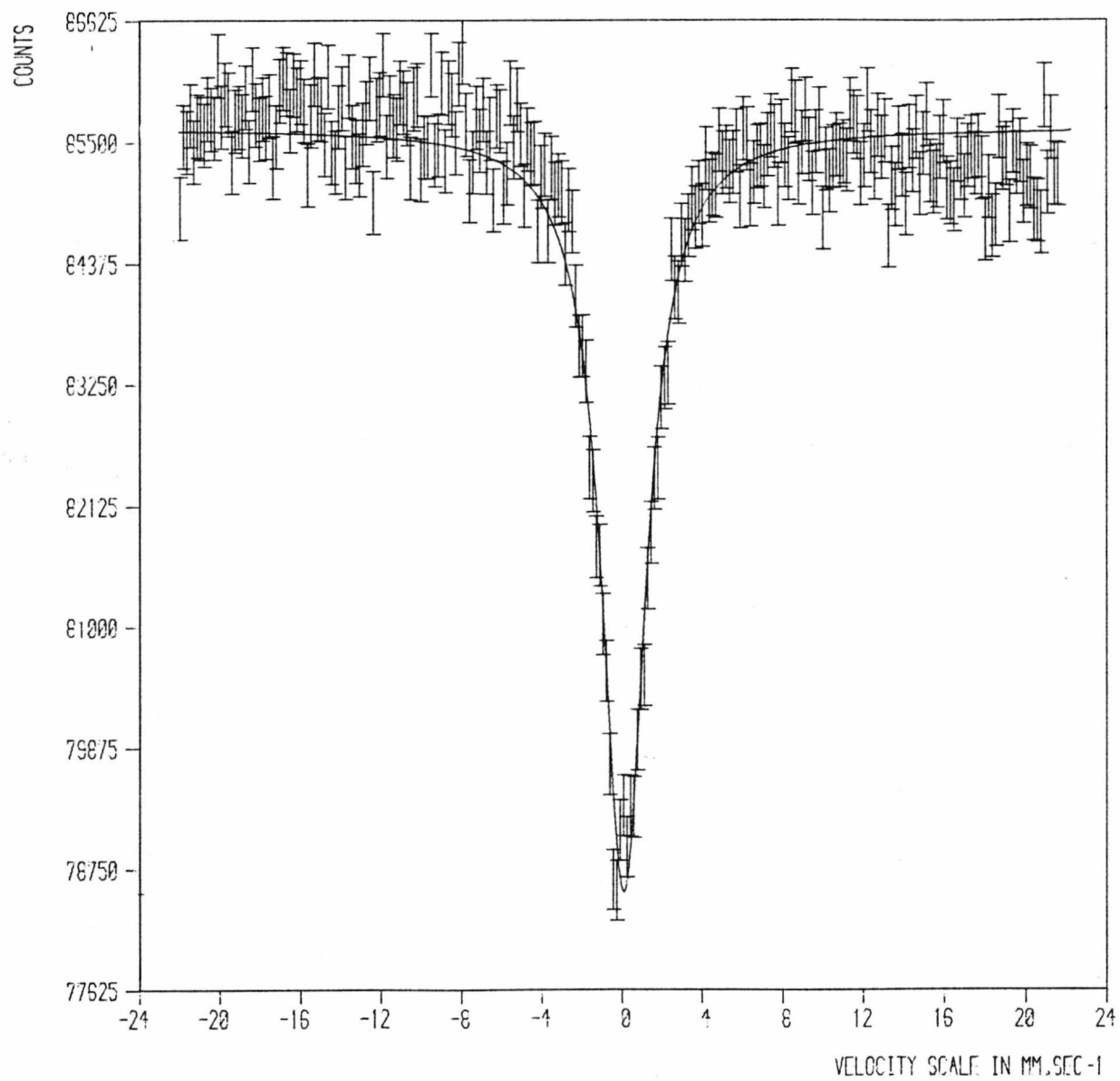
Mössbauer Spectrum of $\text{EuBr}_{2.95}$ at 83 K

Figure 5.9

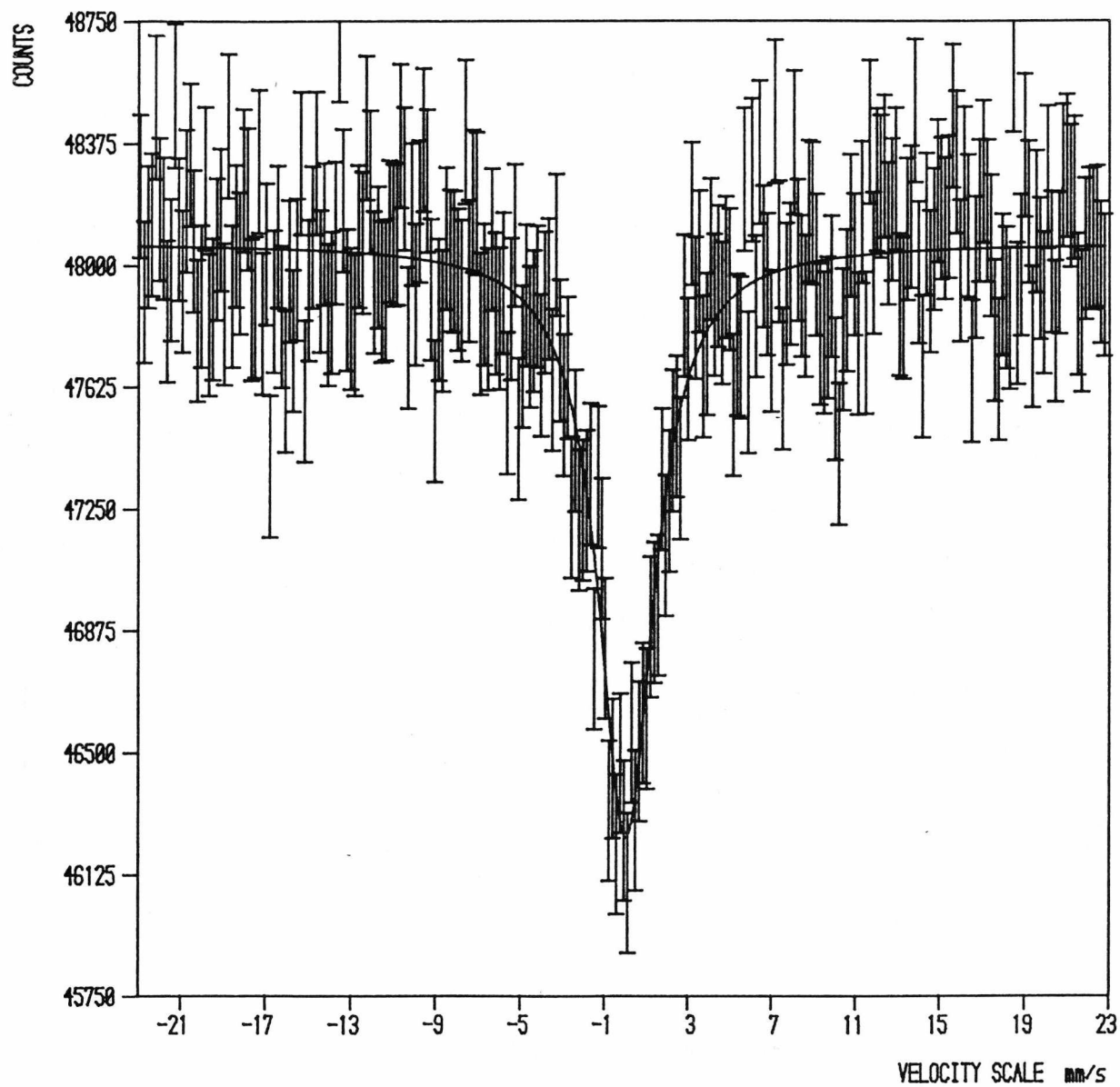
Mössbauer Spectrum of $\text{EuBr}_{2,84}$ at 273 K

Figure 5.10

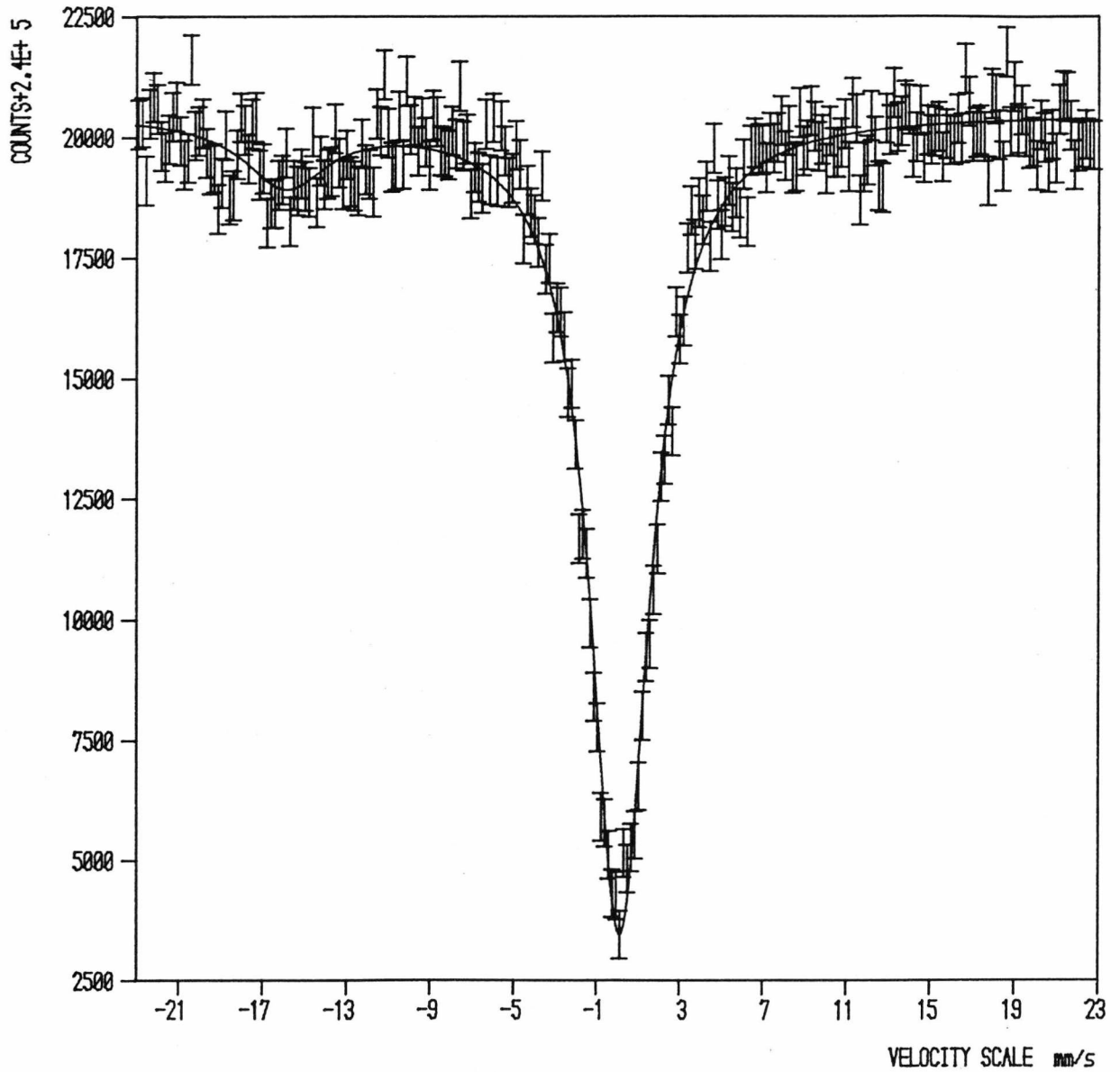
Mössbauer Spectrum of $\text{EuBr}_{2.84}$ at 77K

Figure 5.11 Mössbauer Spectra and Theoretical curves for $\text{EuCl}_{2.89}$ at various temperatures

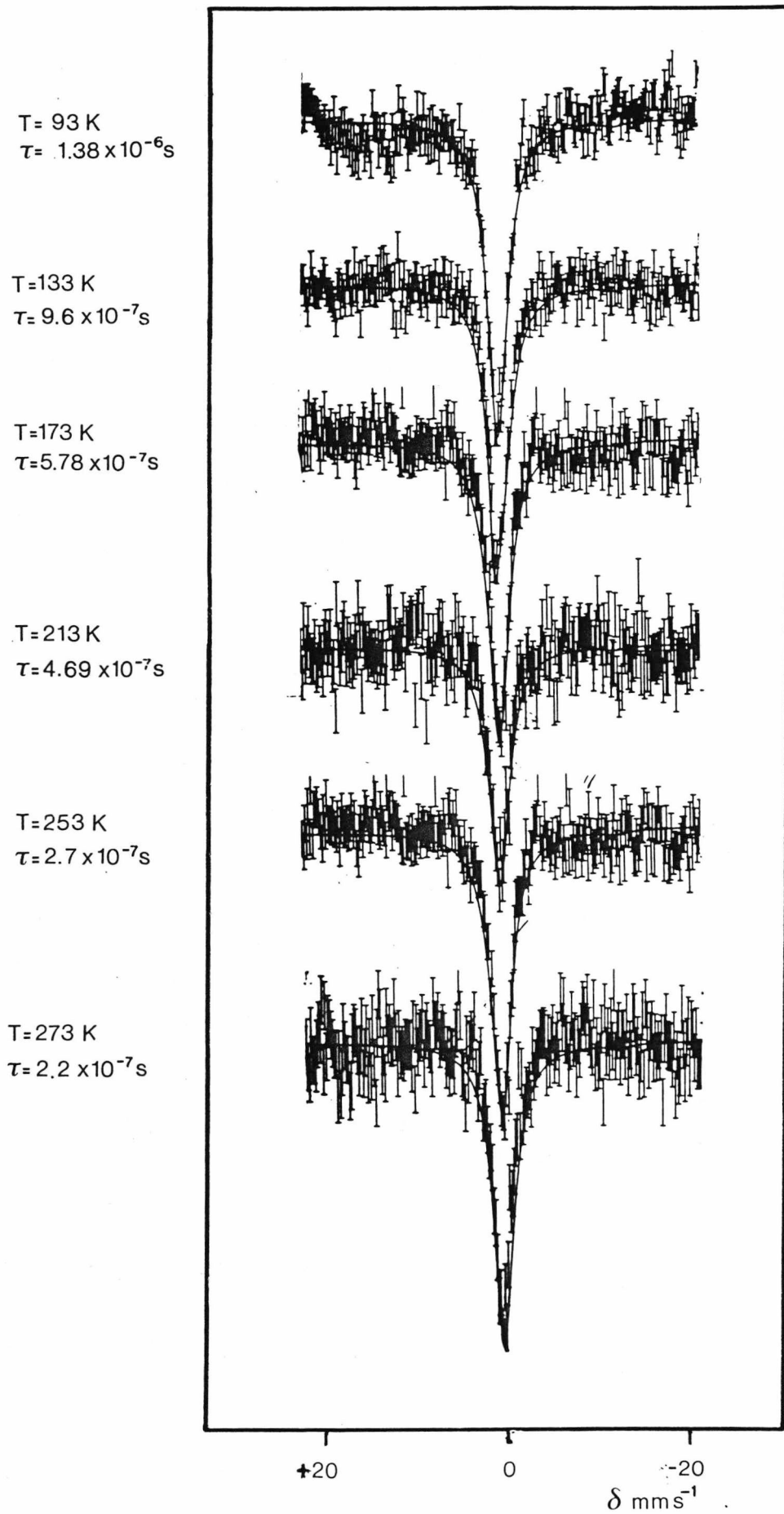


Figure 5.12

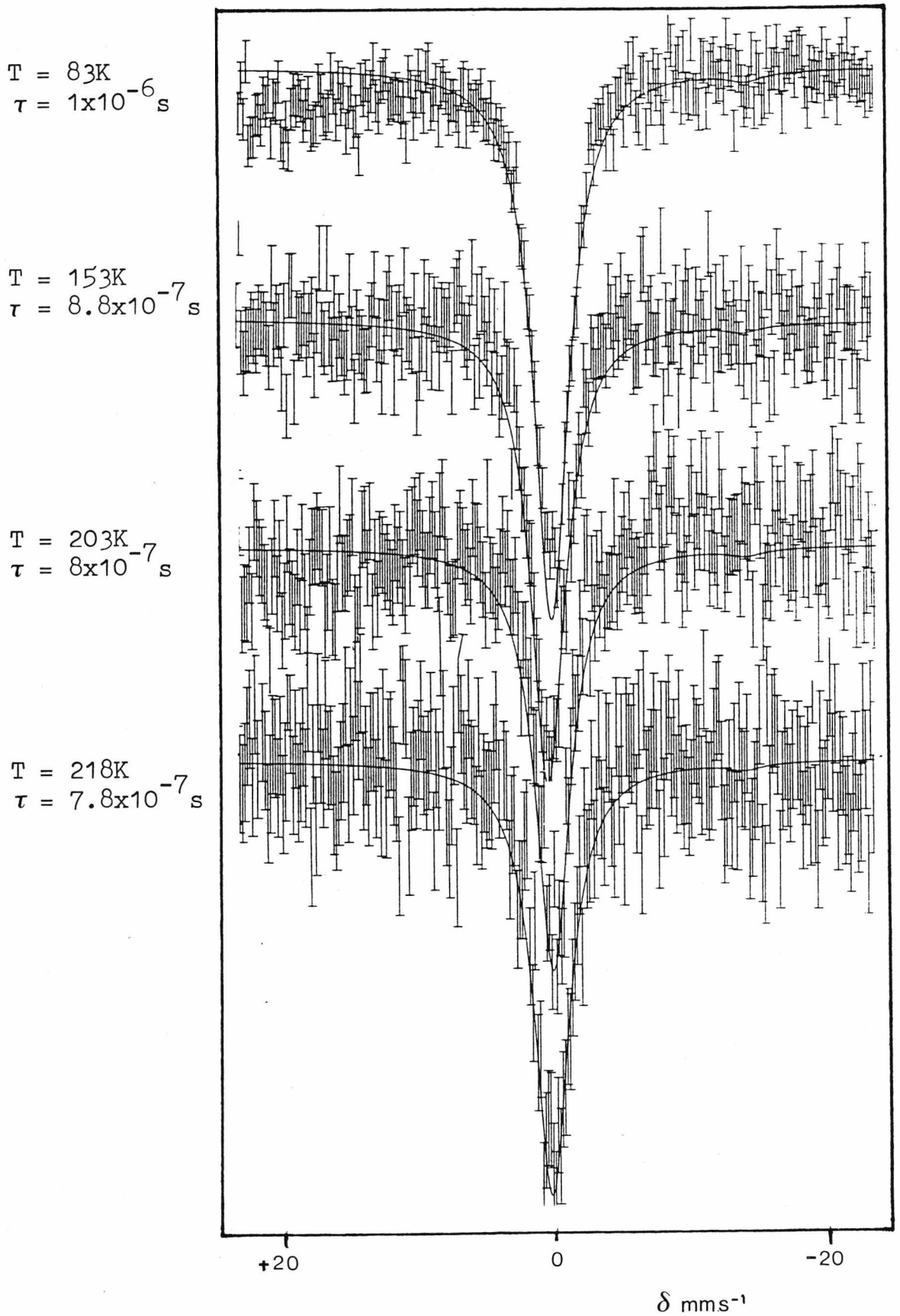
Mössbauer Spectra and Theoretical Curves
for $\text{EuBr}_{2.95}$ at Various Temperatures

Figure 5.12 cont Mössbauer Spectra and Theoretical Curves for $\text{EuBr}_{2.95}$ at Various Temperatures

$$T = 228\text{K}$$
$$\tau = 8 \times 10^{-7}\text{s}$$

$$T = 253\text{K}$$
$$\tau = 6 \times 10^{-7}\text{s}$$

$$T = 291\text{K}$$
$$\tau = 4.8 \times 10^{-7}\text{s}$$

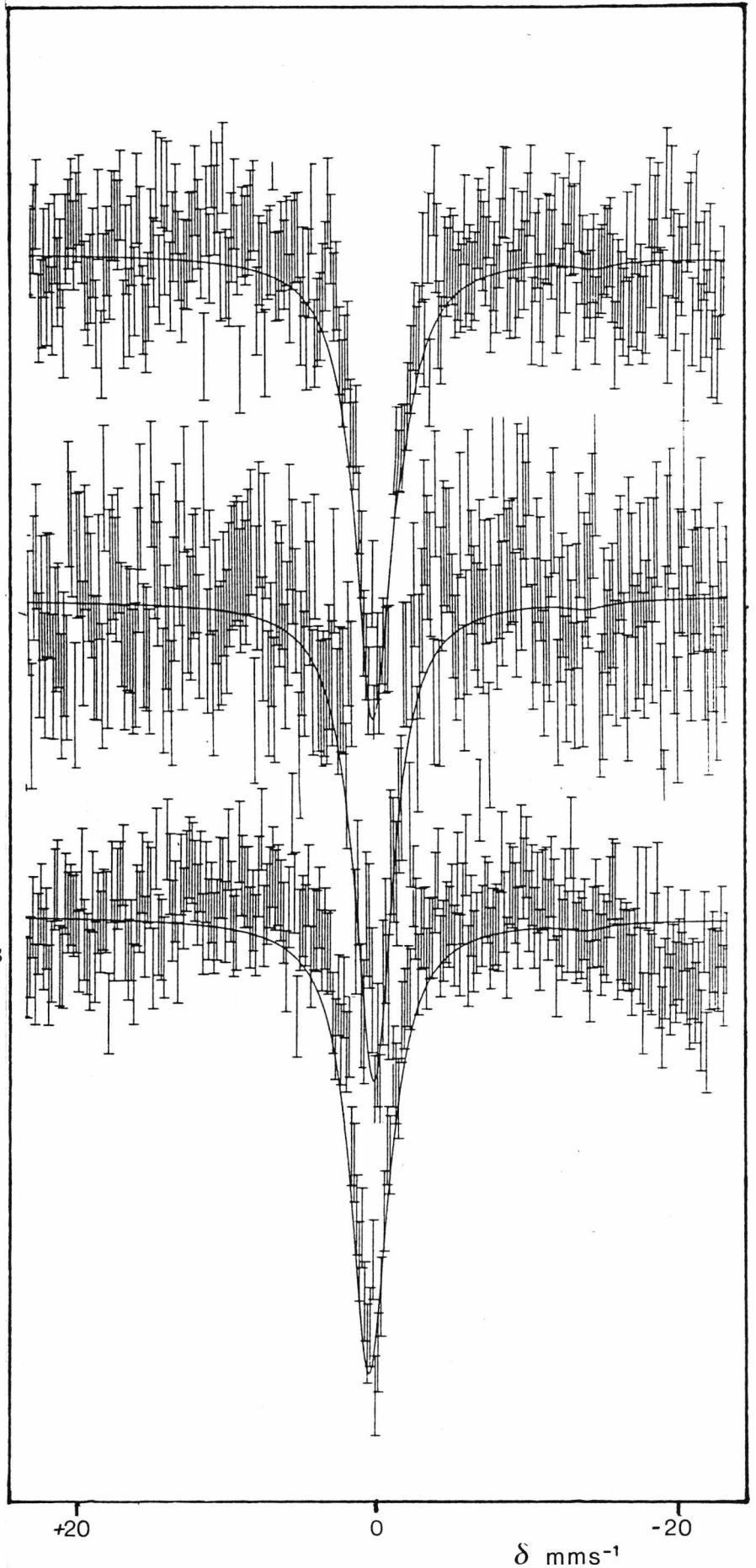


Figure 5.13

$\log_{10} \tau$ versus Reciprocal Temperature
for $\text{EuCl}_{2.89}$

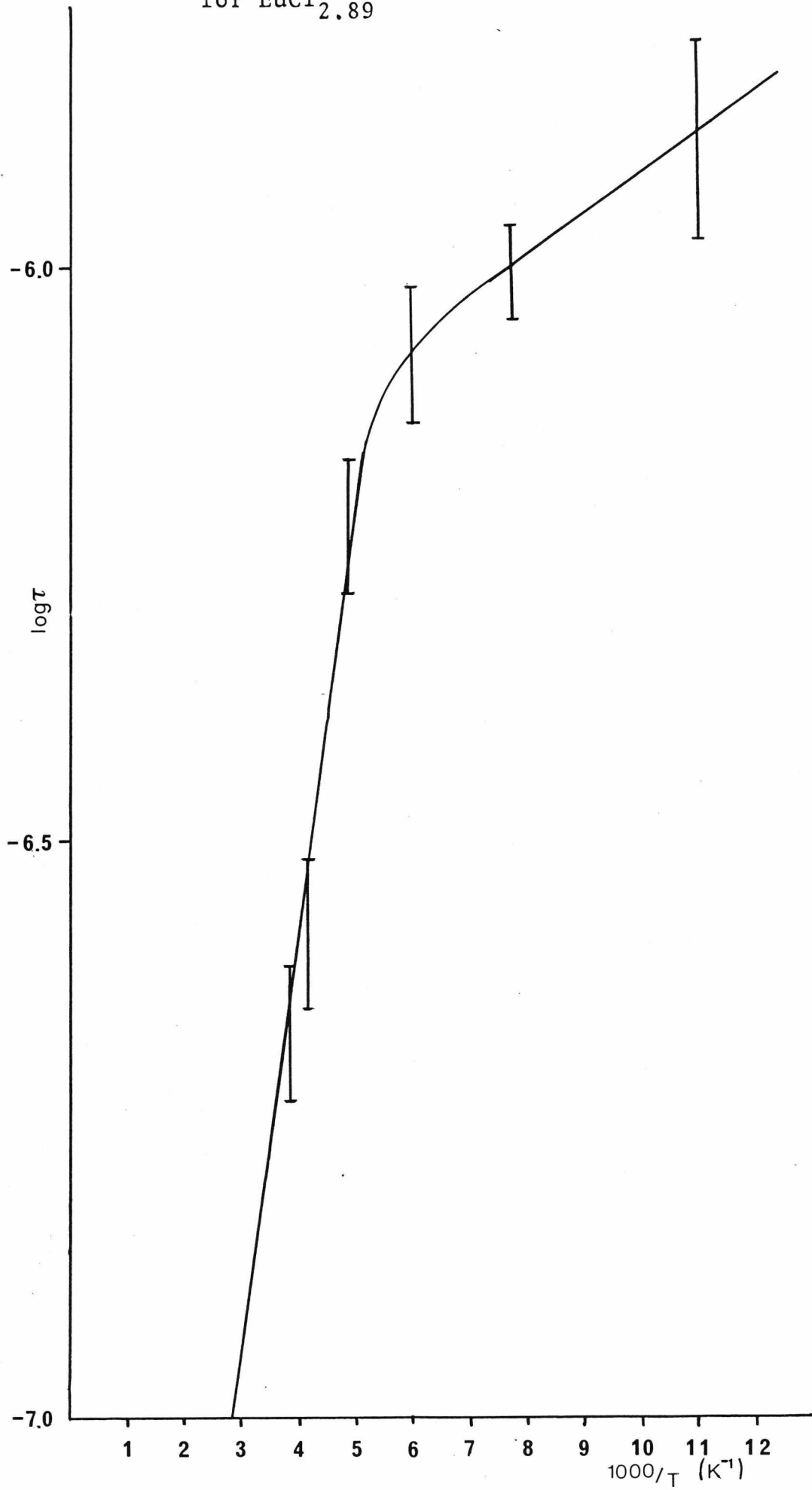
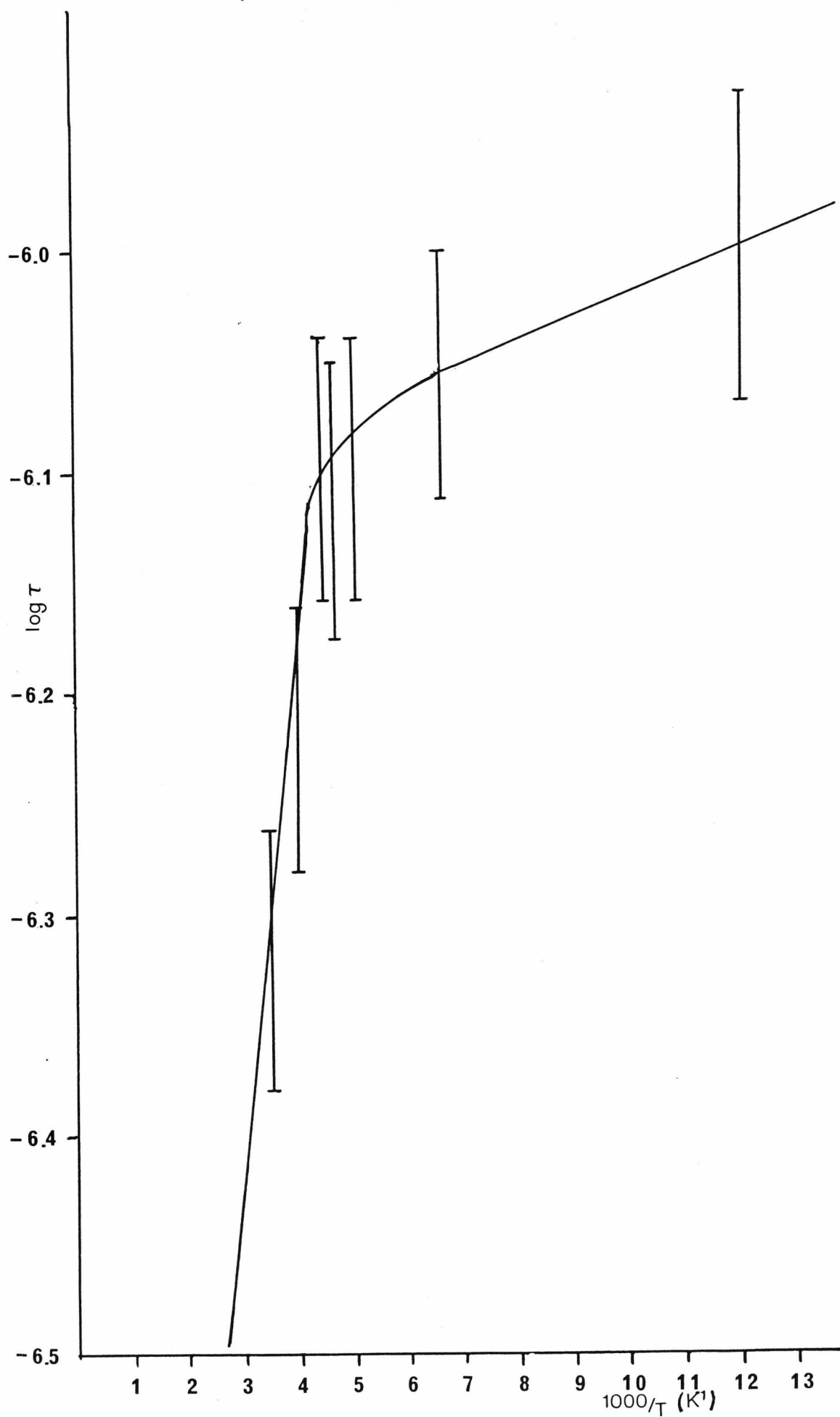
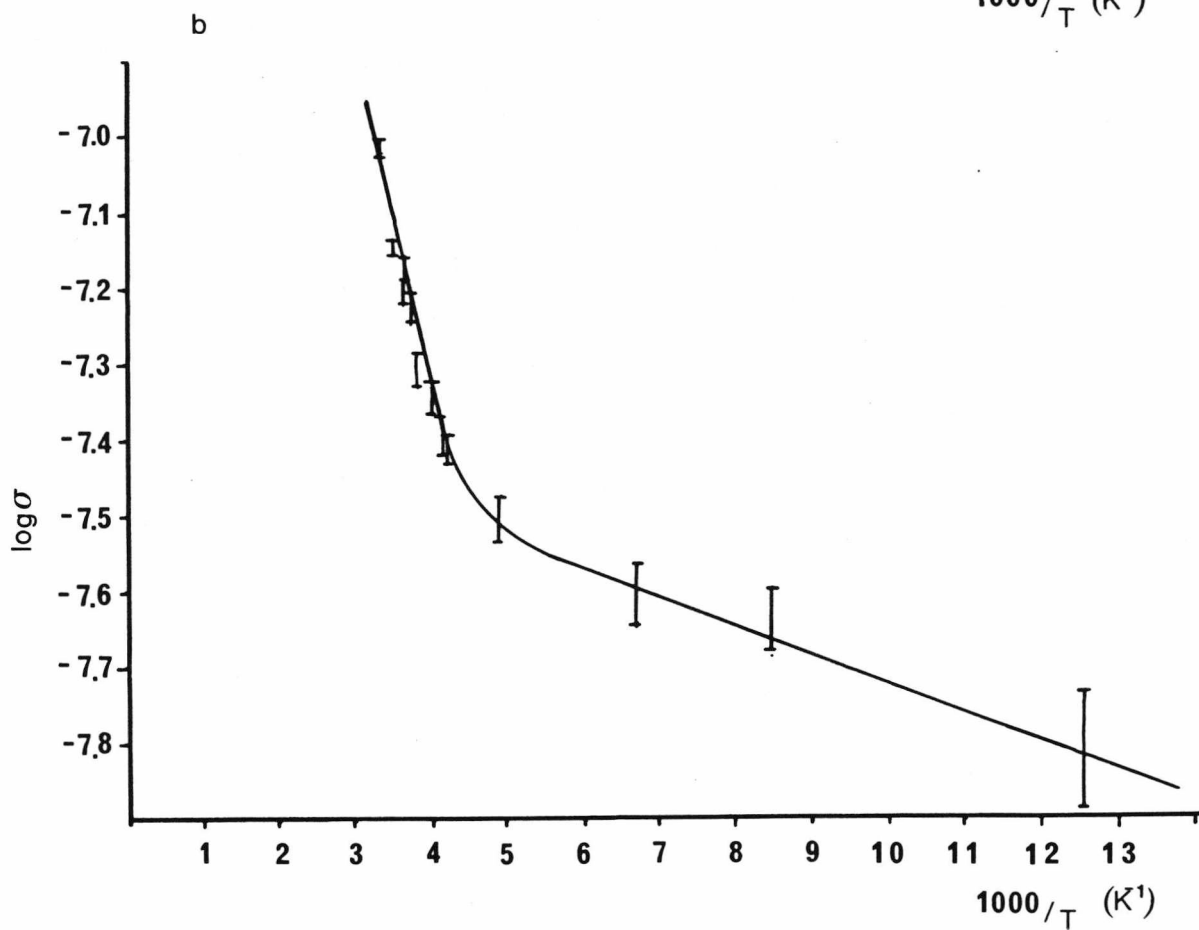
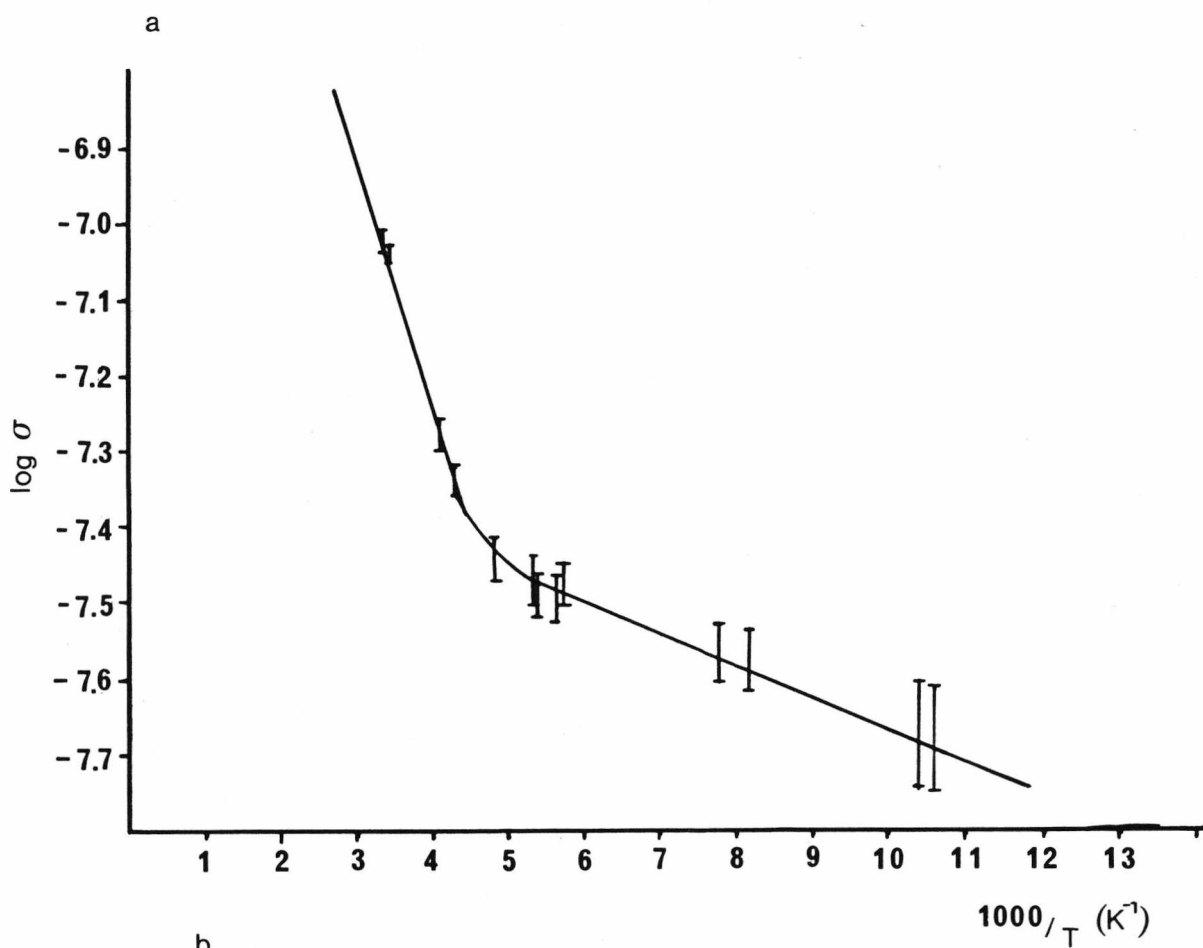


Figure 5.14 $\log_{10} \tau$ versus Reciprocal Temperature
for $\text{EuBr}_{2.95}$



Electrical Conductivity Plot for:

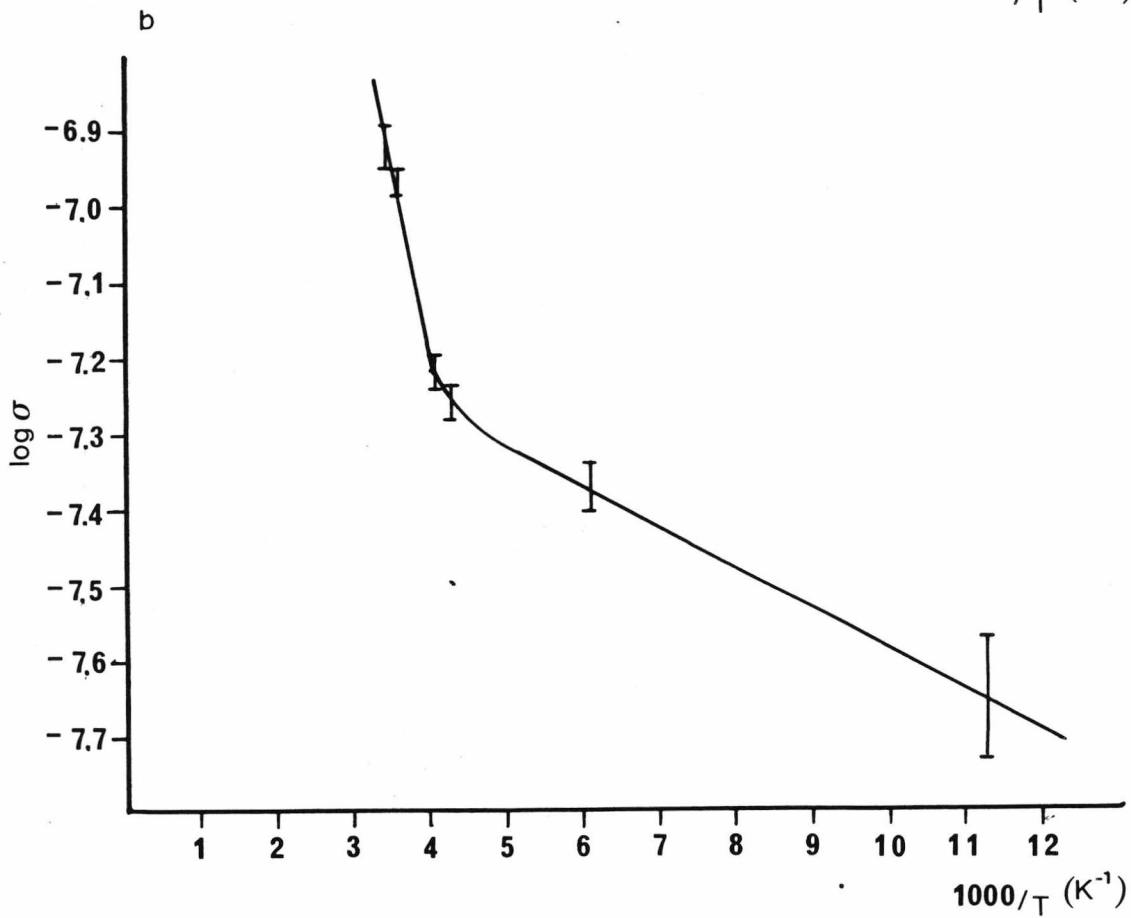
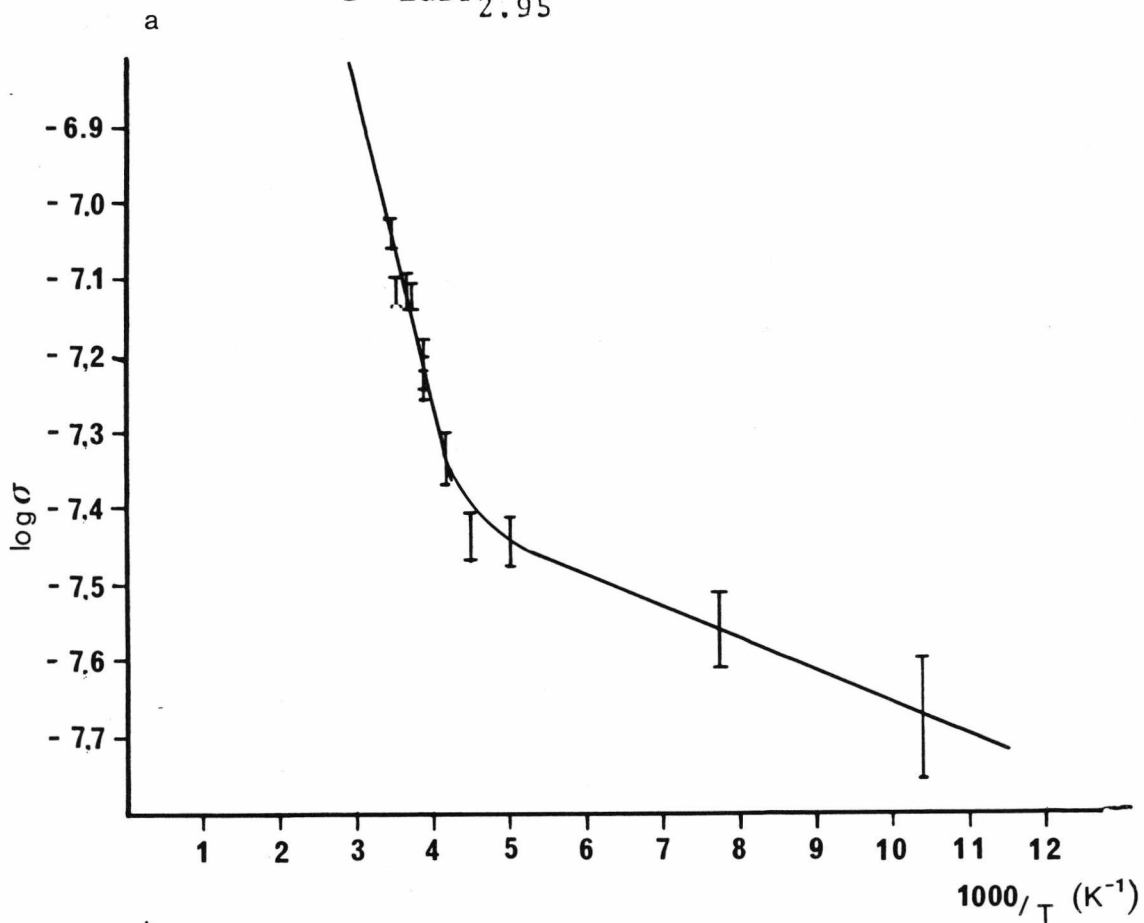
Figure 5.15

a EuCl 2.99
b EuCl 2.96

Electrical Conductivity Plot for:

Figure 5.16

- a $\text{EuBr}_{2.99}$
b $\text{EuBr}_{2.95}$



References

Chapter 5

1. O. Berkooz, M. Malamud and S. Shtrinkman, Solid State Comm. 1968, 6, 185.
2. J. Ball, PhD. Thesis, University of Kent at Canterbury, 1978.
3. C.M. Jenden, PhD. Thesis, University of Kent at Canterbury, 1980.
4. H.H. Wickman, M.P. Klein and D.A. Shirley, Phys. Rev. 1966, 152, 345.
5. H.H. Wickman, Mössbauer Effect Methodology 1966, 2, 39.
6. R.F. Gould (Ed.) "Non-stoichiometric Compounds", Adv. in Chem. Series, 1963, 39, American Chemical Soc. Washington, D.C.
7. E. Catelano, R.G. Bedford and V.G. Silveira, J. Phys. Chem. Solids, 1969, 30, 1613.
8. M. Blume and J.A. Tjon, Phys. Rev. 1968, 165, 446.
9. F. van der Woude and A.J. Dekker, Phys. Stat. Sol., 1965, 9, 775.
10. A.M. Affanas'er and Y. Kagan, Sov. Phys. J.E.TP. 1964, 18, 1139.
11. E. Bradford and W. Marshall, Proc. Phys. Soc. 1966, 87, 731.
12. H. Gabriel, J. Bosser, K. Rander, Phys. Stat. Solid, 1968, 27, 301.
13. A.J.F. Boyle and H.E. Hall, Rept. Prog. Phys., 1962, 25, 441.

14. G.K. Wertheim and J.P. Renseika, Phys. Lett., 1964, 10, 14.
15. H.S. Gutowsky, D.W. McCall and C.P. Slichter, J. Chem. Phys. 1953, 21, 279.
16. J.M. Haschke and H.A. Eick, J. Inorg. Nucl. Chem. 1970, 12, 2153
17. H.P. Klug and L.E. Alexander, "x-ray Diffraction Procedures for Polycrystalline and Amorphous Materials" John Wiley and Sons, New York, 1966.
18. G. Gerth, P. Kienle and K. Buchner, Phys. Lett., 1968, 27A, 557.
19. N.R. Large, R.J. Bullock, P. Glentworth and D.A. Newton, Phys. Lett., 1969, 29A, 352.
20. B. Morosin, J. Chem. Phys., 1968, 49, 3007.
21. J.A. Sommers, PhD. Thesis, University of Michigan U.S.A. 1976.
22. I. Bransky, N.M. Tallan and A.Z. Hed., J. Appl. Phys. 1970, 41, 1787.
23. O. Masseret and J.M.D. Coey, J. De Physique, 1976. 37, 297.
24. J.L. Morán-López and P. Schlottman, Phys. Rev. 1980, 22, 1912.
25. F.L. Carter, J. Solid State Chem., 1972, 5, 300.
26. C.M. Varma, Rev. Mod. Phys. 1976, 48, 219.

27. B. Batlogg, E. Kaldis and P. Wachter
J. Magnetism and Magnetic Materials, 1976, 3,
96.
28. R.L. Cohen, M. Eibschutz and K.W. West, Phys. Rev.
Lett., 1970 24, 383.
29. A. Jayaraman, V. Narayanamurti, E. Bucher and
R.G. Maines, Phys. Rev. Lett., 1970, 25, 1430.
30. D.M. Newns and A.C. Hewson, J. Phys. F. 1980,
10, 2429.
31. C. Kittel, "Introduction to Solid State Physics
5th (ed.), John Wiley and Sons Inc., 1976, New York.

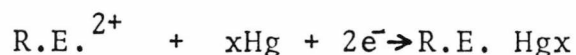
Chapter 6

A Preliminary Investigation into Europium

Mercury Compounds

6.1 Introduction

The lanthanides have presented difficulties in the separation of one element from another. Europium has been separated from rare earth mixtures by electrolytic techniques in the production of insoluble hydroxides at a solid-electrode surface 1930 Yntema¹ electrolyzed rare earth elements using a mercury cathode and later McCoy² reported that the electrolysis could be performed in the presence of complex forming organic acids which prevent the formation of insoluble hydroxides allowing the lanthanide to form an amalgam with the mercury according to the reactions:



This method works well for europium, the efficiency is lower for ytterbium relatively poor for samarium, with other lanthanides not forming the amalgam. Very little information is available on the europium amalgam formed, McCoy reported the existence of a model EuHg_{10} phase and after distilling the mercury rich amalgam under reduced

pressure in a solid Eu_3Hg_2 phase remained. The work described in this chapter concerns an investigation into some of the chemical and physical properties of europium-mercury compounds and attempts to characterize them using chemical analysis x-ray diffraction and Mössbauer spectroscopy.

More recently³⁻⁷ europium-mercury compounds have formed part of a study of rare earth intermetallic compounds with metals of Groups 1B, 11B, 11B of the periodic table. These studies used x-ray diffraction data to find correlations between the rare earth ionic size and the lattice parameters; hence structures of various phases were determined. Europium and Ytterbium were found to behave in an anomalous way, the lattice parameters and magnetic susceptibilities suggested that the ionic cores of the europium and ytterbium ions were divalent as opposed to trivalent for the other rare earth ions. The ratios of europium to mercury in these compounds was determined from the structures of the compounds. However, no additional information is available.

Compounds formed between metallic elements may have greatly differing properties, alloys or discrete chemical compounds, may be produced. The latter, intermetallic compounds are known as Daltonides and do not tolerate great deviations from stoichiometry, while the former, known as Berthallides are intermediate phase structures which can exist

over a finite compositional range. In order to determine the class to which these compounds belong it will be helpful to review briefly some of the ideas concerning intermetallic phases, most text books⁸⁻¹⁰ on metals include chapters on alloys and intermediate phases and the reader is referred to them for further information.

6.2 Factors Influencing the Character of Intermettalic Compounds.

The relative **sizes**, valences of the constituent elements, together with the electron concentration of the compound have been shown to affect the chemical and physical properties of intermetallic compounds. Hume-Rothery¹¹ and his co workers studied many cases and deduced rules for predicting the behaviour of compounds formed between metals and between metals and metalloids. The size factor states that if the solute atoms differ in size from the solvent so the range of solid solubility decreases. If the atomic diameters of the constituent atoms differ by more than 14-15% the size factor is said to be unfavourable. The size of the atom is taken to be that of the pure metallic state of the element, then changes in the electronic state of the atom when alloyed with another metal need not be taken into account beforehand.

The valence effect is that all things being equal the metal of lower valency is likely to dissolve the metal of higher valency. Allied to this is the electrochemical factor by which the electro negativities of the constituents are considered; the greater the difference in the electro-negativities of the constituents the more ionic or covalent character is imparted in the bonds between the constituents, hence the greater the difference in electronegativities the greater the tendency to form compounds rather than solid solutions.

Hume-Rothery¹² noticed that frequently a phase change occurs when a particular electron concentration is reached. The electron concentration is the ratio of valence electrons to atoms, the number of valence electrons is usually given by the group valence but in the case of the transition metals the valence is taken as zero¹³. An example of this is the Copper-Zinc system. A primary solid solution of zinc in copper occurs to just less than 50 atomic percent zinc, this is the α -phase of brass and has the face centred cubic structure of copper. A phase change occurs when more zinc is added this new phase has a body centred cubic structure of the CsCl type; this is known as the β -phase in which the electron to atom ratio is approximately 3:2. The β -phase structure is found frequently in other solid solutions of this type where the electrons to atom ratio is approximately

3:2. Other phases exist in the copper-zinc system as the zinc content is increased at about 60 atomic percent zinc the δ -phase which has a complex cubic structure occurs. 80 atomic percent zinc leads to the ϵ -phase with the hexagonal close packed structure of zinc. Ekman et al¹³ found that specific electron concentrations occur with the δ - and ϵ -phases, 21:13 and 7:4 respectively.

The β -, δ - and ϵ -phases occur in other solid solutions and at approximately the same electron concentration as for the brass phase. The phase changes are seen to occur at lower solute concentrations for solutes of a higher valency. Hence the phase change is directly related to the electron concentration. The compounds or solid solutions for which the above applies are known as electron compounds.

The influence of space filling and symmetry have been investigated by Laves¹⁴ to predict likely phases formed between metallic elements. The space principle states that the atoms will fill space in the most economical way, this is due to metallic bonds being non-directional so that the structure is determined by packing. The symmetry principle states that higher symmetries are preferred. The most common structures in metals are the close packed structures with co-ordination numbers of 12 and the face centred cubic structure with a co-ordination number of 8. Co-ordination numbers of 9, 10 and 11 are unknown indicating that higher symmetry is preferred. From these observations and rules the general character of intermetallic compounds may be predicted. Primary, secondary interstitial solid solutions or

or intermetallic phases may occur, some of which will be mentioned below.

Laves phases¹⁵ occur when atoms A with a strong tendency to metallic binding are in association with a very much smaller atom B. The size difference of A and B is of the order of 20% and simple and integral ratios of A to B are found such as AB_2 . Zintl phases exhibit variable valence and simple salt like structures, they occur when one constituent has an outermost 8-electron shell about half full. Zintl phases are characterized by the stoichiometry of the composition and thus large cation radius; and example is $LiHg_2$.

Intermediate phases may occur where a high degree of ionic or co-valent character is involved in the bonds between the constituents; normal valences of the elements may not be observed due to the metallic bonding. Some compounds show metallic conductivity and reflectivity but have chemical compositions which do follow normal valence rules.

The structures of alloys are dependent on the constituents and the relative proportions of each as has been mentioned. In addition the structure may be disordered at one temperature and ordered at a lower temperature. Thermal vibration increases with temperature so that crystal defects such as vacancies become more mobile as are the atoms or ions. Hence favoured

regions may exist for the constituents and there is long range order although the structure may be said to be disordered. This is a superlattice; on cooling the structure orders to decrease the internal energy. Identification can be made through the increase in the number of lines in a diffraction pattern as previously identical phases become distinct due to ordering. If compounds rather than true metallic solid solutions form, disorder is less prevalent because packing is no longer the major factor in the structure of the phase; so bonding plays a more important role.

6.3 Electrons in Metals

From the preceding section the importance of the behaviour of the electrons can be seen, especially that of the valence electrons. Many theories of electrons in metals start by considering the metal to consist of positive ionic cores held together in a 'sea' of electrons. The electrons come from the valence shells of the atoms and the attraction between them and the ionic cores is responsible for the metallic bonding. Theories on the behaviour of electrons in metals have been produced and improved; all use the idea of an ionic core surrounded by electrons in energy bands. The first theory put forward by Drude^{16,17} used free electrons moving in the spaces between atoms and were treated as molecules of an ideal gas. Hence the name free electron gas model. The electrons normally move randomly

but when an electric force is applied there is a general drift of electrons in one direction so the current is carried.

The energy of a gas at a given absolute temperature, T is

$$\frac{1}{2} m u_x^2 = \frac{KT}{2} \quad (6.1)$$

where m is the mass of the gas molecule, atom or in this case electron. The velocity $u_x^2 =$, and $K =$ Boltzmann's constant so that the total energy for three degrees of freedom is $3/2 KT$.

If an e.m.f. is applied the electrons develop a drift velocity v_D such that

$$i = nev_D \quad (6.2)$$

$i =$ current

$n =$ number of electrons

$e =$ charge on an electron.

From this expression the conductivity may be derived by finding the mean free path traveled by an electron before it collides and comes to rest. Ohms' law and the relationship between the electrical and thermal conductivities may be derived. The model can not explain the specific heat capacity of the metal as an energy of $3/2 kT$ is attributed to every valence electron as well as the atoms in the metal, so the specific heat capacity is over estimated.

In the Sommerfeld model¹⁸⁻²⁰ quantum mechanics are used to describe the motion of an electron which is considered to be wavelike²¹. The wavelength λ , of an electron with energy E , mass m in a potential field V is given by

$$\lambda = \frac{h}{\sqrt{2m(E-V)}} \quad (6.3)$$

where h is Planck's constant

This may be simplified by setting $V = 0$. If a cube of L contains N electrons, Schrodinger's wave equation may be solved giving the electron energies

$$E_n = \frac{h^2}{8m^2L^2} (n_x^2 + n_y^2 + n_z^2) \quad (6.4)$$

$$n = 1, 2, 3, \dots$$

The level, n_x , n_y , n_z may be treated as a volume element of a quadrant of a sphere distance R from the origin. The energy is given as

$$E_n^2 = \frac{h^2 R^2}{8m^2L^2} \quad (6.5)$$

The maximum energy, E_m is the energy of the highest filled level and is found by considering the volume occupied

by the levels

$$\frac{N}{2} = \frac{1}{8} \left(\frac{4}{3} \pi R_m^3 \right)$$

(The factor of 2 is due to each level being able to accommodate two electrons).

$$\text{from this } R_m^3 = \frac{3N}{\pi}$$

$$E_m = \frac{h^2}{8mL^2} R_m^3 = \frac{h^2}{8m} \left(\frac{3N}{\pi L^3} \right)^{2/3} \quad (6.6)$$

$$\text{hence } E_m \propto \left(\frac{N}{V} \right)^{2/3}$$

The energy distribution may be calculated by finding the number of levels between R and $R + dR$ and the effect of temperature is described by the Fermi-Dirac function

$$f(E) = \left(\exp \left\{ \frac{E - E_m}{KT} \right\} + 1 \right)^{-1} \quad (6.7)$$

E_m is the energy of the highest filled level at absolute zero and is known as the Fermi energy. There is very little temperature effect; energy can only be absorbed by electrons which are able to be promoted into a higher band, ie only those with an energy close to E_m . The specific heat capacity is still $3/2 RT$ for the electrons plus atoms but only a very small proportion of the electrons can accept energy and so this contribution is negligible.

The Sommerfeld model assumes that the levels extend to infinity so that insulators and semi-conductor behaviour can not be explained, this is due to a constant potential being used and was improved upon in the Bloch or Brillouin zone model where a modulated potential was used. Bloch^{22,23} proved the important theorem that solutions of the Schrodinger equation for a periodic potential must be of a special form:

$$\psi_{\underline{k}}(\underline{r}) = U_{\underline{k}}(\underline{r}) \exp(i\underline{K} \cdot \underline{r}) \quad (6.8)$$

where the function $U_{\underline{k}}(\underline{r})$ has the period of the crystal lattice and depends on the wave vector \underline{K} . $(|\underline{K}|) = \frac{2\pi}{\lambda}$

Using the new wave function the energy of a level becomes

$$E = \frac{h^2}{8\pi^2 m} \cdot K^2 \quad (6.9)$$

A plot of E vs \underline{K} gives a parabolic curve with discontinuities corresponding to energy gaps or forbidden bands. This theory is now capable of explaining the differences between metals, semiconductors and insulators.

The wave vector may be related to the diffraction condition and so to the crystal lattice

$$n\lambda = 2d \sin \theta \quad d = \text{plane spacing in the lattice}$$

$$\text{so } K = \frac{n\pi}{d \sin \theta}$$

The discontinuities in the E vs \underline{K} curve are associated with the planes of x-ray reflection and define the Brillouin zones of the reciprocal lattice.

6.4 Experimental.

Two methods for the preparation of the europium-mercury compounds were employed. The first followed McCoy's² method of electro-reducing europium(III) at a mercury cathode while the second involved heating stoichiometric proportions of europium metal and mercury together in a sealed ampoule. The first method was found to be unsuitable as the end product was too difficult to predict. Thus all the measurements made on the reaction products reported below made use of the second method.

6.41 Preparation

The first method was prepared by the method of McCoy; this method was originally intended to be used for the separation of europium from accompanying rare earths. The electrolyte is europium acetate in aqueous potassium citrate which prevents the production of insoluble europium hydroxide when the rare earth chloride is electrolyzed in aqueous solution²⁴. The electrolysis is carried out in a beaker with a small bore glass tube attached to the side for the electrical connection to the mercury cathode at

the bottom of the beaker. The surface of the mercury is constantly renewed by a rotating stirring rod and the contents of the beaker are kept below 25°C. A platinum anode is used and a potential of between 6-8 volts with a current density of between 0.04-0.06 A/cm² is required. The resultant amalgam also contains potassium which may be removed by the action of water; several washings with water facilitate its removal.

The electrolyte was prepared by dissolving about 5g of Europium(III) oxide²⁵ (99.9%) in an excess of boiling 15% acetic acid²⁶. The solution is then neutralized with potassium carbonate. Tripotassium citrate is prepared by neutralizing 20g of citric acid in 64 ml of water with 21.6g of anhydrous potassium carbonate. The acetate and citrate solutions are mixed and made alkaline with the addition of a further 2.5g of potassium carbonate.

Electrolysis was conducted in an adapted 50 ml pyrex beaker (figure 6.1) into which 57g of triply distilled mercury was introduced together with 35ml of the electrolyte. The stirrer was introduced and set to just disturb the surface of the mercury. The platinum electrodes were positioned, the anode in the bulk solution and the cathode into the mercury via the side arm. A potential of 8v (with a current of 0.5 A) was applied giving a current density of 0.04A cm⁻². The beaker stood in an ice water bath to keep the electrolyte below 25°C and the electrolysis was carried out for about 100 minutes until the electrolyte no longer bleached litmus paper (ie all of the Eu(II) had

been removed from the electrolyte). The electrolyte was then decanted and the amalgam was washed with distilled water four to five times then left to stand in water for about half an hour to allow the remaining potassium amalgam to be removed. The amalgam was washed again and transferred to a 25ml round bottom flask with a ground glass 'Quick Fit' stopper. The transfer was carried out with water still present as the amalgam was found to tarnish in air. The flask was attached to a vacuum distillation apparatus and evacuated to 0.1 torr and heated with a micro bunsen burner using a quiet flame. The residual water layer is distilled off first followed by the mercury. Distillation is continued until a solid phase is seen in the sample flask. The flask was sealed using a ground glass joint and transferred to the glove box for sample recovery. The sample had the appearance of a silver-grey solid but it was mixed with a liquid phase. The solid tarnished quickly in air and reacted with dilute acid to give metallic mercury and a solution containing europium.

The second method of preparation followed that of later workers³⁻⁶ and simply involved heating together stoichiometric proportions of europium and mercury in a sealed ampoule. The europium in the form of sublimed metal (99.9%)²⁵ was purchased in ampoules containing a known weight of europium sealed under argon. The weights ranged from between 0.3g to about 0.6g. The europium was divided into small pieces with a scalpel in

the glove box. The pieces were placed in a medium walled silica ampoule (figure 6.2) similar in design to that described in chapter 3. An accurately weighed amount of triple-distilled mercury was added leaving the europium in slight excess. The top of the ampoule was secured in place sealing the contents from the atmosphere before the apparatus was removed from the glove box. The ampoule was evacuated on the vacuum line to a pressure of 10^{-3} τ and sealed while under vacuum. The sealed ampoule was placed in a mild steel screwtop container in case of implosion and then heated vertically in an oven at 600°C for between 24 and 48 hours. At the end of the heating period the ampoule was allowed to cool in air and the sample was recovered in the glove box. All the samples had the appearance of silvery grey solids. Samples with a high proportion of mercury melted below 600°C ; only EuHg did not melt at this temperature. In addition to the stoichiometric compounds, two other samples were produced to test the range of solid solubility. They corresponded to the formulae Eu_2Hg_3 and Eu_3Hg_2 , the latter being claimed to exist by McCoy.

6.4.2 Chemical Analysis

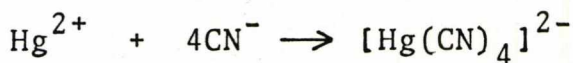
The compounds were analyzed for total metal content and for europium content, both analyses were by E.D.T.A. titrimetric analysis with the mercury being masked by CN^- in the latter determination.

(a) Total metal analysis

The titration is adapted from that used for the determination of europium as described in Chapter 3. About 0.2g of the sample were dissolved in dilute nitric acid. The europium went into solution first leaving metallic mercury which eventually dissolved with gentle heating. When cool the solution was transferred to a 50ml standard volumetric flask and made up to volume with distilled water. An aliquot of 10ml was pipetted into a 250ml conical flask and neutralized with 0.01 NaOH using bromophenol blue as an indicator. Six drops of pyridine were then added and the solution warmed to about 60°C after which four drops of xylenol orange indicator were added. The solution titrated against E.D.T.A. solution ($5 \times 10^{-3}M$) to a sharp red to golden yellow end point.

(b) Europium Analysis

The mercuric ions are masked by CN^- ions according to the reaction²⁷



The cyanide is added as the potassium salt in an amount one and one half times greater than the reaction requires.

A 10ml aliquot of sample was pipetted into a 250ml conical flask to which 10ml of 0.1M KCN is added. The solution

is neutralized as in (a), one drop of pyridine and 0.2ml of acetate buffer are added. The solution is warmed to about 60°C and titrated against E.D.TA. solution to a sharp red to golden yellow end point.

Mössbauer spectra were recorded for the mercury europium materials which were diluted with Al_2O_3 to reduce non-resonant absorption and scattering. Spectra were accumulated for up to five days at 93K. The authenticity of the samples was confirmed by the crystal structure; lattice parameters were determined as described in Chapter 2. Electrical conductivity measurements were attempted on one sample; difficulty was experienced pressing pellets of the sample with the limited quantity available.

6.5 Results

The compounds were all silver grey in colour, brittle and hard. Difficulty was experienced in grinding the solid for the preparation of samples for Mössbauer and x-ray diffraction experiments, the hardness decreasing with increasing mercury content. The samples were found to react with the atmosphere, the reactivity decreasing with increasing mercury content. The formulae assigned to the compounds are determined from the structures found by previous workers³⁻⁶ even though the ratios of europium to mercury differ from those published. The compounds and the associated structured data are given in table 6.1. An interesting structure-type is $\text{GdAg}_{3.6}^{28}$ which can allow a range of stoichiometries. Mössbauer spectra and x-ray diffraction patterns were produced; the results are presented in table 2

with the experimentally determined ratios of europium to mercury. All the isomer shifts lie between about -10mms^{-1} and -11mms^{-1} , that is between the isomer shifts for europium metal and the divalent ionic species. In general the composition of the samples follows that predicted by the crystal structure; larger deviations occur with an increasing mercury content. The Mössbauer spectra are in general poor in quality despite the long accumulation times; they are shown in figures 6.3 to 6.6.

The compound produced by electrolysis and subsequent distillation was found to have a ratio of europium to mercury of 1: 3.6, the isomer shift was found to be $-10 \pm 0.2 \text{ mms}^{-1}$ and the full width at half height $2.1 \pm 0.1 \text{ mms}^{-1}$. The structure could not be determined and so no further use could be made of the sample due to its uncertain composition or homogeneity. The Mössbauer data were not considered sufficient to characterize the sample and it is possible that more than one phase may exist. The Mössbauer spectrum is shown in figure 6.7.

The samples prepared to test the range of solid solubility were treated in the same way as the samples mentioned previously. The sample intended to be Eu_2Hg_3 was found to have a europium to mercury ratio of 1:1.47 but the x-ray diffraction pattern showed lines due to EuHg_2 and EuHg . The Mössbauer data showed that the spectrum could be fitted to two unresolved peaks with isomer shifts close to those of EuHg_2 and EuHg ; the relative intensity

ratio being 1: 4.88 for EuHg_2 and EuHg . The chemical analysis suggests the ratio of EuHg_2 : EuHg is 1: 1.13 showing the great increase in recoil free fraction with decreasing mercury content. The attempt to make the compound Eu_3Hg_2 resulted in a composition with a europium to mercury ratio of 1: 0.79. The x-ray diffraction pattern showed only lines due to an EuHg phase, the isomer shift was found to lie between those of EuHg and EuHg_2 . The results for these compounds are given in table 6.3 the spectra are shown in figures 6.8 and 6.9 respectively.

The attempt to measure the electrical conductivity of the samples was largely unsuccessful with the pellets tending to disintegrate after a short time. However, enough data was accumulated to show that the compounds possess metallic conduction properties. A plot showing resistance increasing with temperature for $\text{EuHg}_{3.6}$ is shown in figure 6.10.

6.6 Discussion

From the limited amount of data available some general comments on the nature of the compounds can be made. The evidence for metallic like character comes from the appearance, all the compounds are a silver grey colour and possess metal like reflectivity, the resistance is seen to increase with temperature as expected for a metal.

The crystal structures are common to those found for metals, hexagonal or body centred cubic lattices indicating the structure is determined by packing rather than the accomodation of directional bonds. The Mössbauer isomer shifts lie between the value for europium metal and those for divalent ionic compounds, a characteristic of rare earth intermetallic species²⁹. The isomer shifts tend towards those associated with the divalent ionic species. The Mössbauer shifts confirm that the compounds have a divalent ionic core as suspected by previous workers³⁻⁶ from the x-ray data but no obvious correlation is forthcoming of the isomer shift with the chemical compositions of the compounds, this will be discussed in more detail later.

The experiments to determine ranges of solid solubility suggest that the range is very limited, unlike that for alloys. The attempt to produce the compound Eu_3Hg_2 resulted in Eu_5Hg_4 or a compound with a ratio of europium to mercury of 1: 0.79. A larger range of solid solubility might be expected since both Eu and EuHg have the same body centred cubic structure. The attempt to prepare Eu_2Hg_3 resulted in EuHg and EuHg_2 phases, apparently without a great deviation in stoichiometry. The two examples indicate that the range of solid solubility is small and suggest a deviation from truly metallic behaviour. In section 6.2 factors influencing the character of intermetallic compounds were

discussed, together with some physical data for europium and mercury they can provide a description of the compounds. The physical data for europium and mercury is shown in Table 6.4. The size of the atoms or more correctly the metallic radii differ by about 21% this makes the size factor unfavourable and limits the range of solid solubility. The divalent ionic radii are very similar but the size factor rule is based on the radii of the atoms in the element and the unfavourable size factor is borne out by the limited range of solid solubility found in those compounds. On consideration of the electron configurations it would seem likely that both europium and mercury might have divalent ionic cores. Mössbauer spectra and x-ray data confirm this for europium, no such data for mercury exists for these compounds. However, mercury has received more attention than europium in metallic phase studies and it is generally found that the element displays the group valence²⁹, (except for the transition metals¹³ which have a valence of zero). If both the europium and mercury have divalent cores then each is equally likely to act as the solvent or solute, all other things being equal. The rules and observations are all general and their application is dependent on other factors, it may be said therefore that the valence rule is not unfavourable for either metal being the solvent. The experimentally determined ratios of europium to mercury show that the compounds are capable of being deficient

in mercury ie Eu_5Hg_4 or deficient in europium ($\text{EuHg}_{3.6}$ has a europium to mercury ratio of 1: 4.07). The electrochemical factor would appear to be very unfavourable to the formation of solid solutions because the mercury being more electro-negative than the europium, will tend to form polar bonds. This would introduce some degree of either ionic or covalent character into the compounds. The compounds would not appear to conform to Hume-Rothery's electron compound behaviour because of their limited range of solid solubility. However, the CsCl type structure of the β -phase does exist for one of these compounds, EuHg . The general character of the compounds can then be summarized as being metallic with a degree of ionic or covalent character leading to compounds with normal valence like compositions.

Quantitative correlations of the isomer shift with properties of the compounds are now attempted. No correlation is found between the ratio of europium to mercury and the isomer shift. (Table 6.2). This is to be expected since the structures of the compounds are all different, except for Eu_5Hg_4 and EuHg so that the effect of the presence of mercury on the isomer shift will not be observed in such a simple manner. The intermetallic distances (Eu-Hg) of the compounds do not show any correlations with the isomer shift as seen in table 6.5, for the same reasons as above. It would seem clear that a quantity independent of the structure is needed as has been found in previous work.⁴ The cube root of the volume of the unit cell is used after Parthe³⁰. No correlation is found for this quantity with the isomer shift

but it does not take into account the numbers of atoms in the unit cell. Since mercury is more electronegative than europium, there will be a tendency for the mercury ionic cores of the compound to gain electrons at the expense of the europium. Therefore the greater the number of mercury atoms surrounding a europium atom, the greater the loss in electron density experienced by the europium atom³¹. The lower the content of europium in the unit cell the lower the electron density around the europium nucleus will be. A new quantity is defined:

$$\sqrt[3]{\frac{n}{V}}$$

where n is the number of europium atoms per unit cell V is the volume of the unit cell. This quantity reflects the number density of europium atoms in the compound and when plotted against the isomer shifts gives a reasonable straight line (figure 6.11). The isomer shift, hence, s -electron density at the europium nucleus is seen to decrease with decreasing europium content in the unit cell. It is interesting to note that europium metal does not fit this pattern, showing that the reduction in electron density at the europium nucleus can be attributed to the presence of mercury.

An extension can be made covering the electron density at the europium nucleus. If the electron configurations of

europium and mercury are considered together with the structural data it may be reasonable to assume that the divalent core of the europium does not play a significant part in the electronic properties of the compound. The $4f^7$ electron configuration is left intact with the 6s electrons contributing to metallic bonding, ionic or covalent bonding or for electrical conduction. The isomer shift is a measure of the s-electron density at the europium nucleus. This electron density can be considered to be made up of contributions from the inner core of the Eu^{2+} electrons plus a contribution from the conduction electrons or 6s electrons. Brix et al^{32,33} have developed a method for estimating the conduction electrons density at the europium nucleus from the isomer shift. The quantity:

$$L(4f^7.\text{CE}) - L(4f^7)$$

can be found by comparing the isomer shifts of the sample and EuSO_4 deemed to have a $4f^7$ electron configuration.

A simple relationship between the electron densities denoted L, and the isomer shifts δ , has been derived

$$\frac{[L(4f^7.\text{C.E}) - L(4f^7)]}{[L(4f^7) - L(4f^6)]} = \frac{\delta_{\text{sample}} - \delta_{\text{EuSO}_4}}{\delta_{\text{EuF}_3} - \delta_{\text{EuSO}_4}}$$

The value of δ (EuSO_4) relative to EuF_3 is taken as -15 mms^{-1} .

The conduction electron density at the nucleus $[L(4f^7.C.E) - L(4f^7)]$ can be found by using

$$[L(4f^7) - L(4f^6)] = 1.9 \times 10^{26} \text{ cm}^{-3}$$

Another quantity, ζ , is defined as the ratio of the conduction electron density of the sample ion to that of the free ion.

$$\zeta = \frac{[L(4f^7 \text{ C.E}) - L(4f^7)]}{[L(4f^7 6s^2) - L(4f^7)]}$$

$$\text{where } [L(4f^7 6s^2) - L(4f^7)] = 2.4 \times 10^{26} \text{ cm}^{-3}$$

The electron configuration of the free atom is $[\text{Xe}] 4f^7 6s^2$ and assuming that the 4f electrons in the sample ions do not play a part in bonding or the electrical properties of the sample the electron configuration of the europium ion may be calculated.

The conduction electron density at the europium nucleus was calculated for all the samples and plotted against $3 \sqrt{\frac{n}{V}}$ (figure 6.12). The values of ζ' were calculated and used to find the electron configurations of the ions, the data are listed in table 4.6.

The dependency of the isomer shift and conduction electron density at the europium nucleus upon $3 \sqrt{\frac{n}{V}}$ is clear from figures 6.11 and 6.12. The conduction electron density

decreases with decreasing europium concentration in the lattice, each europium has to contribute more electrons to its environment if fewer europium atoms are available, this implies a set electron concentration in the sample for a stable lattice. This is in agreement with the Jones theory³⁴ where the energy of the lattice is partly due to the valence electrons the energy of which depends on $\frac{n}{v}$ where n and v have the same meanings as above.

Hyperfine Interactions

No account of possible hyperfine interactions has been taken so far, although it is possible for both magnetic and quadrupole interactions to occur. Quadrupole interactions would arise from assymetry in the electron distribution outside the europium ion core as the $4f^7$ electrons of the europium ion would not contribute to the electric field gradient. Quadrupole interactions would provide information on polar bonding in the lattice. Magnetic interactions would be observed if Mössbauer spectra were recorded at lower temperatures. There are many examples of resolved magnetic hyperfine spectra in the literature²⁹. Study of the magnetic hyperfine spectra of europium will provide information on the core polarization and the conduction electrons as each give a contribution to the hyperfine field. The total hyperfine field H_{hf} is made up of the contribution³⁵

$$H_{hf} = H_{4f} + H_{core} + H_{CE}$$

where H_{4f} is the hyperfine field produced by the spin and orbital motion of the 4f electrons

H_{core} is the core polarization contribution due to a closed shell of s -electrons which are polarized by the exchange interaction with the 4f shell.

H_{CE} is the hyperfine field produced by the conduction electrons.

H_{4f} disappears for the half filled shell of europium and so allows the investigation of the remaining components. Often magnetic and quadrupole interactions occur together but can yield information on the interactions of the europium ion with its environment. No attempt has been made to investigate hyperfine interactions as such specific data was not sought in this preliminary study. Some difficulties exist in obtaining data on hyperfine interactions such as the low temperatures at which spectra are accumulated. A liquid helium cryostat is available in these laboratories but the ^{151}Eu source is not sufficiently intense to be used with it.

Additional work could be performed to discover the nature of the electrons in the conduction band and that of the electrons participating in bonding. This information can come from the study of hyperfine interactions and also from electron paramagnetic resonance studies.

Table 6.1

Structured data on the europium-mercury system

Compound	structure type	Space group	Lattice parameters		Refs.
			a	c	
EuHg	CsCl (b.c.c)	$P\bar{4}3m$	3.88	-	3
EuHg ₂	CeCd ₂ (hex)	$P\bar{6}2m$	4.98	3.71	4
EuHg ₃	Mg ₃ Cd (hex)	$P63/mmc$	-	-	5
EuHg _{3.6}	GdAg _{3.6} (hex)	$P6/m$	13.57	9.74	6,28

Table 6.2

Compositional data, isomer shifts δ , peak widths Γ , and x-ray parameters for compounds prepared in the present work.

Compound	Ratio Eu:Hg	δ (mms ⁻¹)	Γ (mms ⁻¹)	Lattice parameters	
				a	c
EuHg	1:0.98	-10.37 \pm 0.06	3.1 \pm 0.1	3.76 \pm 0.02	-
EuHg ₂	1:1.98	-10.1 \pm 0.4	2.6 \pm 0.1	4.97 \pm 0.06	3.56 \pm 0.05
EuHg ₃	1:3.15	-10.85 \pm 0.02	2.7 \pm 0.1	6.30 \pm 0.08	5.22 \pm 0.05
EuHg _{3.6}	1:4.07	-10.7 \pm 0.1	2.0 \pm 0.2	13.24 \pm 0.01	9.27 \pm 0.06

Table 6.3

Attempted preparations of composition Eu_2Hg_3 and Eu_3Hg_2 and data relating to the actual products.

Compound intended	actual	Ratio Eu:Hg	δ (mms^{-1})	Γ (mms^{-1})	Lattice parameter	
					a (Å)	c
Eu_2Hg_3	EuHg		-10.5 ± 0.2	4.6 ± 0.2	3.50 ± 0.05	-
	EuHg ₂	1:1.47	-10.2 ± 0.3	2.1 ± 0.8	4.82 ± 0.06	3.63 ± 0.04
Eu_3Hg_2		1:0.79	-10.14 ± 0.05	3.6 ± 0.1	3.80 ± 0.04	

Table 6.4

Some physical data for europium and mercury.

Property	Europium	Mercury
Group in periodic table	IIIA	IIB
Electronegativity (Pauling)	1.1	1.9
Structure	b.c.c	rhombic (complex)
Atomic radii (Å)	1.98	1.56
Metallic radii (Å)	1.99	1.57
Ionic radii (Å)		
+ I	-	1.27
+ II	1.09	1.10
+ III	0.95	-
electron configuration	[Xe] 4f ⁷ 6s ²	[Xe] 4f ¹⁴ 5d ¹⁰ 6s ²

Table 6.5

Isomer shifts and intermetallic distances for the europium-mercury compounds.

Compound	δ (mms ⁻¹)	Eu-Hg distance (Å)
Eu ₅ Hg ₄	-10.14 ± 0.05	3.29
EuHg	-10.37 ± 0.06	3.26
EuHg ₂	-10.1 ± 0.4	4.00
EuHg ₃	-10.85 ± 0.02	5.02
EuHg _{3.6}	-10.7 ± 0.2	4.00*

* weighted average

Table 6.6

Conduction electron densities L.CE $(n/v)^{1/3}$ values, ζ' and electron configurations of the europium ionic cores of the compounds.

Compound	L.CE $\times 10^{-26} \text{ cm}^{-3}$	$(n/v)^{1/3}$ (\AA^{-1})	ζ'	electron configuration
Eu_5Hg_4	0.62	0.287	0.26	$4f^7 6s^{0.52}$
EuHg	0.59	0.266	0.24	$4f^7 6s^{0.48}$
EuHg_2	0.62	0.283	0.26	$4f^7 6s^{0.52}$
EuHg_3	0.53	0.169	0.22	$4f^7 6s^{0.44}$
$\text{EuHg}_{3.6}$	0.55	0.205	0.21	$4f^7 6s^{0.46}$

Figure 6.1

Electrolytic cell for the preparation
of the europium-mercury amalgam

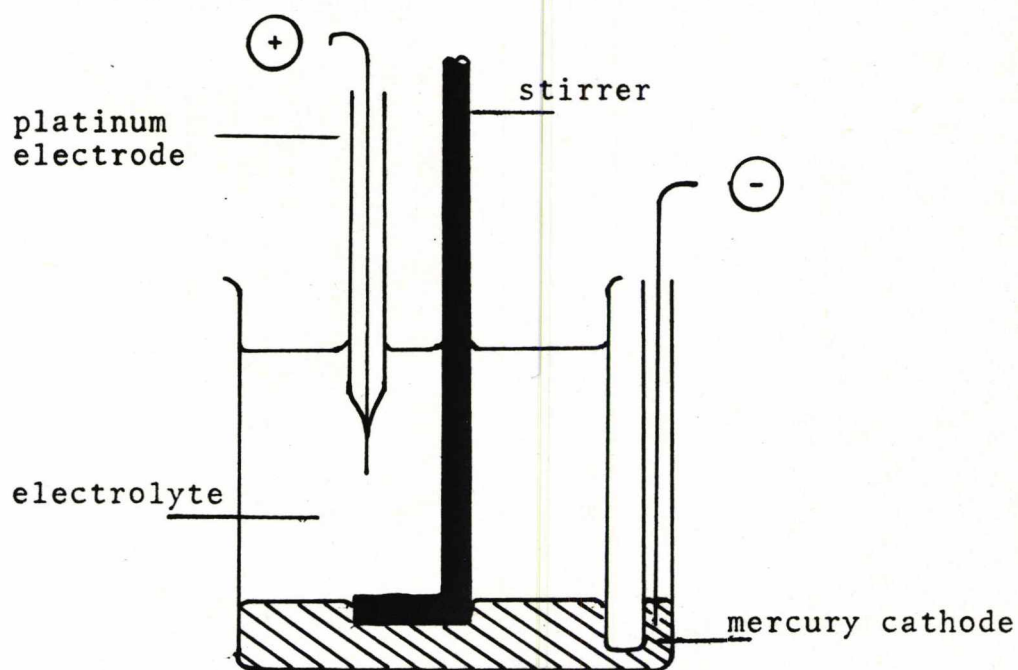


Figure 6.2

Ampoule and vacuum system for the preparation of europium-mercury compounds

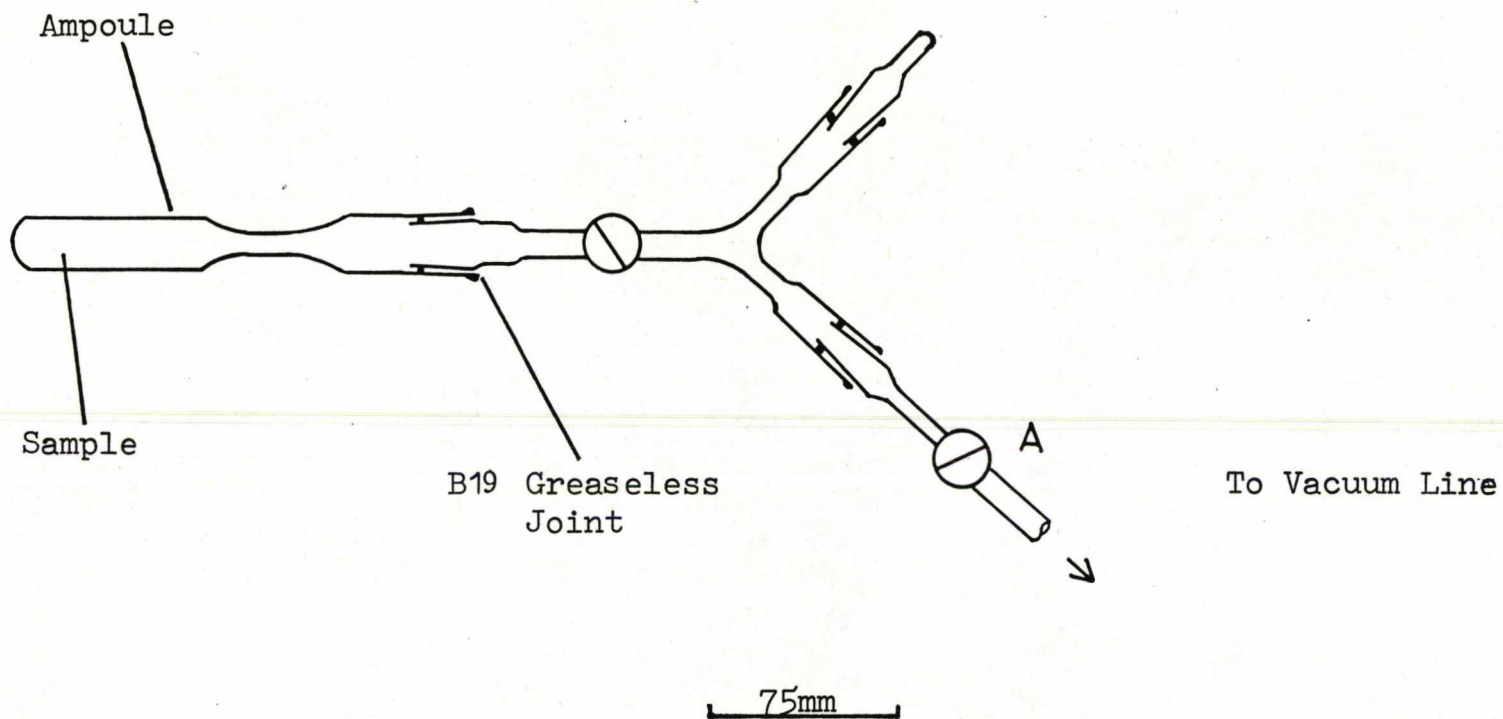


Figure 6.3

Mössbauer spectrum of EuHg

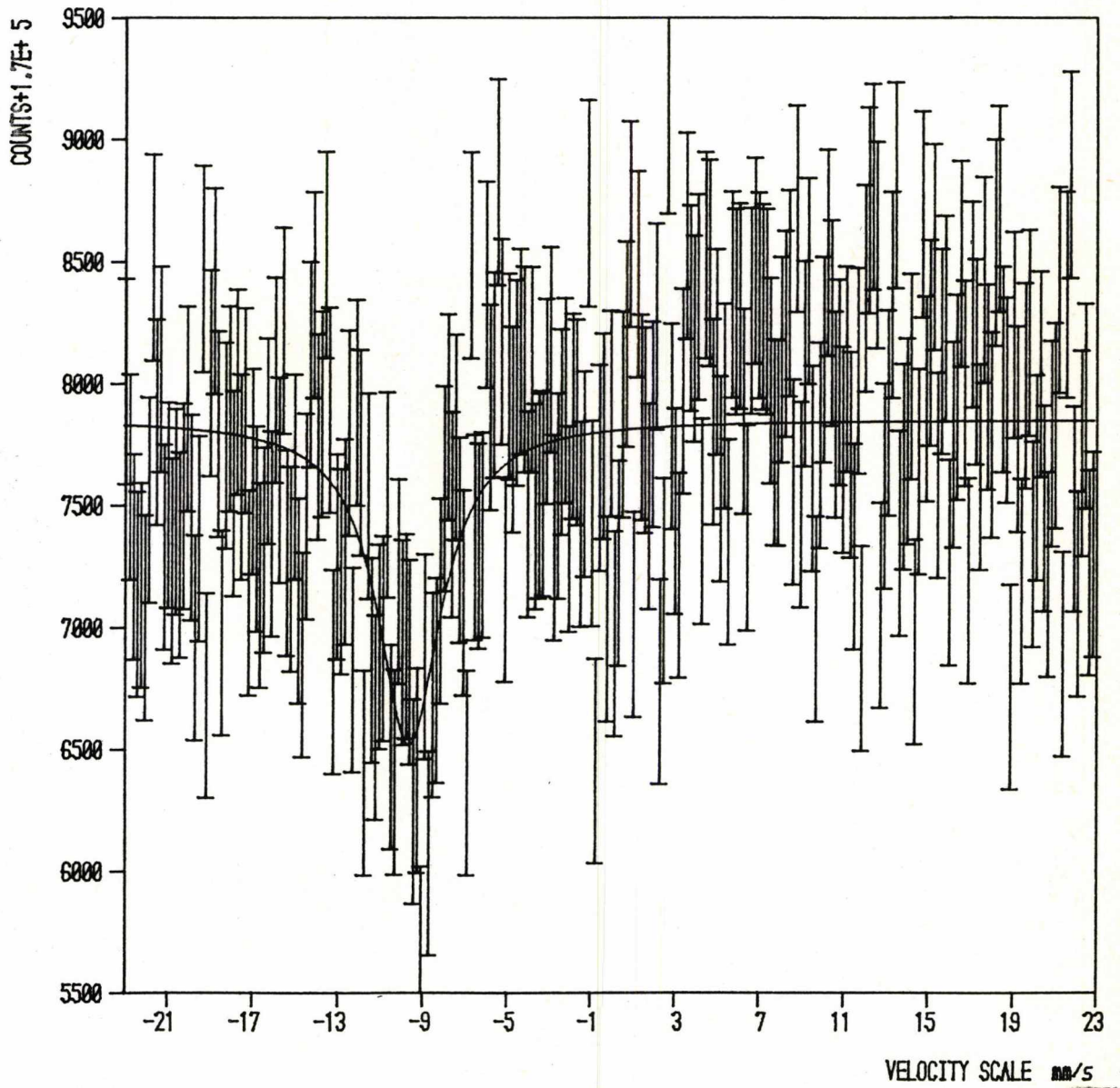


Figure 6.4

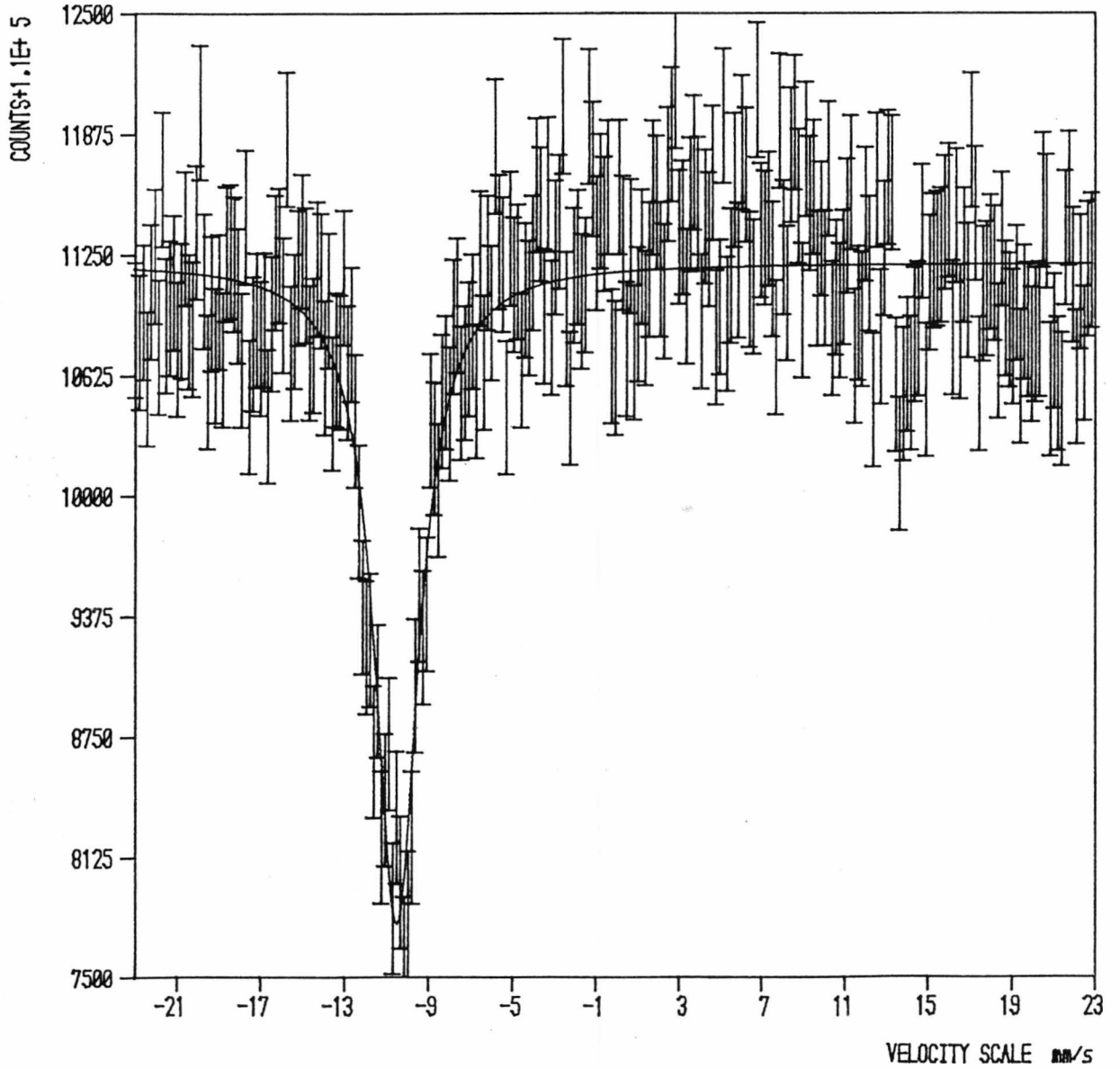
Mössbauer spectrum of EuHg_2 

Figure 6.5

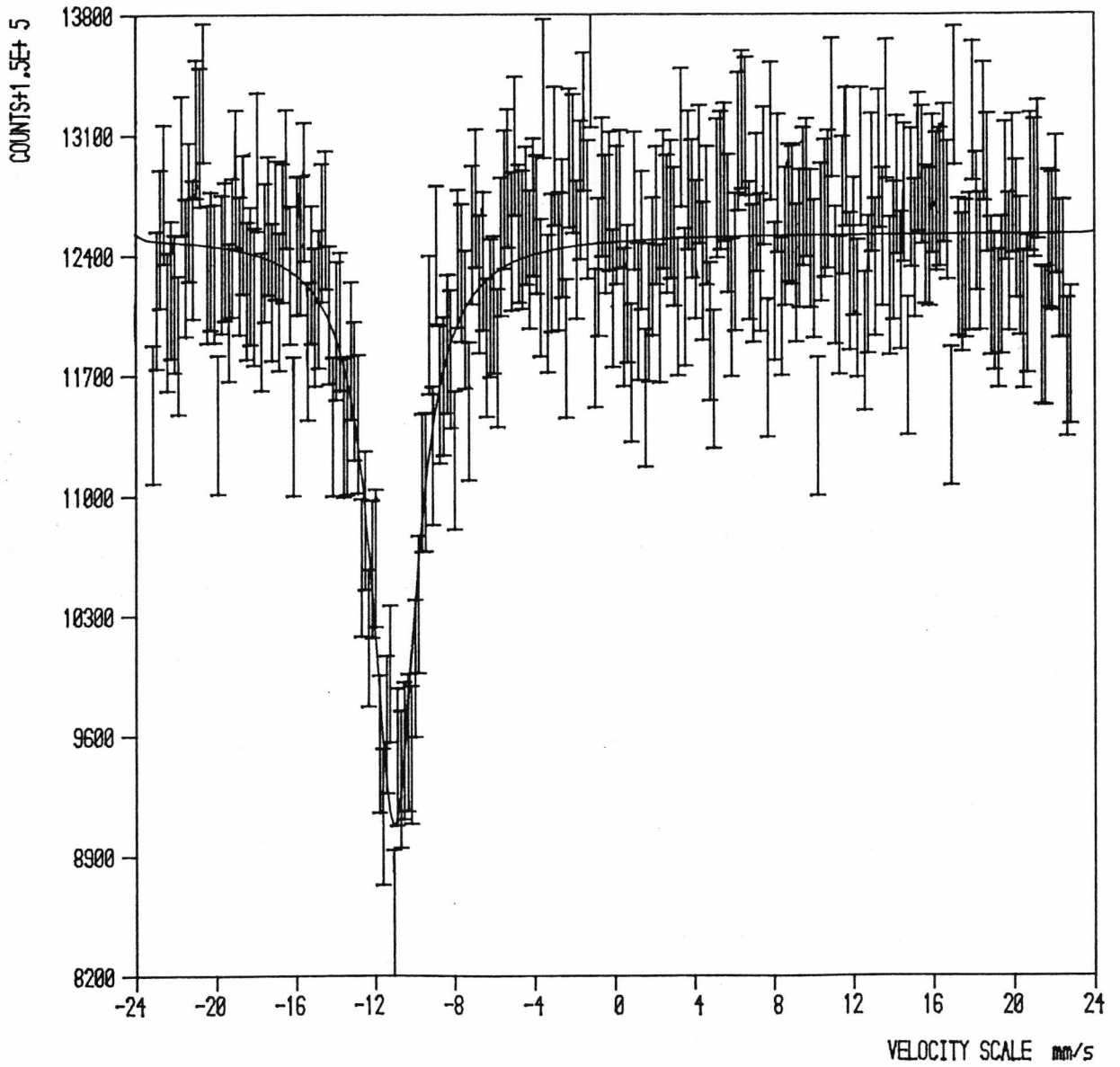
Mössbauer spectrum of EuHg_3 

Figure 6.6

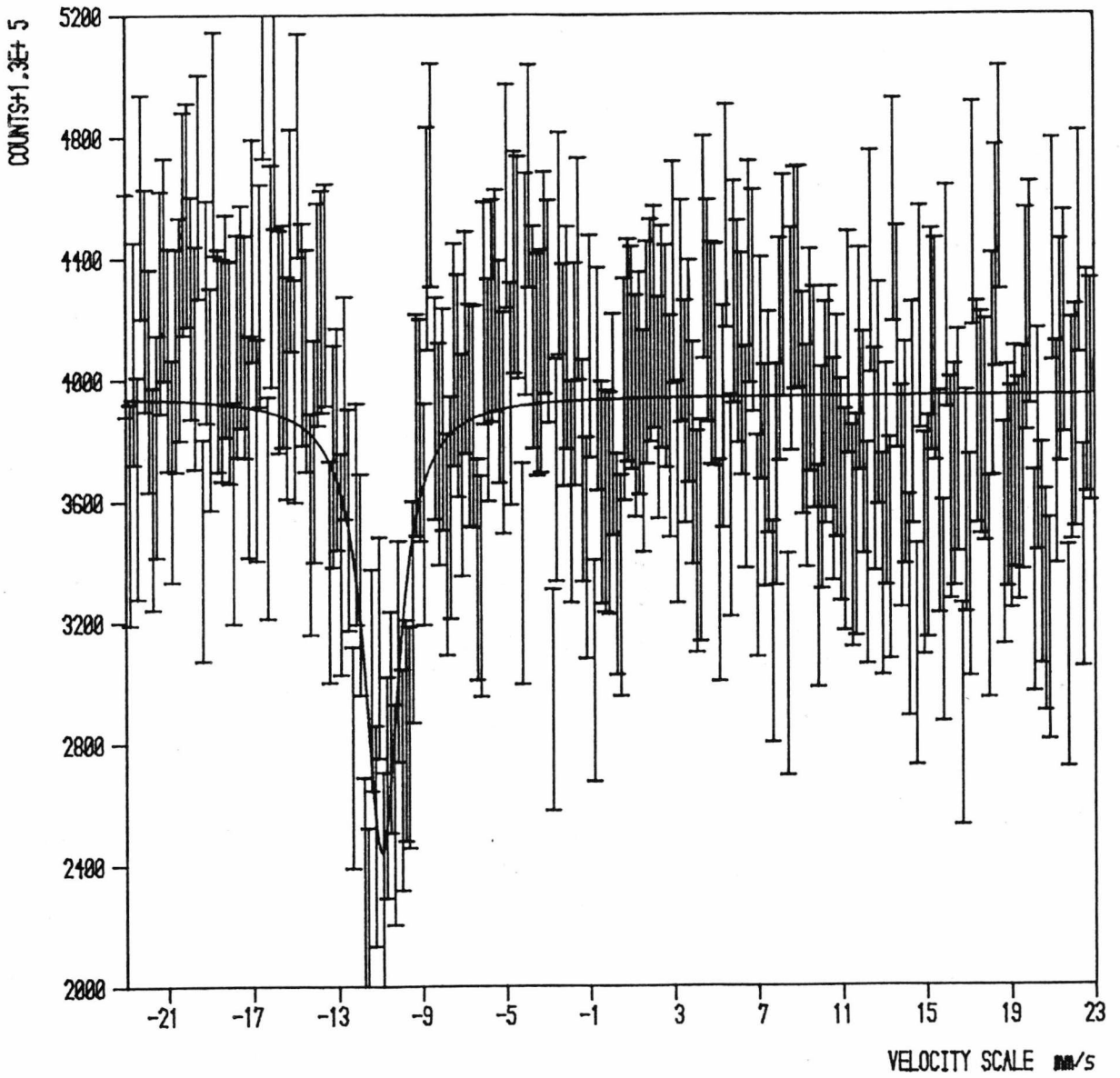
Mössbauer spectrum of $\text{EuHg}_{3.6}$ 

Figure 6.7

Mössbauer spectrum of europium-mercury compound produced by electrolysis and subsequent distillation

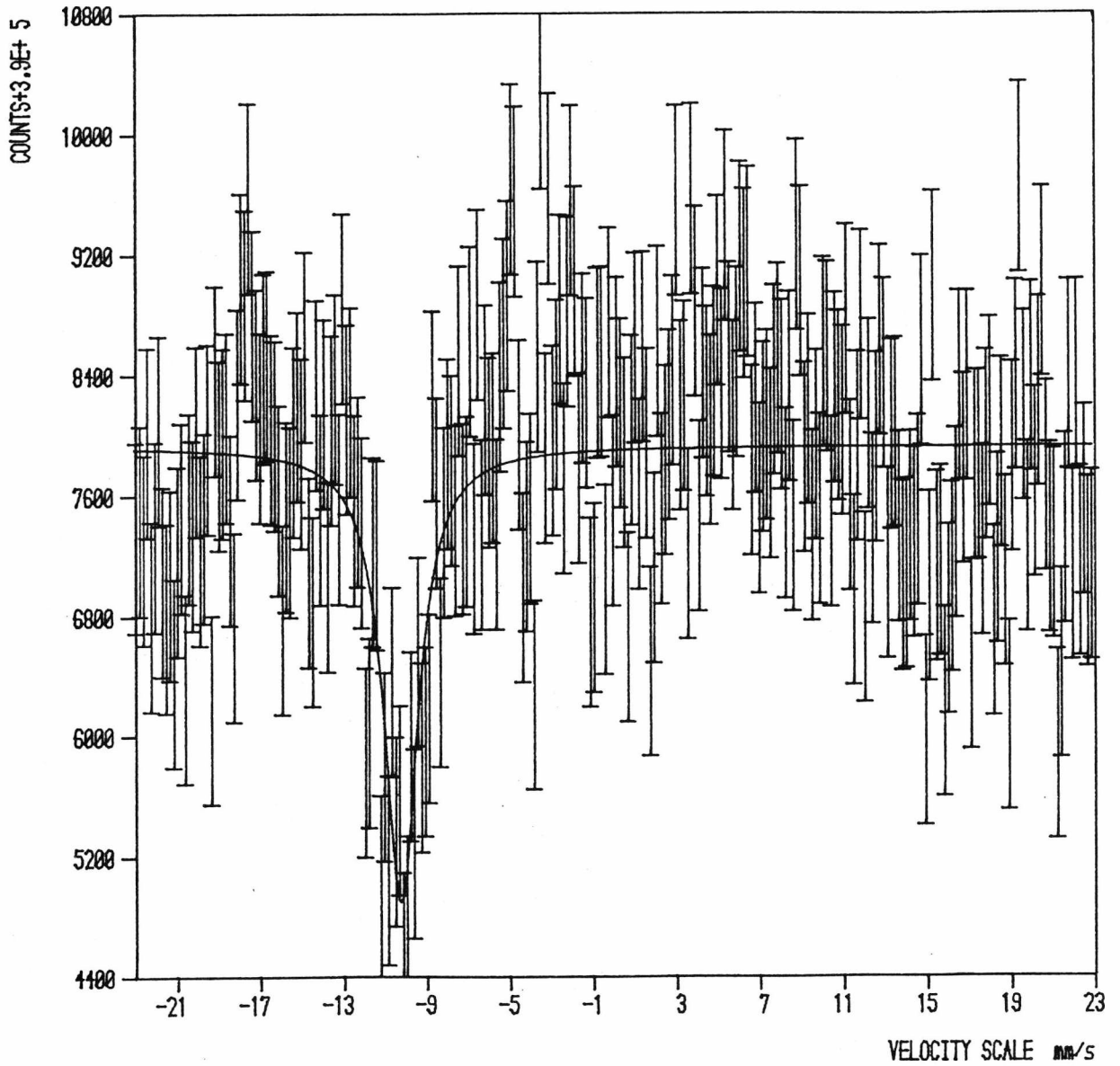


Figure 6.8

Mössbauer spectrum of the attempted
 Eu_2Hg_3 phase

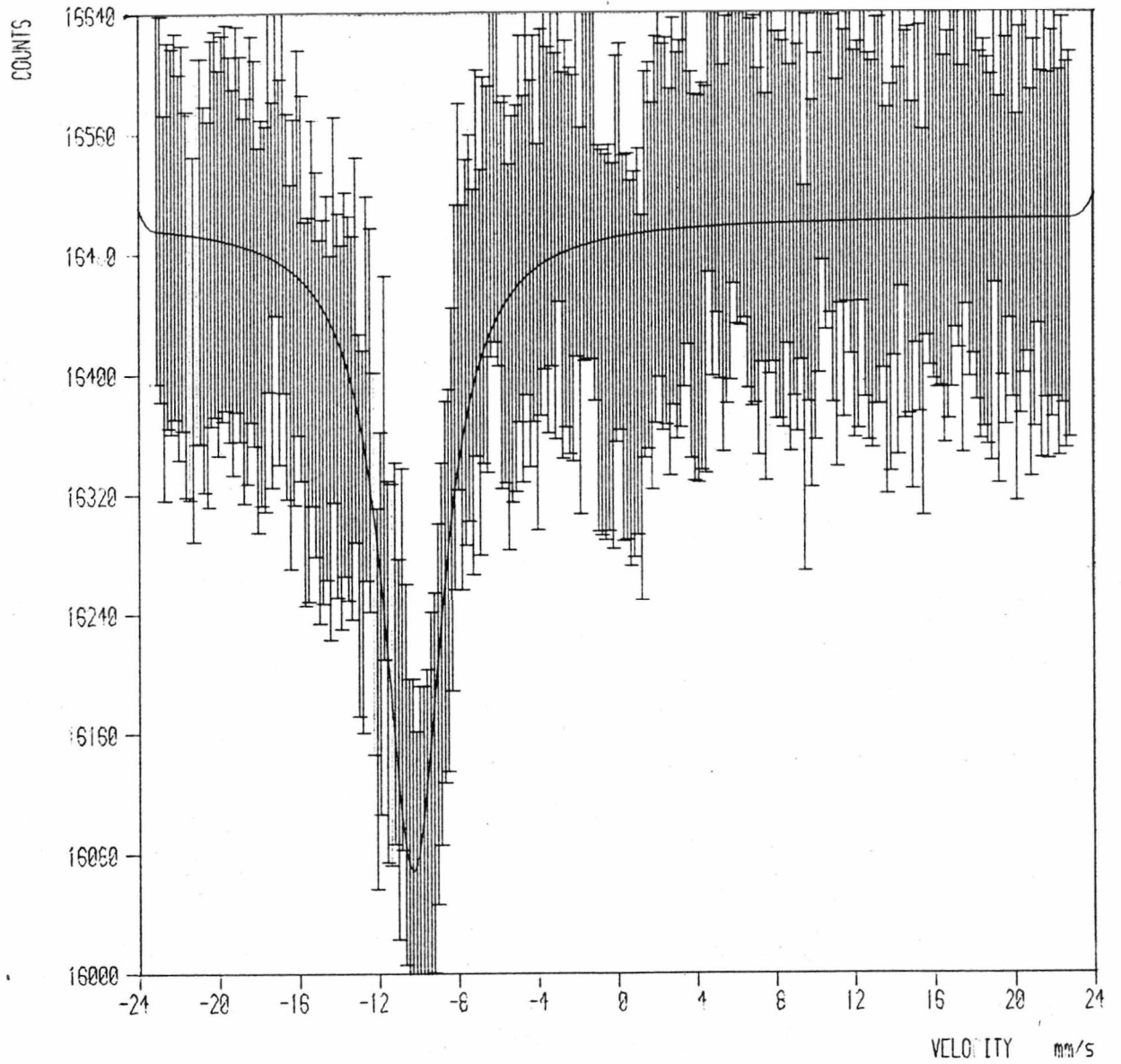


Figure 6.9

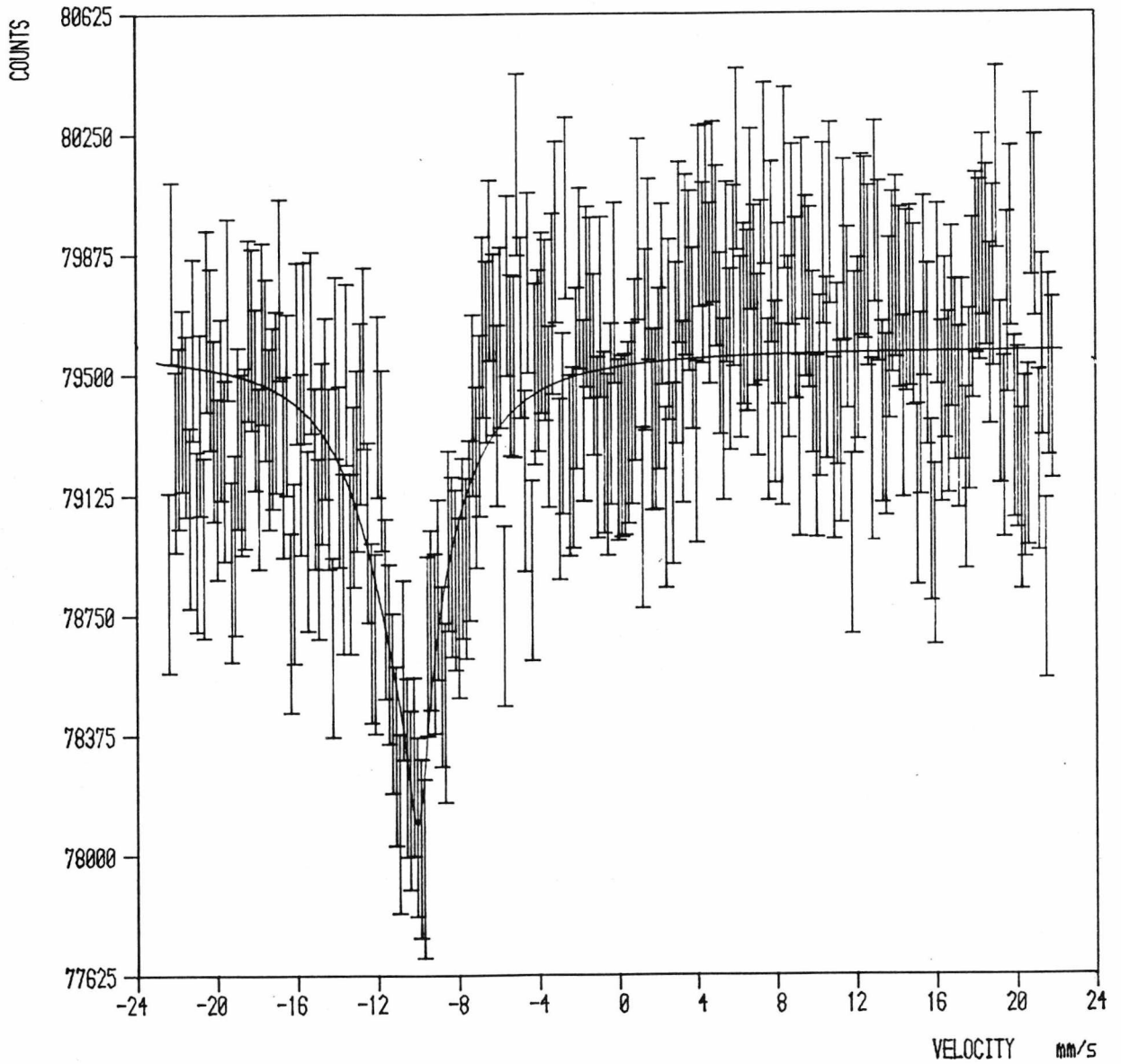
Mössbauer spectrum of Eu_5Hg_4 

Figure 6.10 Plot of resistance vs temperature
for $\text{EuHg}_{3.6}$

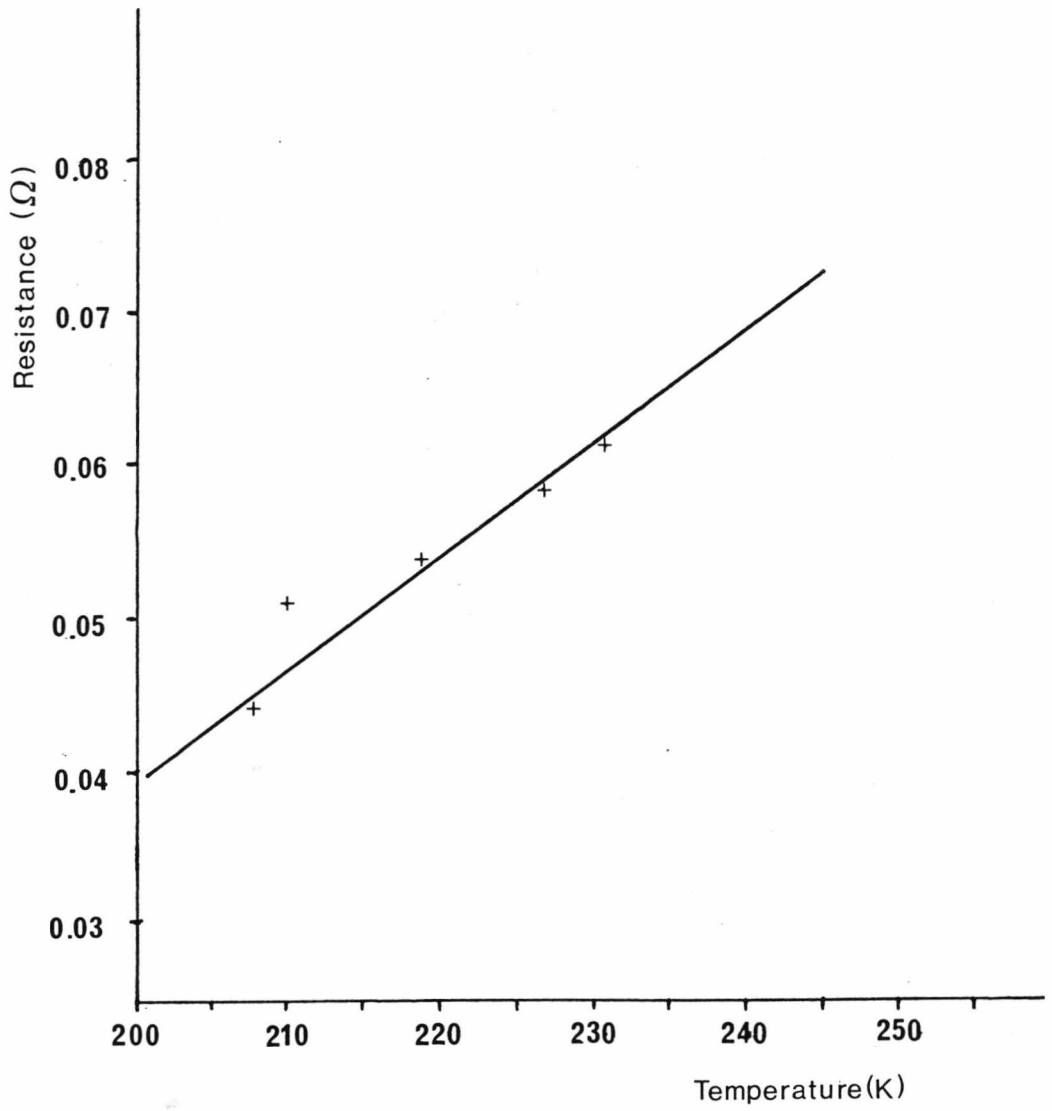


Figure 6.11

Plot of isomer shift (δ)
vs $(n/v)^{1/3}$

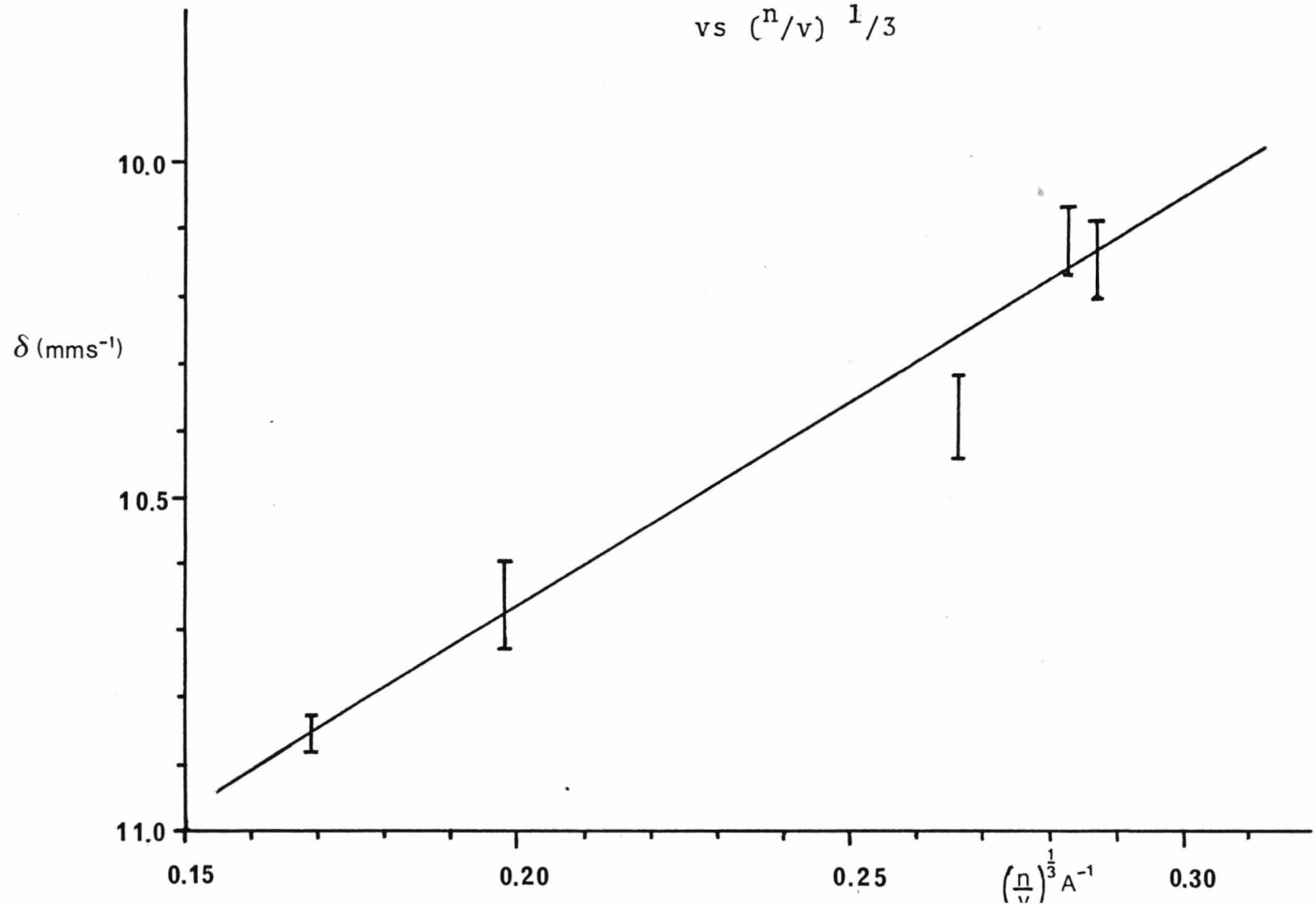
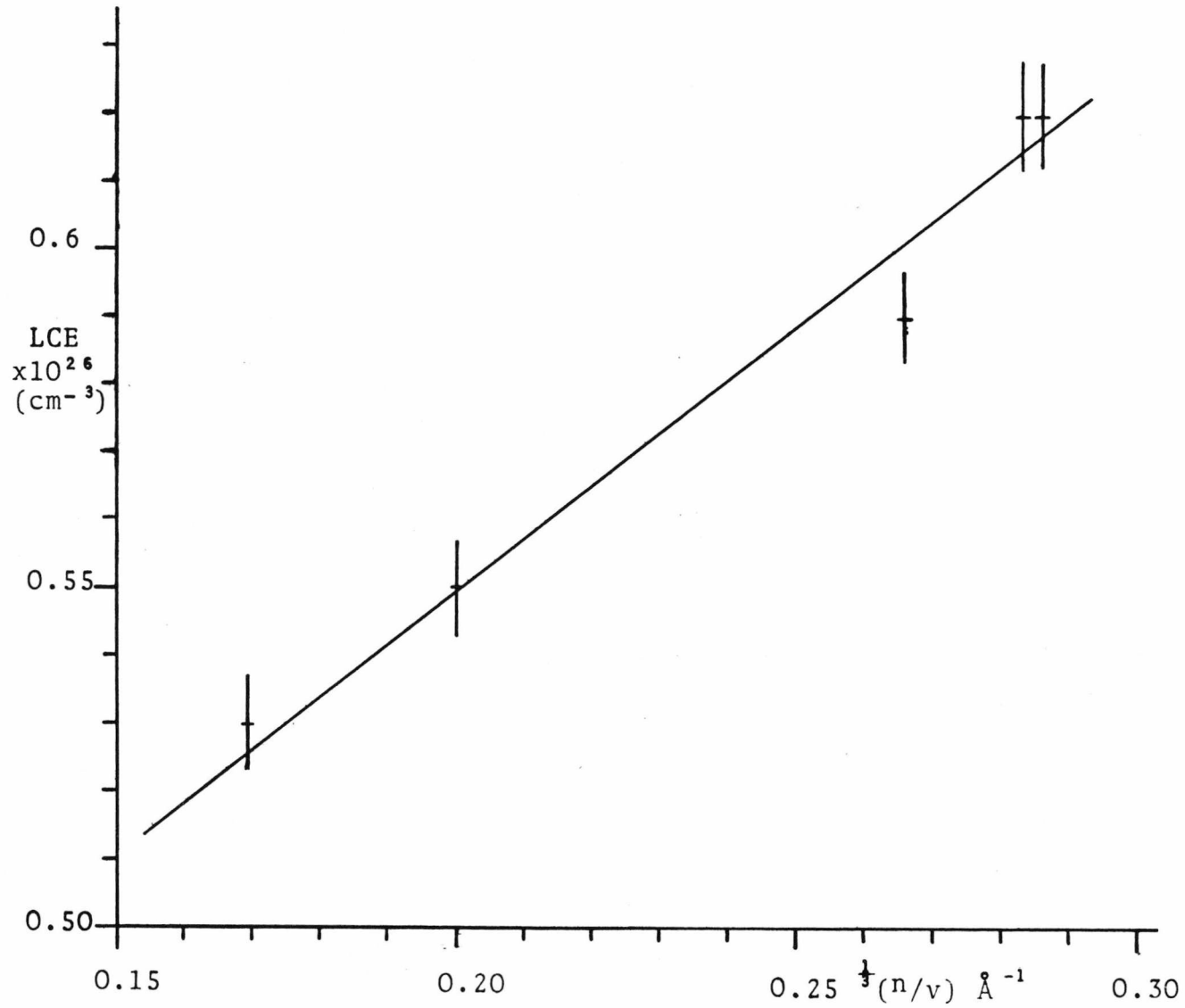


Figure 6.12

Conduction electron density (LCE)

vs $\sqrt[3]{(n/v)}$



References

Chapter 6

1. L.F. Yntema, J. Amer. Chem. Soc., 1930, 52, 2782.
2. H.N. McCoy, Inorganic Synthesis, 1946, 2, 65.
3. A. Iandelli and A. Palenzona, J. Less-Common metals, 1965, 9, 1.
4. A. Iandelli and A. Palenzona, J. Less-Common Metals, 1968, 15, 273.
5. A. Palenzona, J. Less-Common Metals, 1966, 10, 290.
6. F. Merlo and M.L. Fornasini, J. Less-Common Metals, 1979, 64, 221.
7. A. Iandelli and A. Palenzona, A. Atti, Acad. Naz, Lincei, Cl. Sci, Fis. Nat., Rend., 1964, 37, 165.
8. A. Taylor, "X-ray Metalography" John Wiley and Sons, inc. New York, 1961 (chapter 11)
9. A. Wood, "The Study of Metal Structures and their Mechanical Properties" Pergamon Press, New York, 1971.
10. N.F. Mott and H. Jones, "The Theory of the Properties of Metals and Alloys" Clarendon Press, Oxford, 1936.
11. W. Hume-Rothery and G.V. Raynor, "The Structure of Metals and Alloys" Inst. Metals Monogr., 1, London, 1954.
12. W. Hume-Rothery, J. Inst. Metals, 1926, 35, 295.
13. W. Ekmann, A. Westgren and A.J. Bradley, Z. Physik. Chem. (Leipzig) (B) 1931, 12, 51.
14. F. Laves, "Crystal Structure and Atomic Size" Theory of Alloy phases, American Society for Metals, 1956, p 124.
15. F. Laves, Naturwissenschaften (1939), 27, 65.

16. P. Drude, Ann. d. Physik, 1900, 1, 566.
17. P. Drude, Ann. d. Physik, 1900, 3, 369.
18. A. Sommerfeld, Naturwissenschaften, 1927, 15, 825.
19. A. Sommerfeld, Naturwissenschaften, 1928, 16, 378.
20. A. Sommerfeld, Z. Physik, 1928, 47, 1.
21. L. de Broglie, Phil. Mag., 1924, 47, 446.
22. F. Block, Z. Phys., 1928, 52, 555.
23. F. Block, Z. Phys., 1929, 59, 208.
24. Hopkins and Audrieth, Trans. Am. Electrochem. Soc., 1934, 66, 135.
25. Rare Earth Products, Widness, England.
26. Fisons Ltd. Roughborough, Leicestershire, England.
27. A.I. Vogel, "Text Book of Quantitative Inorganic Analysis" 4th ed., Longman, New York, 1978.
28. D.M. Bailey and G.R. Kline, Acta Cryst., 1971, B27, 650.
29. G.K. Shenoy and F.E. Wagner (ed) "Mossbauer Isomer Shifts". North Holland Publishing Co., New York, 1978.
30. E. Parthé, Colloques. int. du C.N.R.S., No 157, (Paris), 1965, P 195.
31. F.J. van Steenwijk and K.H.J. Baschow, Physica B, 1977, 85, 327.
32. P. Brix, S. Hüfner, P. Kienle and D. Quitmann, Z. Physik, 1965, 187, 67.
33. P. Brix, S. Hüfner, P. Kienle and D. Quitmann, Physics lett., 1964, 13, 140.
34. H. Jones, Proc. Roy. Soc. (London) A, 1934, 144, 225.
35. K. Tomala, Hyperfine Interactions, 1979, 7, 71.

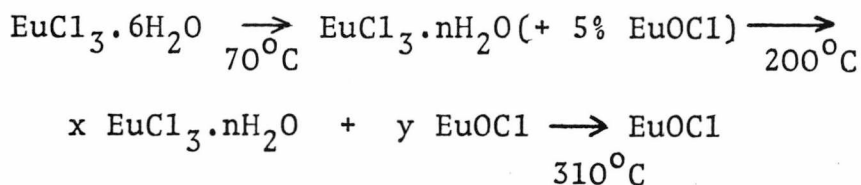
Chapter 7Summary of Results, Conclusions and Suggestions for
Further Work.7.1 Introduction

The results and conclusions of the previous three chapters are summarized in turn in this chapter. Suggestions for further work and modifications to the equipment are given at the end of each section below.

7.2 The Thermal Decomposition of Hydrated Europium(III)
Chloride and Bromide

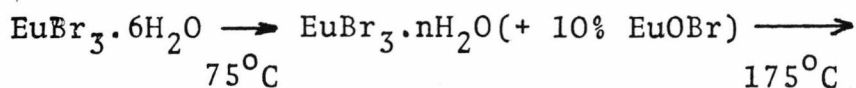
The work described in chapter three led to two reaction sequences being proposed.

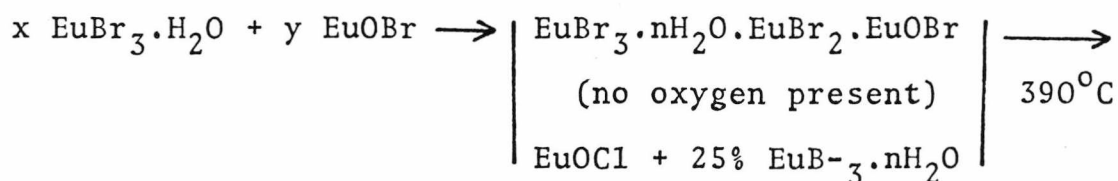
For the chloride system it is:



$$\frac{1}{2} \leq n \leq 1 \quad ; \quad 1 \leq x/y \leq 2.$$

and for the bromide system,





EuOBr

$$0 \leq n \leq \frac{1}{2} \quad ; \quad 2 \leq x/y \leq 4.$$

Evidence for the reaction mechanism of hydrolysis came from mass spectrometry which showed that the volatile reaction products were water and the appropriate hydrogen halide. Infra-red spectroscopy showed that water of hydration was present in all intermediate compounds. The presence of oxygen was found to affect the reaction path in the bromide case; in its absence europium(II) bromide was formed. For the first time, an unequivocal identification has been made of europium(II) among the reaction products of the hydrated bromide. It is hoped that the present study will clarify discrepancies encountered in previously published work.

7.3 Electron Hopping in Anhydrous Europium(III) Chloride and Europium(III) Bromide

Electron hopping was observed in both the bromide and chloride systems by Mössbauer spectroscopy and activation energies were confirmed by electrical conductivity measurements.

A transition was discovered leading to two activation energies existing above and below the transition temperature. The transitions were found to occur at 198K and 272K for the chloride and bromide systems respectively. The activation energy found for the chloride system is 0.08 ± 0.02 eV above the transition temperature. This is in agreement with Jendens' results (0.03 and 0.07 eV) for the high temperature region. The activation energies found for the bromide system are 0.04 ± 0.02 and 0.002 ± 0.002 eV above and below the transition temperature respectively. The activation energies found from electrical conductivity measurements agree with those found by Mössbauer spectroscopy. However the values found from the Mössbauer data lack precision, this is because the "goodness of fit" of the theoretical curves to the experimental data is judged by eye. In future work a modified least squares fitting program which is based on the theoretical relaxation model could be used. This will increase the accuracy and simplify the operation of the program.

Further work could be carried out on similar systems using samarium as the cation. Electron hopping is known to occur in Sm_3S_4 ² while SmS ³ is a well known example of an intermediate valence compound. The mixed system EuSm_2S_4 has been studied⁴, Mössbauer measurements on the europium but not samarium have been performed. A suitable isotope of samarium for Mössbauer spectroscopy would be ¹⁵²Sm as this exhibits a larger isomer shift between di and tri-valent oxidation states (when compared to the line width) than ¹⁴⁹Sm. The precursor of ¹⁵²Sm would be ¹⁵²Eu with a half life of 12 years.

The precursor for ^{149}Sm is ^{149}Eu with a half-life of only 106 days, making it a very expensive Mössbauer source. The disadvantage of ^{152}Sm is its large γ -ray energy of 121.8 KeV compared with 22.5 KeV for ^{152}Sm .

Other techniques can be used to investigate the process of electron-hopping by determination of the electronic environment of the cation. X-ray photo electron spectroscopy (XPS) shares with Mössbauer spectroscopy, the ability to observe the microscopic nature of the ion of interest. The time scale of XPS is much shorter than for Mössbauer spectroscopy (ca. 10^{-17} sec and 10^{-11} sec respectively) so will give information which is temperature independent.

7.4 The Europium-Mercury System

The initial study reported here showed the compounds to be metallic in nature but having a normal valence type of behaviour in bonding. The range of solubility was found to be low although a range of solid solubility does exist. The Mössbauer spectra showed the europium to have a divalent ionic core consistent with the x-ray data of previous workers⁵⁻⁸. The isomer shift hence s-electron density at the nucleus was found to be dependent upon the quantity $\sqrt[3]{\frac{n}{V}}$ where n is the number of europium ions in a unit cell of volume V.

Further work could include an investigation of the range of solid solubility of the samples, this could be used to test the relationship of the isomer shift over a range of samples of the same structure. Electrical conductivity measurements could be made more easily if the samples were produced in rod form of a suitable diameter. Then a length could be cut and used. Electron paramagnetic resonance (EPR) as well as XPS could be used to investigate the distribution of the valence electrons and the bonding within the samples. Hyperfine interactions have not been studied but should give useful information on the electron distribution complementary to that from EPR and XPS measurements.

7.5 Experimental Apparatus

The cryostat and Mössbauer spectrometer functioned satisfactorily and good quality Mössbauer spectra were produced. If magnetic hyperfine interactions are to be studied, lower temperatures will have to be attained and a liquid helium cryostat will be required. Such a cryostat is available in these laboratories, but a new ^{151}Eu source will be required for use with it. The ^{151}Eu source used in the course of this work was found to leak due to aging of the support material and was capped to prevent further leakage; this had the effect of attenuating the γ -ray flux to about half the initial value. It is felt that a more powerful source is required if the helium cryostat is to be used.

The x-ray diffraction patterns were not of good quality due to the absorption of the $\text{CuK}\alpha$ radiation by europium; this leads to errors in the determination of the lattice parameters. A Mo target would be more satisfactory and provide more accurate and reliable x-ray data.

The electrical conductivity cell worked satisfactorily for most purposes. However the large amount of material of high heat capacity used in its construction leads to long stabilization times when changing temperature. A smaller cell of approximately one third the size could be designed the casing of which could be glass. The new cell would stabilize more rapidly on changing the operating temperature, relying on the bath of coolant for temperature stability.

ReferencesChapter 7

1. C.M. Jenden, PhD. Thesis 1980, University of Kent at Canterbury, England.
2. M. Eibschutz, R.L. Cohen, E. Bühler and J.H. Wernick, Phys. Rev., 1972, B6, 18.
3. A. Jayaraman, V. Naraganamurti, E. Bucher and R.G. Maires, Phys. Rev. Lett. 1970, 25, 1430.
4. G.K. Shenoy et al in "Rare Earths and Actinides" Conf. digest No 3, Institute of Physics (London), 1971, p201.
5. A. Iandelli and A. Palenzona, J. Less-common Metals, 1965, 9, 1.
6. A. Iandelli and A. Palenzona, J. Less-common Metals, 1968, 15, 273.
7. A. Palenzona, J. Less-common Metals, 1966, 10, 290.
8. F. Merlo and M.L. Fornasini, J. Less-Common Metals, 1979, 64, 221.

